# Project SPARC Team Organization

## Instructor: Dr. A. K. Jakubowski

**Virginia Polytechnic Institute and State University**

**May, 1990**

Team Leader: Tyler Evans

### Orbital Mechanics / Aerodynamics

Eric Hammer (group leader)
Troy Hetrick
Ray Poff
Aimée Thornton
Roni Winkler

### Propulsion Systems

Theodore Bugtong (group leader)
Steve Davenport
Brett Flanders

### Vehicle Structures, Aerobrake, and Crew Support Systems

Stuart Deitrick (group leader)
Tyler Evans
Jason Lachowicz
Hank Lee
Susan MacDowell
Steve Massey

### Document Editors

Susan MacDowell
Steve Massey

### Graphics Editors

Theodore Bugtong
Jason Lachowicz
Hank Lee
Aimée Thornton

# Abstract

Future United States' space facilities include a Space Station in low Earth orbit (LEO) and a Geosynchronous Operations Support Center, or GeoShack, in geosynchronous orbit (GEO). One possible mode of transfer between the two orbits is an aerobraking vehicle. When traveling from GEO to LEO, the Earth's atmosphere can be used to aerodynamically reduce the velocity of the vehicle, which reduces the amount of propulsive change in velocity required for the mission. An aerobrake is added to the vehicle for this purpose, but the additional mass increases propellant requirements. This increase must not exceed the amount of propellant saved during the aeropass. The following report addresses the design and development of an aerobraking vehicle that will transfer crew and cargo between the Space Station and GeoShack. The vehicle is referred to as Project SPARC, a SPace-based Aeroassisted Reusable Craft. SPARC consists of a removable 45' diameter aerobrake, two modified Pratt & Whitney Advanced Expander Engines ($I_{sp}$ = 487 sec) with a liquid oxygen/liquid hydrogen propellant, a removable crew module with a maximum capacity of five, and standard sized payload bays providing a maximum payload capacity of 28,000 lbm. The aerobrake, a rigid, ellipsoidally blunted elliptical cone, provides lift at zero angle-of-attack due to a 73° rake angle, and is covered with a flexible multi-layer thermal protection system. Maximum dry mass of the vehicle without payload is 20,535 lbm, and the maximum propellant requirement is 79,753 lbm at an oxidizer to fuel ratio of 6/1. Key advantages of SPARC include its capability to meet mission changes, and its removable aerobrake and crew module.



PAGE ii INTENTIONALLY BLANK

PRECEDING PAGE BLANK NOT FILMED

# SPARC

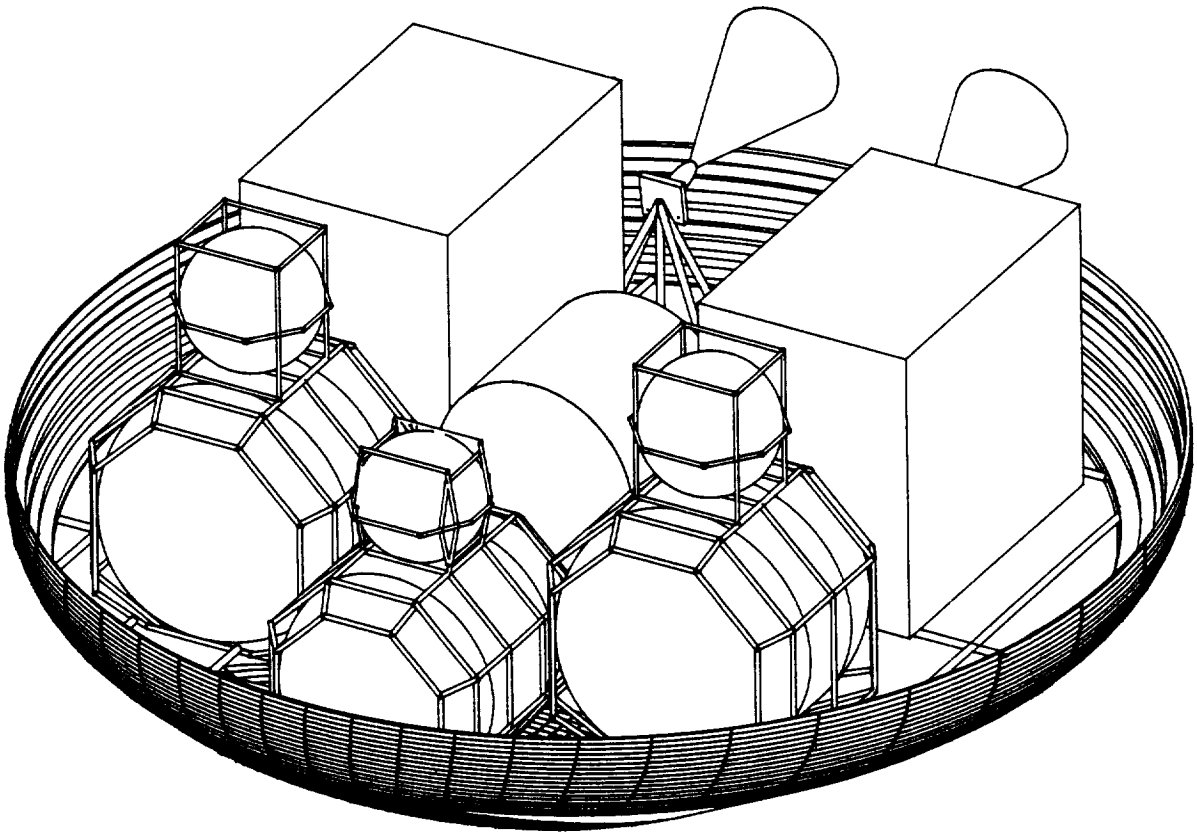



PAGE iv INTENTIONALLY BLANK PRECEDING PAGE BLANK NOT FILMED

# Nomenclature

| | |
|---|---|
| ABS | quilted alumino borosilicate fabric |
| ACS | atmospheric control system |
| $A_e/A^*$ | engine exit area-to-critical area ratio |
| AEE | advanced expander engine |
| AFE | aeroassisted flight experiment |
| CADAM | Computer-Graphic Augmented Design & Manufacturing |
| $C_D$ | drag coefficient |
| $C_L$ | lift coefficient |
| $C_m$ | moment coefficient |
| $C_{m\alpha}$ | slope of moment coefficient with respect to angle of attack |
| DOF | degree of freedom |
| E(1) | longitudinal Young's Modulus |
| E(2) | transverse Young's Modulus |
| EMU | extravehicular mobility unit |
| EVA | extravehicular activity |
| F.S. | factor of safety |
| FTu(1) | longitudinal ultimate strength |
| FTu(2) | transverse ultimate strength |
| $G_{12}$ | shear modulus |
| GEO | geosynchronous earth orbit |
| GNC | guidance, navigation, and control |
| GPS | global positioning system |
| h | altitude |
| HLLV | heavy lift launch vehicle |
| IRU | inertial reference unit |
| $I_{sp}$ | specific impulse |
| L/D | lift-to-drag ratio |
| $(L/D)_{newtonian}$ | analytically determined lift-to-drag ratio, based on newtonian impact theory |
| $(L/D)_{max}$ | maximum lift-to-drag ratio |
| $(L/D)_{experimental}$ | experimentally determined lift-to-drag ratio |
| LEO | low earth orbit |
| $\dot{m}$ | mass flow rate |
| $m/(C_D A)$ | ballistic coefficient |
| MLI | multi-layer insulation |
| MMV | manned maneuvering unit |
| NCRP | National Council on Radiation Protection |
| NOTS | Naval Ordinance Test Station |
| Q-felt | silica fiber felt blanket insulation |
| $\dot{q}$ | convective stagnation point heating rate |



PAGE VI INTENTIONALLY BLANK

PRECEDING PAGE BLANK NOT FILMED

| | |
|---|---|
| $\dot{q}_{max}$ | maximum convective stagnation point heating rate |
| R | aerobrake base plane radius |
| $R_a$ | apogee radius |
| RCS | reaction control system |
| $R_N$ | stagnation point nose radius |
| $R_p$ | perigee radius |
| RTV | room temperature vulcanized |
| SDV-3R | shuttle derived vehicle |
| SPARC | SPace-based Aeroassisted Reusable Craft |
| $S_{ref}$ | aerobrake reference area |
| SSAM | Static Structural Analysis for Microcomputers |
| $S_{surf}$ | aerobrake surface area |
| t | thickness |
| $T_{12}$ | ultimate shear strength |
| TOF | time of flight |
| TPS | thermal protection system |
| V | velocity |
| $w_o/w_f$ | oxidizer-to-fuel ratio |
| $\alpha$ | absorptivity |
| $\delta$ | aerobrake rake angle |
| $\Delta V$ | change in velocity |
| $\varepsilon$ | emissitivity |
| $\varepsilon_b$ | aerobrake bluntnose ellipticity |
| $\varepsilon_{cone}$ | aerobrake cone ellipticity |
| $\theta_{xy}$ | aerobrake cone half angle in xy-plane |
| $\theta_{xz}$ | aerobrake cone half angle in xz-plane |
| $\rho$ | density |
| $\tau$ | aerobrake skirt circular arc angle |
| $\phi$ | flight path angle |

# Table of Contents


Project SPARC Team Organization . . . . . i
Abstract . . . . . iii
SPARC . . . . . v
Nomenclature . . . . . vii
Table of Contents . . . . . ix
List of Tables . . . . . xi
List of Figures . . . . . xii

**Chapter 1 Introduction** . . . . . 1
1.1 Project Background . . . . . 3
1.2 Mission Scenario . . . . . 3

**Chapter 2 SPARC Configuration** . . . . . 5
2.1 Vehicle Design Evolution . . . . . 7
2.2 Configuration Selection . . . . . 9
2.3 Stability Analysis . . . . . 21
2.4 Center of Gravity Analysis . . . . . 21
2.5 Mass Moments of Inertia . . . . . 22

**Chapter 3 Trajectory Analysis** . . . . . 25
3.1 Introduction . . . . . 27
3.2 Orbital Mechanics . . . . . 27
3.4 Time of Flight . . . . . 29
3.5 Atmospheric Pass . . . . . 31

**Chapter 4 The Aerobrake** . . . . . 41
4.1 Introduction . . . . . 43
4.2 Geometry and Aerodynamics . . . . . 43
4.3 Structure and Materials . . . . . 43
4.4 Thermal Protection System . . . . . 46

**Chapter 5 Propulsion Systems** . . . . . 51
5.1 Introduction . . . . . 53
5.2 Propellant . . . . . 53
5.3 Main Engines . . . . . 54
5.4 Engine Mount . . . . . 57
5.5 Selection of Fuel Tank Shape . . . . . 59
5.6 Main Propellant Tanks . . . . . 63
5.7 Auxiliary Tanks . . . . . 65
5.8 Insulation . . . . . 65
5.9 Propellant Lines . . . . . 65

**Chapter 6 Structures** . . . . . 79
6.1 Introduction . . . . . 81
6.2 Materials . . . . . 81
6.3 Main Truss Structure . . . . . 83
6.4 Structural Analysis . . . . . 83
6.5 Payload Accommodation . . . . . 90
6.6 Tank Support . . . . . 92
6.7 Docking . . . . . 97

**Chapter 7 Crew Module** . . . . . 103
7.1 Introduction . . . . . 105
7.2 Cabin Environment . . . . . 105
7.3 Atmospheric Control System . . . . . 105
7.4 Interior Design . . . . . 107
7.5 Extravehicular Activity . . . . . 110
7.6 Crew Module Hull Structure . . . . . 111
7.7 Pressure Shell . . . . . 111
7.8 Insulation . . . . . 115
7.9 Radiation . . . . . 115

**Chapter 8 Navigation, Communication, & Power Systems** . . . . . 119
8.1 Guidance, Navigation, Control (GNC) . . . . . 121
8.2 Communications and Data Processing . . . . . 121
8.3 Electrical Power System . . . . . 122

**Chapter 9 Cost Analysis & Assembly** . . . . . 125
9.1 Cost Analysis . . . . . 127
9.2 On Orbit Assembly . . . . . 127

**Chapter 10 Design Summary** . . . . . 131
10.1 Summary . . . . . 133

**References** . . . . . 135

**Appendices** . . . . . 145
Appendix A Stability Equations . . . . . 147
Appendix B Mass Moments of Inertia . . . . . 148
Appendix C DRAG Program . . . . . 149
Appendix D Propellant Analysis Program . . . . . 155

# List of Tables


Table 2.1 Vehicle Mass Summary . . . . . 20
Table 3.1 Flight Summary . . . . . 28
Table 3.2 Multiple Aeropass Scenarios . . . . . 30
Table 3.3 Analytic Perigee Solution Summary . . . . . 33
Table 3.4 Critical Values . . . . . 40
Table 4.1 Aerobrake Characteristics . . . . . 44
Table 4.2 Aerobrake Shell and TPS Mass Summary . . . . . 50
Table 5.1 Propellant Calculations . . . . . 53
Table 5.2 Characteristics of Vehicle Engine Candidates . . . . . 54
Table 5.3 Modified AEE Characteristics . . . . . 56
Table 5.4 Tank Characteristics for Tank Shape Selection . . . . . 62
Table 5.5 Tank Characteristics . . . . . 64
Table 5.6 Propellant Line Characteristics . . . . . 70
Table 5.7 Thruster Characteristics . . . . . 75
Table 5.8 RCS Mass Summary . . . . . 75
Table 6.1 Material Properties . . . . . 82
Table 6.2 Propellant Tank Characteristics . . . . . 97
Table 7.1 Mass Summary of Atmospheric Storage Tanks . . . . . 106
Table 7.2 ACS Mass Summary . . . . . 107
Table 7.3 Volumetric Allocations . . . . . 110
Table 7.4 Crew Module Mass Summary . . . . . 114
Table 8.1 GNC Summary . . . . . 121
Table 8.2 Communications and Data Processing Summary . . . . . 122
Table 8.3 Power Requirements . . . . . 122
Table 8.4 Power System . . . . . 123
Table 9.1 SPARC Cost Analysis . . . . . 128
Table 9.2 SPARC Component Useable Lifetime . . . . . 129
Table 10.1 Design Parameter Summary . . . . . 134

# List of Figures


Figure 2.1 SPARC Configuration . . . . . 8
Figure 2.2 SPARC Configuration . . . . . 8
Figure 2.3 SPARC Configuration . . . . . 8
Figure 2.4 Configuration I . . . . . 10
Figure 2.5 Configuration II . . . . . 11
Figure 2.6 Configuration III . . . . . 13
Figure 2.7 Configuration IV . . . . . 14
Figure 2.8 Configuration V . . . . . 14
Figure 2.9 Final Configuration Top View . . . . . 15
Figure 2.10 Final Configuration Front View . . . . . 16
Figure 2.11 Final Configuration Side View . . . . . 17
Figure 2.12 Payload Configurations . . . . . 19
Figure 2.13 $C_m$ versus $\alpha$ . . . . . 23
Figure 2.14 Allowable Center of Gravity Envelope . . . . . 23
Figure 2.15 Center of Gravity History and Engine Mount Angle . . . . . 24
Figure 3.1 Flight Summary . . . . . 27
Figure 3.2 2-Pass Senario . . . . . 29
Figure 3.3 3-Pass Senario . . . . . 29
Figure 3.4 Relative Geometry . . . . . 30
Figure 3.5 Flowchart . . . . . 32
Figure 3.6 Perigee Altitude vs. Conic Perigee Altitude . . . . . 35
Figure 3.7 Total Heat versus Time (20,000-lbm Mission) . . . . . 35
Figure 3.8 Velocity versus Time (20,000-lbm mission) . . . . . 36
Figure 3.9 Altitude versus Time (20,000-lbm mission) . . . . . 36
Figure 3.10 Deceleration versus Time (20,000-lbm Mission) . . . . . 37
Figure 3.11 Heating Rate versus Time (20,000-lbm Mission) . . . . . 37
Figure 3.12 Total Heat versus Time (6,000-lbm Mission) . . . . . 38
Figure 3.13 Velocity versus Time (6,000-lbm Mission) . . . . . 38
Figure 3.14 Altitude versus Time (6,000-lbm Mission) . . . . . 39
Figure 3.15 Deceleration versus Time (6,000-lbm Mission) . . . . . 39
Figure 3.16 Heating Rate versus Time (6,000-lbm Mission) . . . . . 40
Figure 4.1 Aerobrake Structure . . . . . 45
Figure 4.2 Quilted Multilayer TPS Concept . . . . . 48
Figure 5.1 Engine Performance . . . . . 56
Figure 5.2 Engine Actuation . . . . . 58
Figure 5.3 Shape Factor - Oxidizer Tank (Front) . . . . . 60
Figure 5.4 Shape Factor - Fuel Tank (Front) . . . . . 60
Figure 5.5 Shape Factor - Fuel Tanks (Back) . . . . . 61
Figure 5.6 Shape Factor - Oxidizer Tank (Profile/Bottom) . . . . . 61
Figure 5.7 Shape Factor - Fuel Tank (Profile/Bottom) . . . . . 62
Figure 5.8 Propellant Tank and Cross Section . . . . . 66

Figure 5.9 Heat Flux versus # of Insulation Layers . . . . . 67
Figure 5.10 Engine Schematic . . . . . 68
Figure 5.11 Propellant Lines . . . . . 71
Figure 5.12 Oxygen Line Location . . . . . 72
Figure 5.13 Hydorgen Line Location . . . . . 72
Figure 5.14 Reaction Control System . . . . . 74
Figure 5.15 Reaction Control System Schematic . . . . . 77
Figure 6.1 Truss Support Structure (Top View) . . . . . 85
Figure 6.2a Location of Section Views . . . . . 86
Figure 6.2b Section Views A Through D . . . . . 87
Figure 6.2c Seciton Views E Through H . . . . . 88
Figure 6.3 Typical 5-Member Joiner . . . . . 89
Figure 6.4 Payload Structure . . . . . 91
Figure 6.5a Oxygen Main Tank Support . . . . . 93
Figure 6.5b Oxygen Auxiliary Tank Support . . . . . 94
Figure 6.6a Hydrogen Main Tank Support . . . . . 95
Figure 6.6b Hydrogen Auxiliary Tank Support . . . . . 96
Figure 6.7 Docking (Side View) . . . . . 99
Figure 6.8 Docking (Top View) . . . . . 100
Figure 6.9 Docking (Rear View) . . . . . 102
Figure 7.1 Atmospheric Control System Schematic . . . . . 108
Figure 7.2 Crew Module Interior Floor Plan . . . . . 109
Figure 7.3 Crew Module 3-D Wire Frame . . . . . 112
Figure 7.4 Support Bracket . . . . . 113
Figure 7.5 Crew Module Cross Section . . . . . 116

# Chapter 1

# Introduction

*1.1 Project Background*

*1.2 Mission Scenario*

## 1.1 Project Background

In the near future, the United States will place a Space Station in a low Earth orbit (LEO) which will serve as a laboratory for advanced experiments, a center for satellite operations and servicing, and a home for the astronauts who will perform these operations. Since space is limited on the Space Station, and travel between the Earth and the Space Station is expensive, it is proposed that extra supplies and equipment (i.e. propellant, lab supplies, life support equipment, and tools) be stored on another satellite in a geosynchronous orbit (GEO).

The Geosynchronous Operations Support Center, or GeoShack, will accomplish this purpose as well as serve as a way-station for future missions to the Moon, Mars, or elsewhere. Furthermore, the GeoShack will be a repair station for existing satellites often eliminating the need for them to be returned to the Earth's surface for servicing. Subsequently, it is necessary that a space-based vehicle transport equipment and crew to and from the GeoShack, and return supplies to the Space Station when needed. This vehicle is the subject of the following report: the design of an orbital transfer vehicle: Project SPARC (SPace-based Aeroassisted Reusable Craft)

## 1.2 Mission Scenario

### 1.2.1 Aerobraking Requirements

In recent years, a great deal of interest and research has been focused on the use of the planetary atmospheres to assist in orbital transfers. Specifically, when traveling from GEO to LEO, the Earth's atmosphere can be used to aerodynamically reduce the velocity of the vehicle, thus reducing the amount of propulsive $\Delta V$ required for the mission. An aerobrake must be added to the vehicle for this purpose, adding mass, which in turn, increases the propellant requirements. In order for the aeromaneuver to be economical, this increase must not exceed the amount of propellant saved by the aeropass in the first place.

Disadvantages of an aerobraked vehicle include the excessive heating rate that would be experienced during the atmospheric pass and the difficulties encountered in maintaining aerodynamic stability. It therefore becomes necessary to design an aerobrake that will provide adequate thermal protection of the entire vehicle, be aerodynamically stable, and create enough drag to sufficiently slow down the vehicle.

### 1.2.2 Mission Requirements

Three mission scenarios have been specified for transfer between the Space Station and the GeoShack. The first is a round-trip transfer for a 6,000-lbm payload and crew of five, the second is transfer of a 20,000-lbm payload and crew of five to the GeoShack and return of the crew only, and the third is transfer of a 28,000-lbm payload to the GeoShack with no return to the Space Station. This final mission is expendable and the vehicle will be discarded into a higher orbit.



INTENTIONALLY BLANK

PRECEDING PAGE BLANK NOT FILMED

# Chapter 2

# SPARC Configuration

*2.1 Vehicle Design Evolution*

*2.2 Configuration Selection*

*2.3 Stability Analysis*

*2.4 Center of Gravity Analysis*

*2.5 Mass Moments of Inertia*

PAGE 4 INTENTIONALLY BLANK

PRECEDING PAGE BLANK NOT FILMED

## 2.1 Vehicle Design Evolution

The first step of the design process was the selection of an aerobrake configuration. Three initial designs were considered (Figures 2.1 through 2.3).

Figure 2.1 is a ballute design with forward-firing engines and axial placement of the propellant tanks, payload bay and crew module. The ballute is a non-lifting, inflatable, balloon-like structure that surrounds the vehicle during atmospheric entry and serves as a variable-drag device responding on demand to accommodate atmospheric variations. Advantages include a low mass, compact storage requiring less hangar space at the Space Station, and no on-orbit assembly requirement.

Major disadvantages of this configuration include a high susceptibility to longitudinal instability if the location of the center of pressure is not carefully controlled relative to the center of gravity during drag modulation, and directional instability during turbulence and density fluctuations through the non-uniform atmosphere. Another problem with the ballute is the combined magnitude of the non-equilibrium radiative and convective heat fluxes near peak heating. These fluxes "are well in excess of the capability of the material proposed for the thermal protection of this structure. In fact, there is no existing flexible-reusable material that will accommodate the predicted surface heat fluxes." (Menees, 1983) Furthermore, the ballute will have to be replaced after every mission and placement of the reaction control system required to provide guidance corrections during flight is difficult because the craft is partially enveloped by the ballute during the aeropass. Due to these complications, this concept was eliminated from design considerations.

Figure 2.3 illustrates the use of rear firing engines with a centrally located payload module and a ballute aerobrake. The bent biconic was also considered for this configuration because of its high lifting capability and subsequent ability to provide pane-inclination change during the aeropass. Since the biconic has a reduced drag surface however, the corresponding ballistic coefficient must be increased to provide the required $\Delta V$. The perigee altitude must therefore be much closer to the surface of the Earth compared to the larger area "drag brakes" causing both the radiative and convective heating loads to drastically increase. Menees states that "the high stagnation point convective heating rates...place the bent biconic well beyond the capability of contemporary, reusable materials." (Menees, 1983) Due to these problems, the biconic aerobrake was ruled out. Other disadvantages of this configuration are the stability problems associated with rear-placed engines, and the lack of accessibility to the centrally located payload bay. Due to these complications, this configuration was eliminated from design considerations.

Figure 2.2 has a fixed aerobrake with side-firing engines and the main vehicle structure mounted above the aerobrake. Two aerobrake designs can be accommodated with this configuration: a symmetric aerobrake and a conical lifting aerobrake. The symmetric lifting aerobrake creates a constant drag with a small variable-lift capability providing the maneuverability to compensate for atmospheric variations. Analysis has shown, however, that the symmetric aerobrake is subject to higher thermal loading than the conical aerobrake (Menees, 1983) and is subject to roll-instability during certain phases of the aeropass. The conical lifting aerobrake, possessing all the



PRECEDING PAGE BLANK NOT FILMED

SPARC Configurations

Figure 2.1

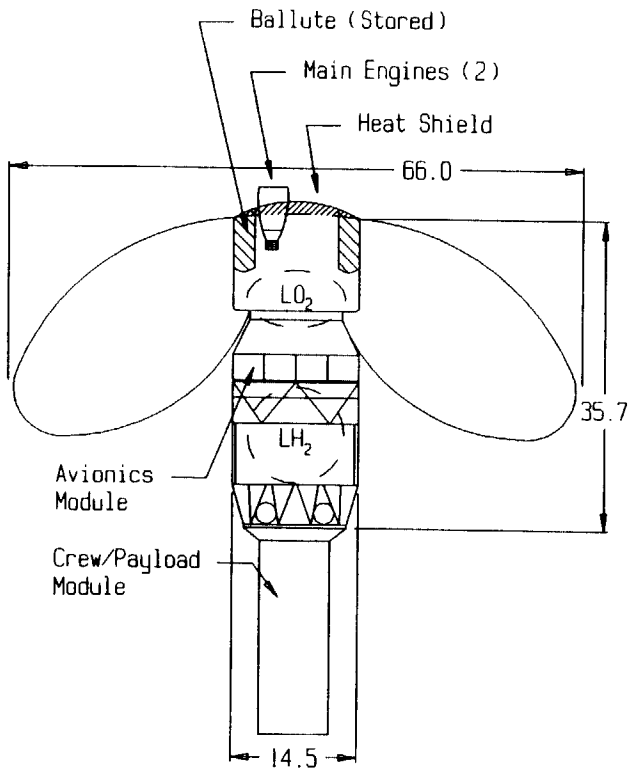


Figure 2.2

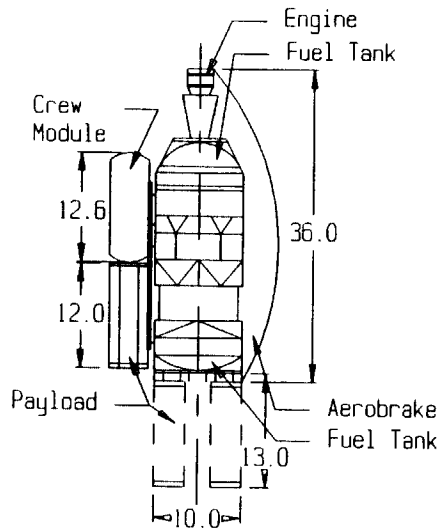


Figure 2.3

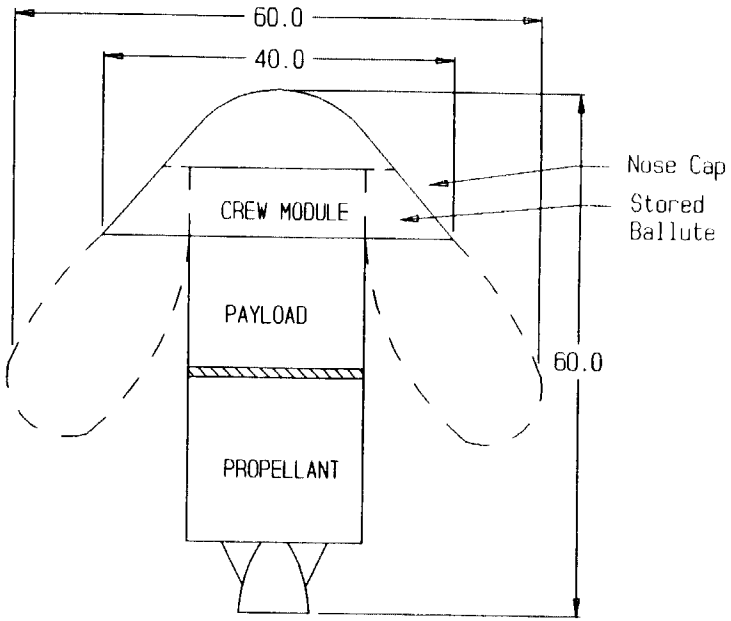


All Dimensions in Feet

ORIGINAL PAGE IS
OF POOR QUALITY

advantages of a symmetric aerobrake, is raked at an angle to provide lift at zero angle of attack. The frustrum is contoured to alleviate the high edge-heating effects and the asymmetric shape overcomes the roll-instability characteristic of the symmetric aerobrake. For these reasons, the fixed conical lifting aerobrake design was chosen.

An advantage of this configuration is the side-firing engines. Consideration was also given to engines that fire through doors in the aerobrake then retract during aeromaneuvering, but these doors create discontinuities on the surface of the aerobrake causing excessive thermal loads and possible failure points. Two other options were available: engines that fire through the aerobrake or engines that fire away from the aerobrake. Since crew safety is paramount, this type of engine placement was rejected and a side-firing engine orientation was chosen. The configuration in Figure 2.2 meets the design requirements most effectively and was therefore chosen for development.

## 2.2 Configuration Selection

### 2.2.1 Structural Design Considerations

There are numerous factors that were considered in the design of the SPARC configuration including propellant mass and tank size, crew accommodations, flexibility to variable payload requirements and the necessity of an expendable version. For each scenario, a center of gravity as far forward as possible is desired to provide for stability and control of the vehicle during the atmospheric pass. Furthermore, adaptability to mission changes and allowance for emergency situations are design criteria.

### 2.2.2 Initial Fixed Aerobrake Configurations

Two preliminary configurations were considered for the orientation of the structure within the aerobrake, and they are shown in Figure 2.4 and Figure 2.5. Figure 2.4 features one rectangular payload bay which meets the payload volume requirements of the largest mission, a large cylindrical crew module (35' length, 6' radius), and a box-like truss structure to connect the tanks, crew module, and the payload bay. A 58'-diameter aerobrake is necessary to shield the components from aerodynamic heating. The expendable version is considered an emergency situation in which the entire vehicle is lost. The tanks, crew module, and payload bay are all mounted in the same plane, the vehicle plane, located at the bottom of the skirt of the aerobrake. The engines are mounted to the truss structure surrounding the hydrogen tanks to provide an even thrust distribution about the x-axis.

Figure 2.5 features a separate payload bay for each mission which is connected to an attachment plate and mounted to the truss structure surrounding the tanks. The oxygen tank is offset from the hydrogen tanks to better utilize the aerobrake area, and a rectangular crew module (11' x 6.5' x 5.4') makes use of the space between the offset tanks. The crew module is connected much like the payload modules which enable it to be removed for the expendable mission. In such a case, an external set of avionics is positioned between the offset tanks to provide the necessary control

Figure 2.4 Configuration I

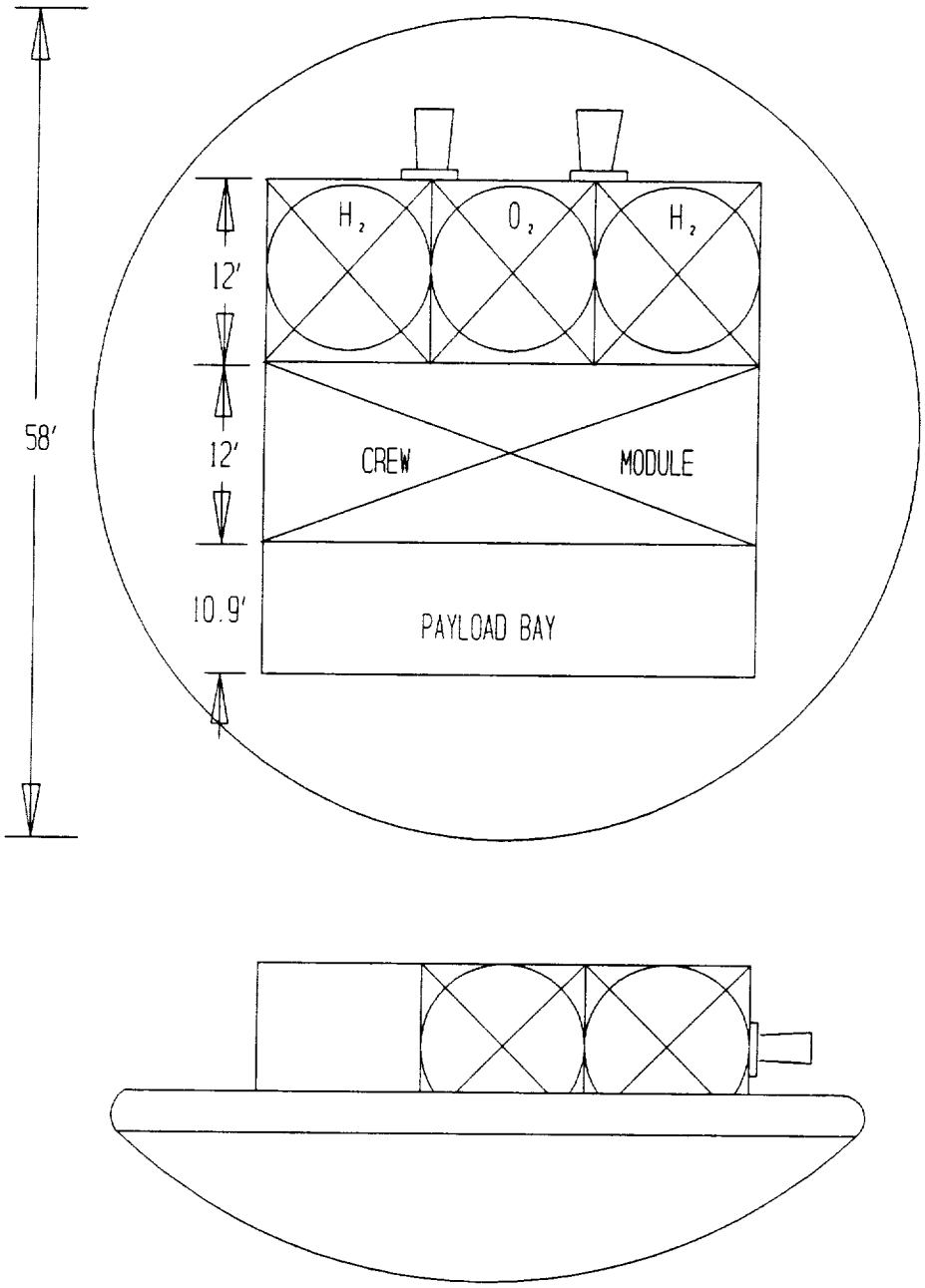

Figure 2.5 Configuration II

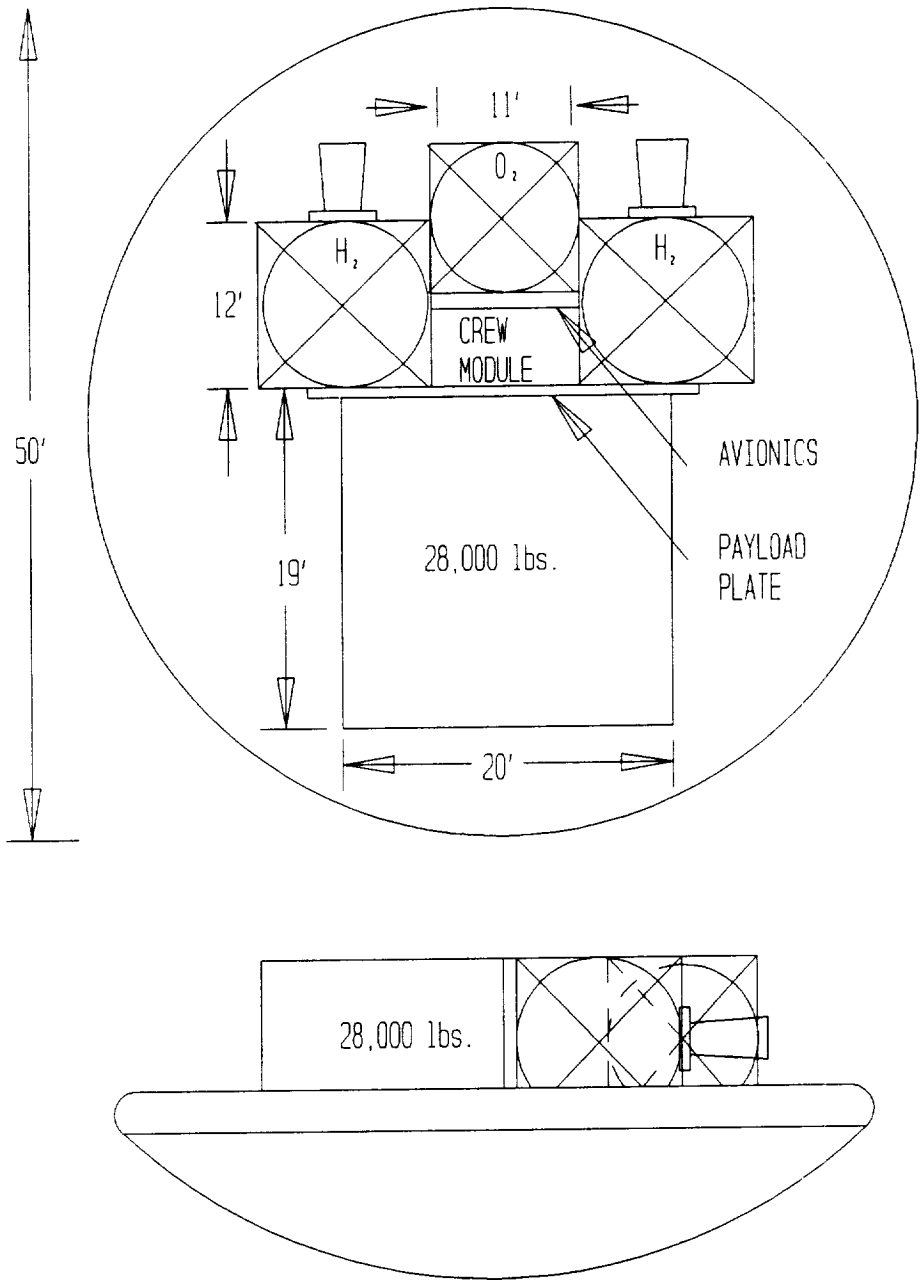

of the vehicle. A 50'-diameter aerobrake is necessary to protect the structural components during the atmospheric pass. The tanks, crew module, and the multiple payload carriers are mounted on the vehicle plane, and the engines are mounted on the truss structure surrounding the hydrogen tanks, symmetrical about the x-axis. With the exception of the crew module, the vehicle will be lost during the expendable mission.

After careful consideration of both preliminary configurations, the first was discarded due to inflexibility of the payload bay, and an oversized crew module. The second was chosen for further development.

### 2.2.3 Final Preliminary Configuration

The final preliminary configuration, Figure 2.6, features a payload/crew module truss support structure which allows for the attachment or detachment of the payload carriers and the crew module depending on the mission requirements. The crew module is 10' x 10' x 8' which provides additional room for storage and an air lock necessary for extravehicular activity. This module can be removed for the expendable mission and retained for future use, and the main truss structure provides better tank support and attachment points to the aerobrake. The idea of a removable aerobrake was considered for the expendable mission so that the truss structure is self-supporting for thrusting to GEO. With the smaller crew module and the creation of an octagonal tank support structure, the diameter of the aerobrake was reduced to 45' decreasing the vehicle mass. The key change, however, was the placement of the engines. To compensate for the large center of gravity fluctuations occurring during each mission, the engines were placed at the rear of the vehicle. This location, farthest from the center of gravity, reduces the gimballing necessary by creating a larger moment arm for thrusting. Additional truss members are included to support the engines.

### 2.2.4 Final Configuration Design

The first revision, Figure 2.7, was a cylindrical crew module with an inside diameter of 9.5'. (A cylinder acts as a much better pressure vessel than a rectangular module.) This module provides meteoroid and radiation protection for a crew of five, and a storage area which also serves as a safe haven from solar flare radiation. The airlock feature of the previous design was re-evaluated and discarded due to its excessive mass; in its place are extra tanks which allow for three repressurizations and a 48-hr supply of atmosphere. This crew module design was used in the final configuration.

Figure 2.8 shows a rail system which replaces the payload support structure and provides for the adjustment of both the payload bay(s) and crew module for cg considerations. The main propellant tanks were changed to circular cylindrical tanks with hemispherical end caps and are designed to carry the maximum amount of propellant needed.

The final configuration (Figures 2.9 through 2.11) is a compilation of the previous revisions. The rail system was discarded since only minimum repositioning of the payload bays could be

Figure 2.6 Configuration III

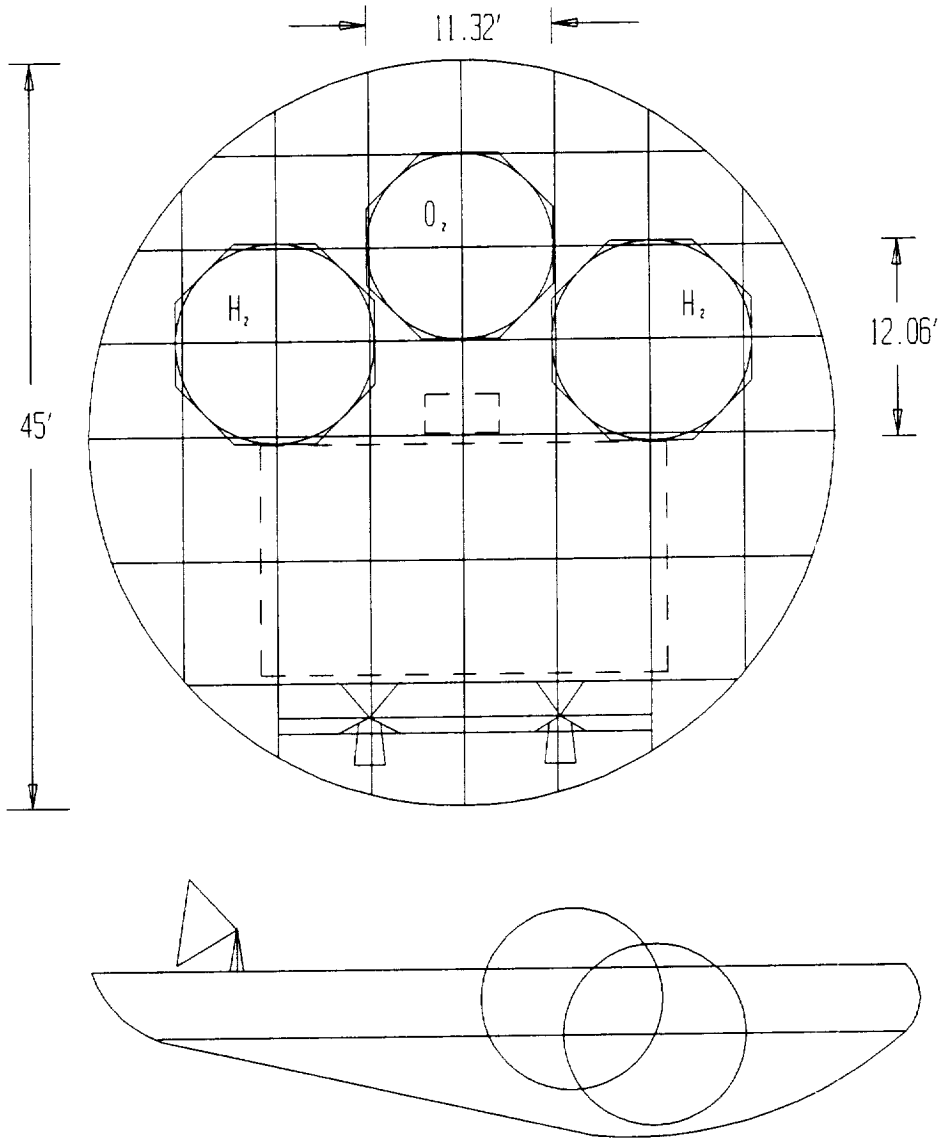

Figure 2.7 Configuration IV

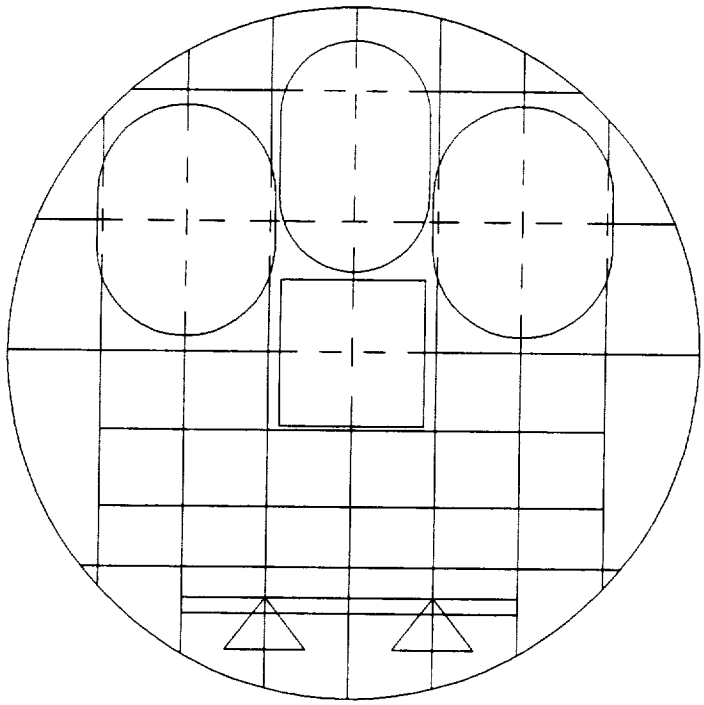

Figure 2.8 Configuration V

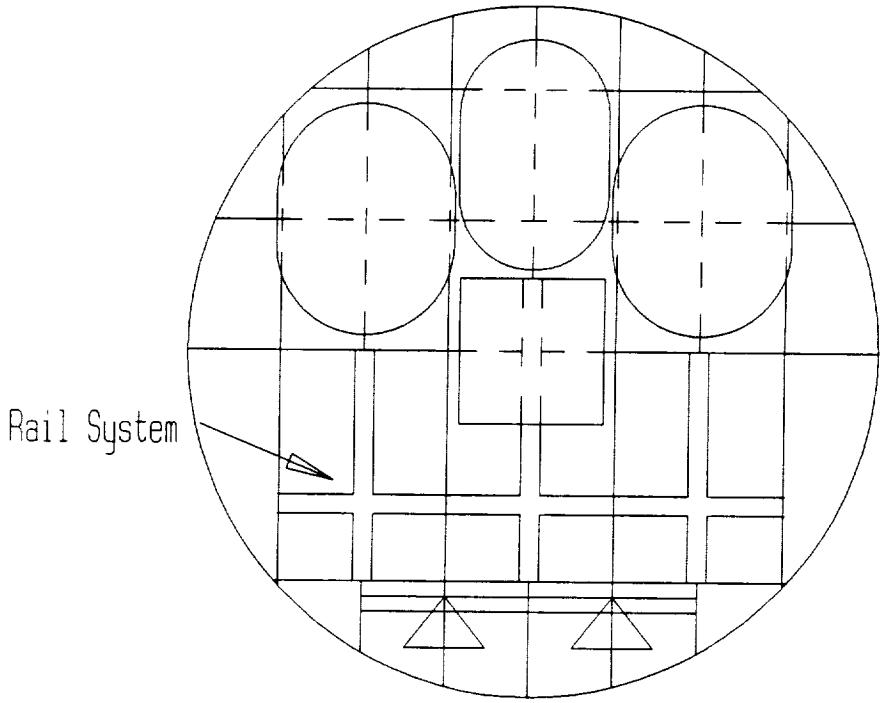

FIGURE 2.9 FINAL CONFIGURATION TOP VIEW

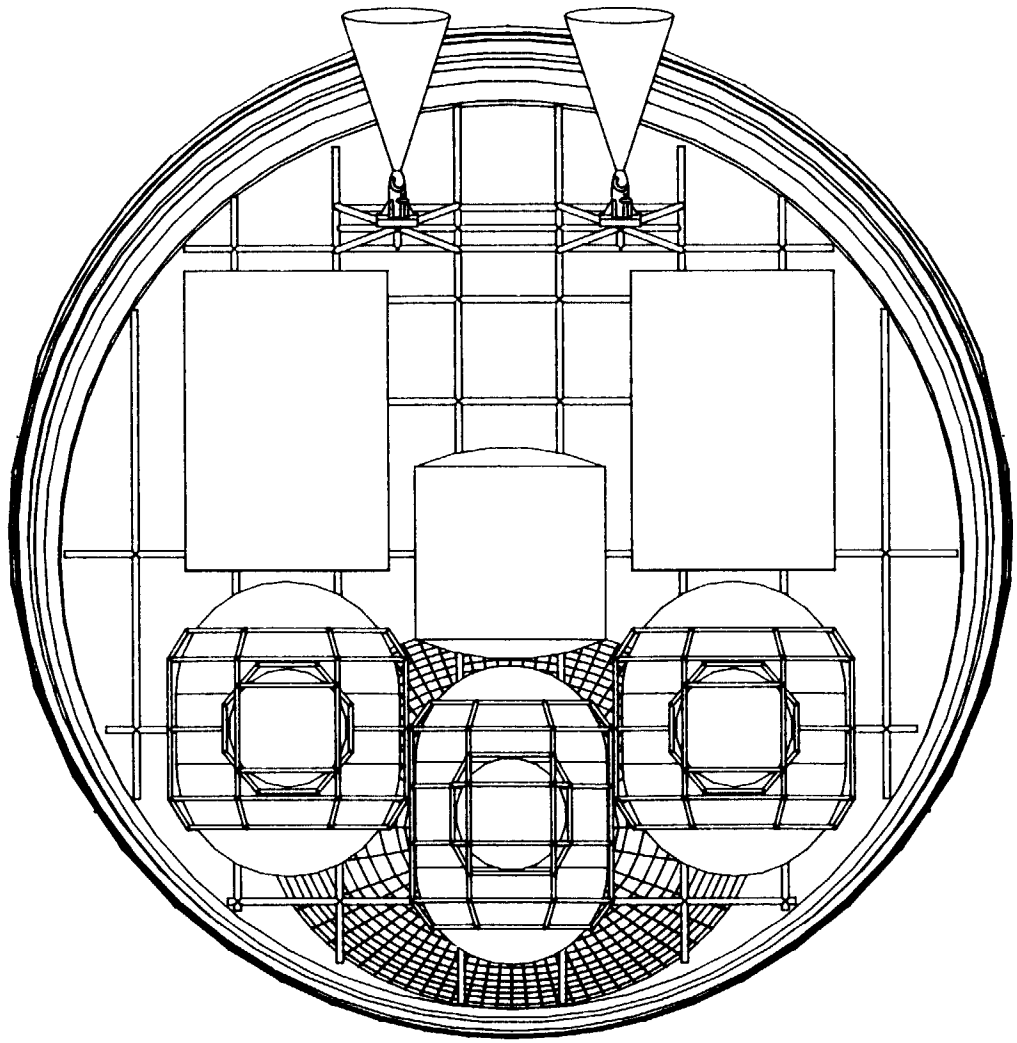

FIGURE 2.10 FINAL CONFIGURATION FRONT VIEW

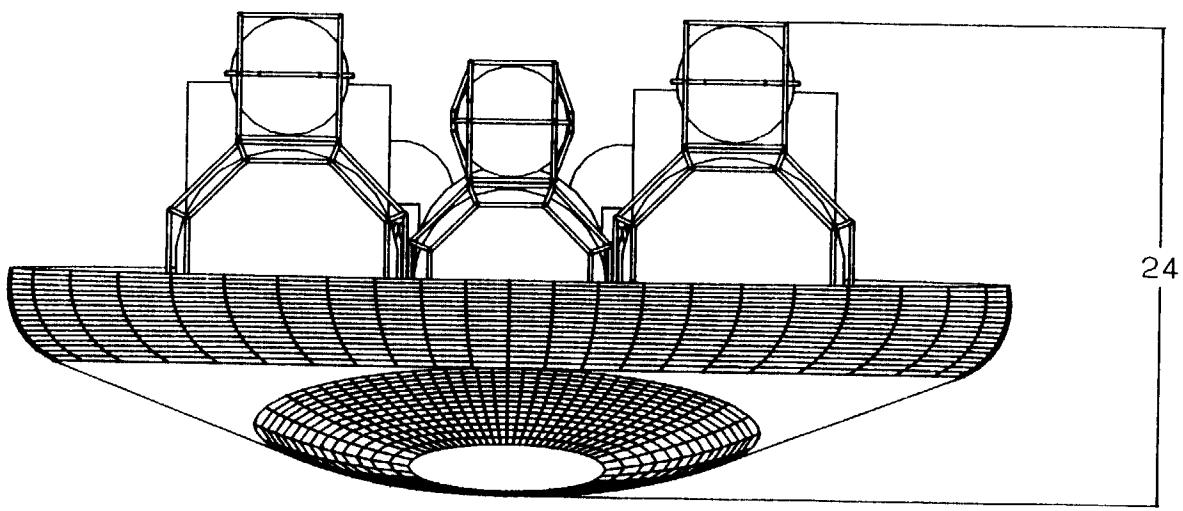


ALL DIMENSIONS IN FEET

FIGURE 2.11 FINAL CONFIGURATION SIDE VIEW

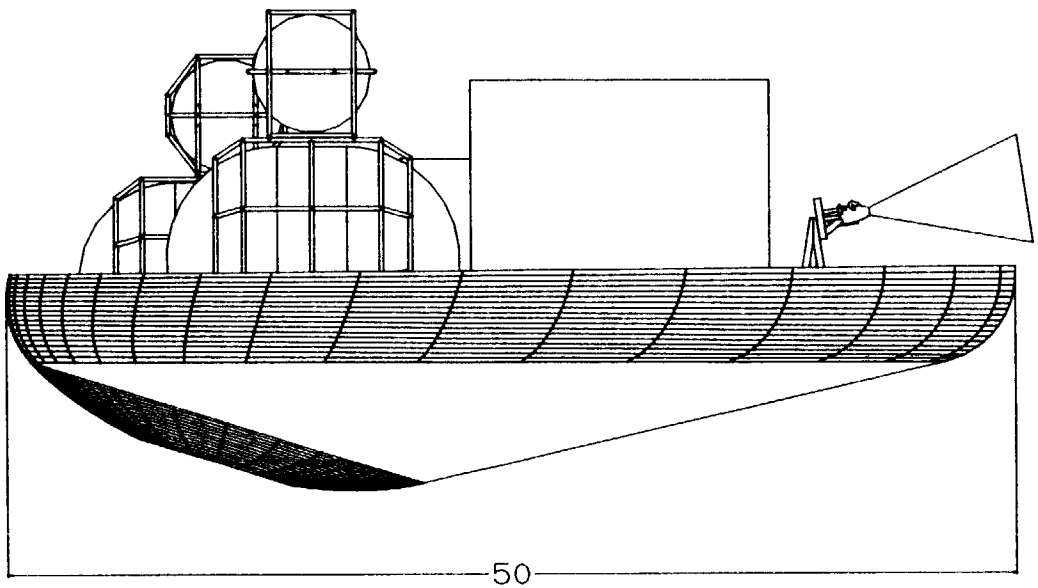


NOTE: MAXIMUM LENGTH SHOWN
BRAKE PLANE DIAMETER = 45
ALL DIMENSIONS IN FEET

accomplished, and truss members were put in its place onto which the payload bays are connected. Flexibility of the orientation of the payload bays is provided as shown in Figure 2.12. The main propellant tanks contain only enough fuel for the 28,000 and 6,000-lbm missions, and spherical auxiliary tanks are added for the 20,000-lbm mission to provide the additional propellant needed. These tanks are removable and can be taken off when not in use. Sufficient protection from heating and wake impingement during aeropass is still provided by a 45' diameter aerobrake. Vehicle axes are defined as follows: the origin is located at the center of the circular base plane, the positive x-axis points away from the engines, the positive z-axis points down through the aerobrake, and the positive y-axis forms a right-handed coordinate system.

Emphasis during the design process was placed on the overall flexibility of the vehicle. The challenging aspect in the design of the final configuration was trying to meet all mission payload requirements while saving as much of the vehicle as possible during the expendable mission. With a variable number of payload bays and the removable aerobrake and crew module, this challenge was met.

Figure 2.12 Payload Configurations

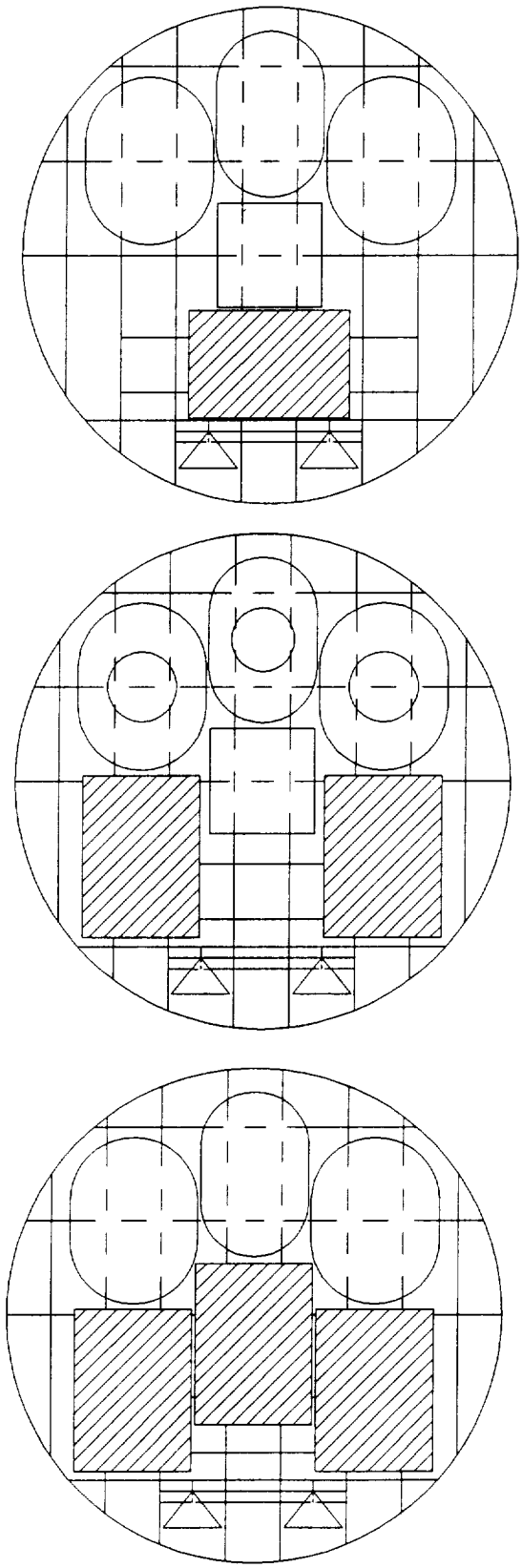

Table 2.1 Vehicle Mass Summary

| Constant Masses | |
|---|---|
| Component | Mass (lbm) |
| Truss Structure (joints, payload support) | 1,095 |
| Engines (2) | 850 |
| Engine Support | 500 |
| RCS (4) | 2,260 |
| Main $LO_2$ Tank | 98 |
| Main $LH_2$ Tank | 471 |
| Main Tank Support | 1,064 |
| Piping | 5 |
| Avionics, Communication, Navigation | 1,379 |
| **Total Constant Masses** | 7,722 |

| Variable Masses | | | |
|---|---|---|---|
| Component | 6,000-lbm Mission | 20,000-lbm Mission | 28,000-lbm Mission |
| Aerobrake | 3,326 | 3,326 | 0 |
| Crew Module | 5,094 | 5,094 | 0 |
| Payload | 6,000 | 20,000 | 28,000 |
| Payload Bay(s) | 1,656 | 3,312 | 4,968 |
| Oxidizer (full) | 46,226 | 61,673 | 61,673 |
| Fuel (full) | 7,704 | 10,279 | 10,279 |
| Auxiliary $LO_2$ Tank (full) | 0 | 6,713 | 0 |
| Auxiliary $LH_2$ Tank (full) | 0 | 1,154 | 0 |
| Auxiliary Tank Support | 0 | 58 | 0 |
| Acquisition Device | 779 | 939 | 779 |
| **Total Variable Masses** | 70,785 | 112,566 | 105,669 |
| **Total Vehicle Mass** | 78,507 | 113,338 | 113,421 |

## 2.3 Stability Analysis

There are two reasons for conducting a longitudinal stability analysis: to determine if the vehicle is statically stable during the aeropass and to determine an allowable region for the vehicle center of gravity. The analysis incorporates the use of the Newtonian Impact Theory (Appendix A) on hypersonic bodies which is applied to a simplified model of the aerobrake (a raked elliptical cone with no nose bluntness). According to Aeroassisted Flight Experiment (AFE) data, the effects of nose bluntness provide no significant changes when compared to data without nose bluntness. Other assumptions of the analysis include zero roll, yaw, and sideslip angles, and a linear relationship between the moment coefficient (Cm) and angle of attack ($\alpha$) between zero and ten degrees.

The derivative of Cm with respect to $\alpha$ ($Cm_\alpha$) is negative, as shown in Figure 2.13, satisfying the requirement for static stability. From the longitudinal analysis, an allowable region for the location of the vehicle center of gravity was determined (Figure 2.14). This region extends below the aerobrake skirt.

The results of the analysis were in good agreement with AFE wind tunnel data with the exception of the trim angle of attack. The AFE trims at 17° and the SPARC trims at 28°. This discrepancy is most likely due to the fact that only the aerobrake, and not the additional mass of the structural components was included in the analysis.

## 2.4 Center of Gravity Analysis

There are two objectives of a center of gravity analysis: to ensure aerodynamic stability and to determine an engine mount angle that will minimize the amount of gimballing required to direct the thrust vector through the center of gravity. The mass of the structure, and thus the center of gravity, changes significantly during the total mission as the propellant is depleted and the payload is delivered. For this reason, the center of gravity was calculated for three different stages of the mission: at launch from LEO, when the vehicle enters the atmosphere, and with the tanks "empty" upon return to LEO. The history of the cg location was plotted, and an appropriate angle for the engine mounts was determined.

The vehicle was split up into components which were estimated as point masses (Table 2.1). For the purpose of calculating the center of gravity, the piping and RCS masses were added to that of the truss structure and concentrated as a point mass at the center of gravity of the aerobrake (determined from CADAM). Also, the tank support and acquisition device masses were added to the tank mass, and the avionics mass was added to the crew module. The mass of fuel in each tank was calculated at each of the desired times from the $\Delta V$ remaining in each mission and was added to the mass of the corresponding tank at each point. It should be noted that the 20,000-lbm mission is the only one which requires and uses the auxiliary tanks, and that they are considered empty at and beyond GEO. Further, the 20,000-lbm payload is dropped off at GEO and therefore subtracted from the total vehicle mass there. For the 28,000-lbm mission, the aerobrake and crew

module are removed but the mass of the avionics, communication and navigation systems remains.

Since the vehicle is symmetric about the x-axis (along the thrust direction), the y-component of the center of gravity is zero. A computer program facilitated repeated calculations of the x and z components of the center of gravity as the mass of the vehicle changed throughout the design process. The results of the program are plotted as a history of the center of gravity for each mission (Figure 2.15). As each mission progresses, the center of gravity shifts toward the engines. The result is approximately a straight line oriented at an 8.4° angle to the vehicle plane. For this reason, the engines are mounted at an 8.4° angle, minimizing the gimballing required to keep the line of thrust through the vehicle's center of gravity.

The center of the engine mounting plate is located 6.8' above the vehicle plane and 6.5' from the farthest edge of the aerobrake providing adequate clearance above the vehicle for gimballing, engine exhaust, and nozzle retraction before aerobraking. The support structure for each engine consists of five members attached to the center of the mounting plate in a pyramid configuration.

## 2.5 Mass Moments of Inertia

A computer program was written to calculate the vehicle mass moments of inertia by transferring the moments of inertia of each vehicle component to the vehicle cg with the parallel axis theorem. Calculations for each mission are made at launch, at aeropass, and upon return to LEO (Appendix B). The largest moments of inertia (28,000-lbm mission at launch) were used to determine the angular turn rate necessary for the design and placement of the RCS thrusters.

Figure 2.13 $C_m$ versus $\alpha$

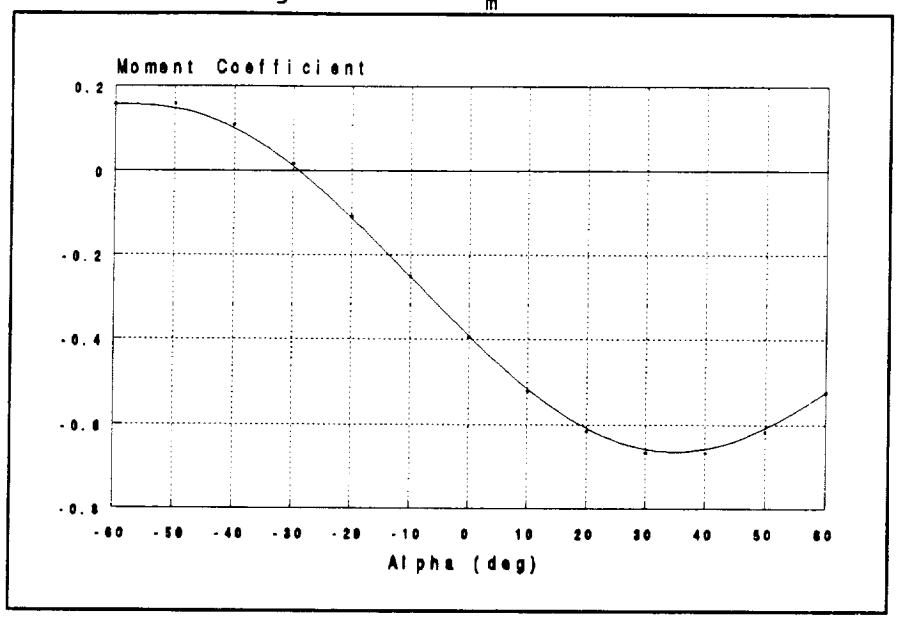


Figure 2.14

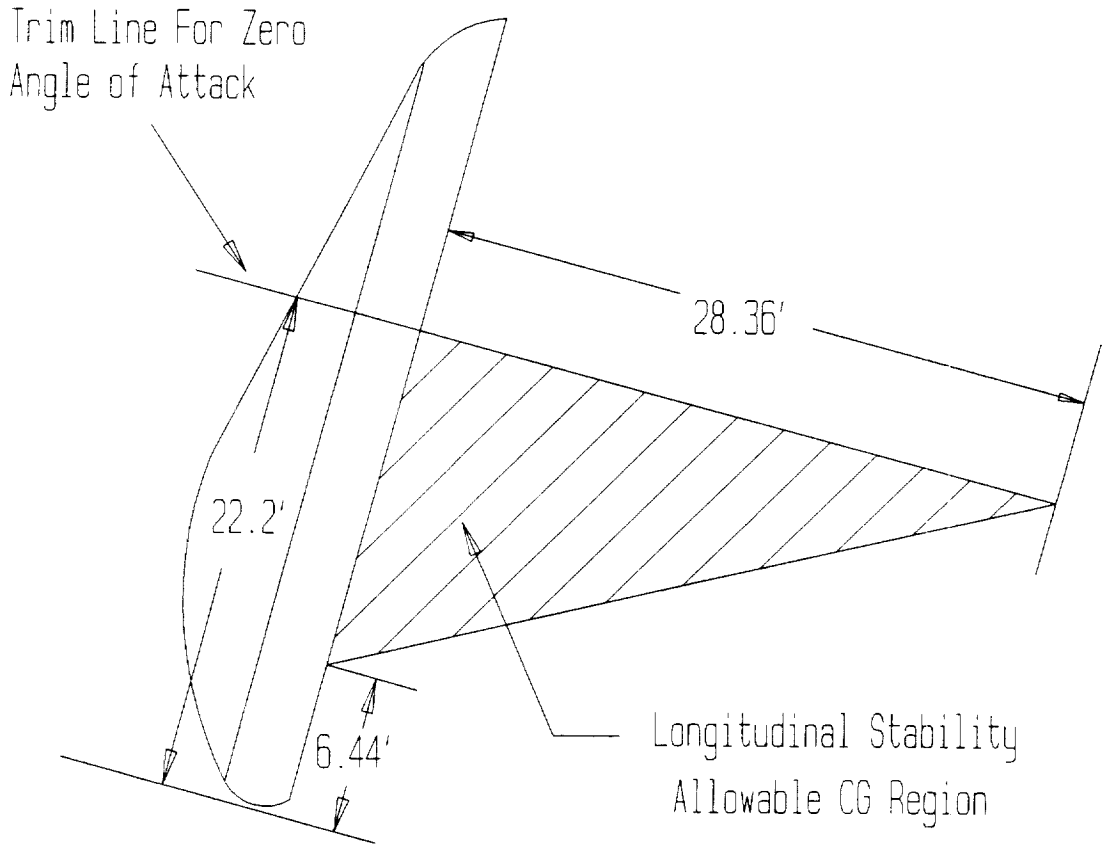

Figure 2.15 CG History and Engine Mount Angle

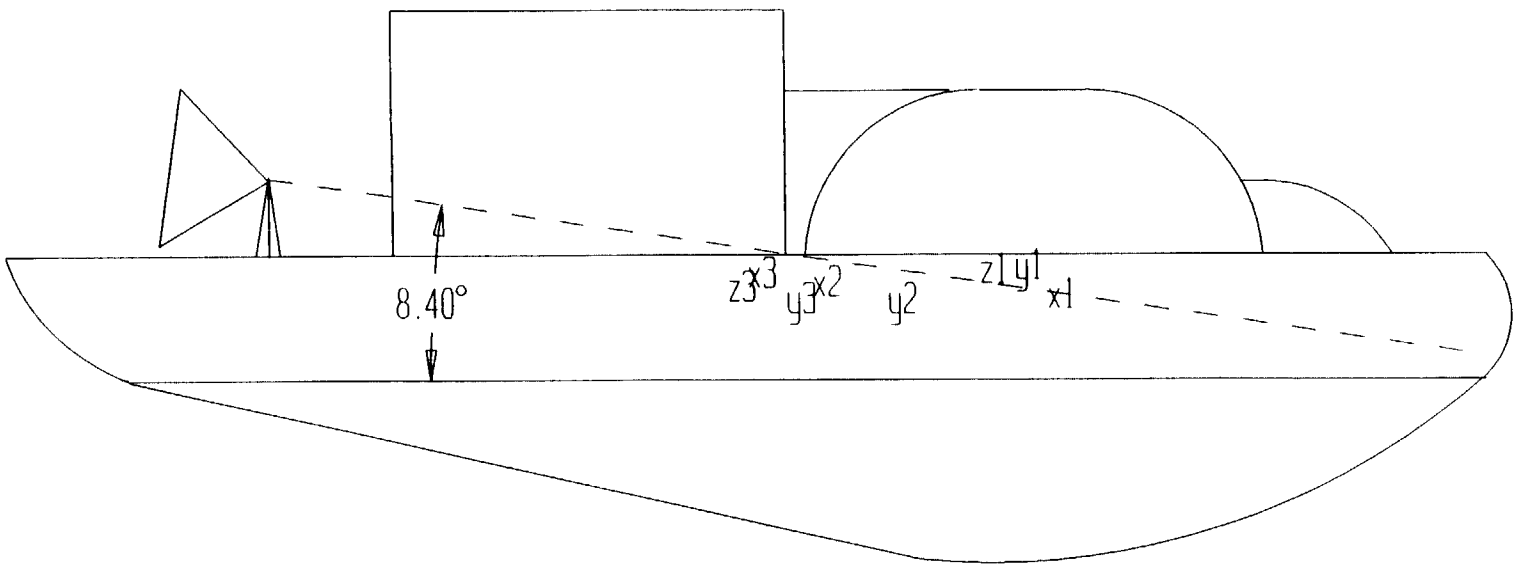


x = 6000# mission  1 = full
y = 20000# mission  2 = at aeropass
z = 28000# mission  3 = empty

# Chapter 3

# Trajectory Analysis

*3.1 Introduction*

*3.2 Orbital Mechanics*

*3.3 Multiple Aeropass Scenarios*

*3.4 Time of Flight*

*3.5 Atmospheric Pass*

## 3.1 Introduction

The purpose of this section is to discuss all aspects of the SPARC flight. Specifically, the mission analysis has been broken down into two different sections: orbital mechanics and the aeropass. The 28,000-lbm expendable mission is not included in this analysis since there is no aeropass.

The $\Delta V$ for an all-propulsive mission was calculated to be 30,700 fps, 36% greater than the aerobraked mission.

## 3.2 Orbital Mechanics

Orbital calculations are based on the following assumptions: GEO has a radius of 22,744 nmi and an inclination of 0°, LEO has a radius of 3,616 nmi and an inclination of 28.5°, the sensible atmosphere reaches an altitude of 400,000', and the aeropass attains a minimum altitude of 262,470'.

The total $\Delta V$ was calculated using a Hohmann transfer, a bi-elliptic maneuver, and a double perigee burn maneuver. The Hohmann transfer resulted in a total $\Delta V$ of 22,570 fps (Table 3.1), as did the double perigee burn maneuver. Since the time of flight for the double perigee burn is longer, it was decided that this maneuver would only be used in a situation that called for more time between LEO and GEO. Total $\Delta V$ calculations reveal that the bi-elliptic maneuver is only preferable for transfers to orbits with a radius of greater than 55,103 nmi, therefore the Hohmann transfer is used.

Figure 3.1 Flight Summary

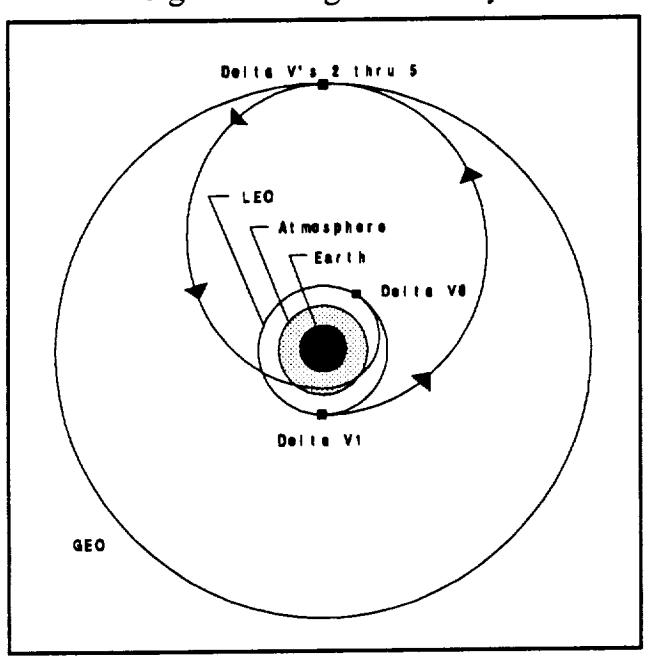




PAGE 26 INTENTIONALLY BLANK

PRECEDING PAGE BLANK NOT FILMED

Table 3.1 Flight Summary

| Impulse | Segment | Time (hr) | Δ V (fps) |
|---|---|---|---|
| 1 | Decircularization at LEO | 0.0 | 7,929 |
| | LEO to GEO | 5.3 | 0 |
| 2 | Plane Change (28.5°) | 0.0 | 2,610 |
| 3 | Circularization at GEO | 0.0 | 4,805 |
| | Minimum Stay at GEO | 0.4 | 0 |
| 4 | Decircularization at GEO | 0.0 | 4,874 |
| 5 | Plane Change (23.82°) | 0.0 | 2,159 |
| | GEO to Atmospheric Entry | 5.2 | 0 |
| | Atmospheric Entry to Atmospheric Exit | 3.9 min | 0 |
| | Atmospheric Exit to LEO | 4.6 min | 0 |
| 6 | Circularization at LEO | 0.0 | 193 |
| **Total** | | 11.0 | 22,570 |
| **All Propulsive: Δ V = 30,700 (fps)** | | | |

## 3.3 Multiple Aeropass Scenarios

Multiple aeropass scenarios (Figure 3.2 and 3.3) are also considered as a means of decreasing the maximum heat flux encountered during any one atmospheric pass. The heating rate for each pass (Table 3.2) is determined with the engineering correlation equation for a sphere in terms of the aerobrake nose radius, free stream velocity, and free stream density (Scott, 1984). The apogees used for the first and second passes are 7,500 and 5,050 nmi, respectively (Walburg, 1982).

Multiple pass missions do not travel as low into the atmosphere as single pass missions do, resulting in lower heating rates and lower accelerations. They are also less sensitive to off-nominal conditions which is beneficial in correcting flight path errors or providing extra flight time when necessary. However, multiple aeropasses do increase the total heat load on the vehicle. Although the heating rates for the single pass case exceed the heating rate limits of existing thermal protection systems, a single aeropass scenario is feasible considering future advances in thermal protection systems.

To find an expression for the maximum effective plane change during the aeromaneuver in terms of $(L/D)_{max}$ and entrance and exit velocities, the equations of motion are integrated and solved using Chapman's variables for altitude, speed, and arc length. This yields a maximum

Figure 3.2 2-Pass Senario

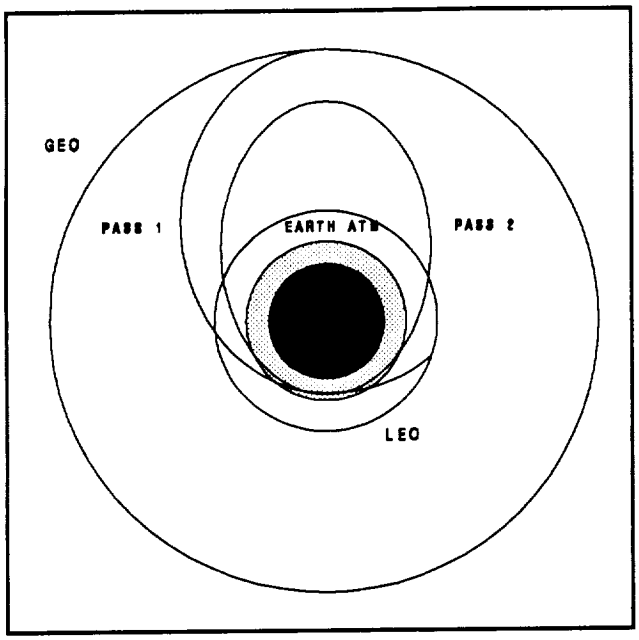


Figure 3.3 3-Pass Senario

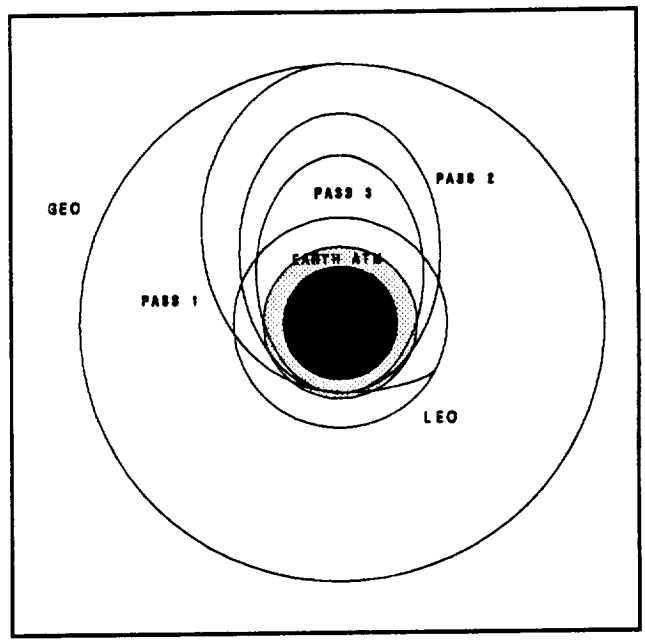


aerodynamic plane change of 4.68° for the vehicle configuration leaving a propulsive plane change of 23.82°.

### 3.4 Time of Flight

The time of flight calculations depend on a number of factors: the synodic period, the time it takes for the geometry between the Space Station and the GeoShack to repeat, the radius of the orbit traversed, and the number of aeropasses incurred during the mission. As expected, the time of the mission greatly increases with the addition of multiple aeropasses. The required relative geometry between LEO and GEO is shown on Figure 3.4. When leaving LEO, the GeoShack must be 100°3' (counter clockwise) away, and when leaving GEO, the Space Station must be 90°5' (counter clockwise) away. The time of flight for the entire mission, with one aeropass and an atmospheric perigee of 262,974', is 10.6 hr. The delay time, or synodic period, which is 1.6 hr, and any time spent at the GeoShack before the return flight, is not included in the time of flight.

Table 3.2 Multiple Aeropass Scenarios

| 6,000lbm Mission | | | | | | |
|---|---|---|---|---|---|---|
| | **Single Pass Scenario** | **2 Pass Scenario** | | **3 Pass Scenario** | | |
| | Pass 1 | Pass 1 | Pass 2 | Pass 1 | Pass 2 | Pass 3 |
| Perigee Altitude (ft) | 265028 | 270771 | 271842 | 270771 | 272137 | 286804 |
| Maximum Acceleration (g's) | -.03141 | -.02279 | -0.2144 | -0.2279 | -0.2109 | -0.0947 |
| Heat Load (Btu/ft$^2$) | 1131.76 | 963.35 | 934.96 | 963.35 | 927.29 | 612.57 |
| Time of Flight (hr) | 0.0305 | 6.6312 | 1.4188 | 6.6312 | 1.4188 | 0.9722 |

| 20,000lbm Mission | | | | | | |
|---|---|---|---|---|---|---|
| | **Single Pass Scenario** | **2 Pass Scenario** | | **3 Pass Scenario** | | |
| | Pass 1 | Pass 1 | Pass 2 | Pass 1 | Pass 2 | Pass 3 |
| Perigee Altitude (ft) | 263739 | 272055 | 273125 | 272055 | 273420 | 288078 |
| Maximum Acceleration (g's) | -0.3616 | -0.2275 | -0.2129 | -0.2275 | -0.2104 | -0.0945 |
| Heat Load (Btu/ft$^2$) | 1172.55 | 929.18 | 901.77 | 929.18 | 894.31 | 590.73 |
| Time of Flight (hr) | 0.0305 | 6.6312 | 1.4189 | 6.6312 | 1.4189 | 0.9722 |

Figure 3.4 Relative Geometry

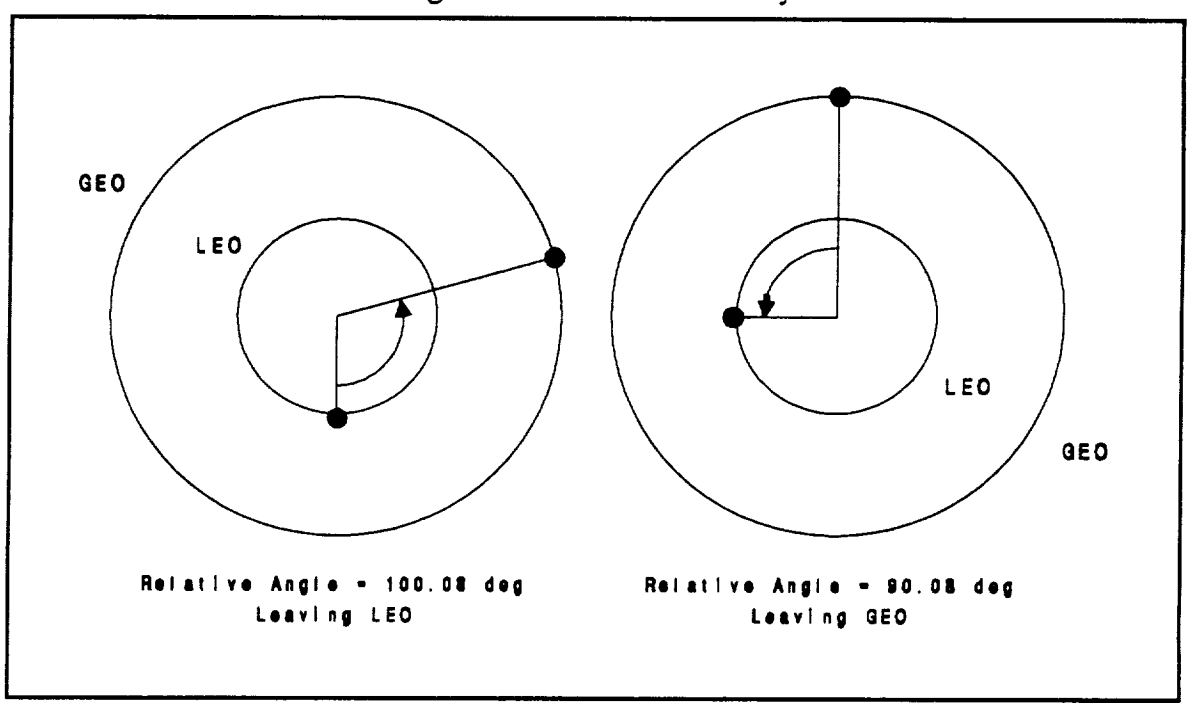

### 3.5 Atmospheric Pass

In the preliminary design of the SPARC configuration, it is desirable to have a simple analytical method for characterizing the aerothermodynamic regime at skip trajectory perigee as a function of vehicle lift to drag ratio (L/D) and ballistic coefficient ($m/C_DA$). An approximate perigee solution was derived from the generalized equations of motion and uses the following assumptions: a locally exponential atmosphere, planar motion, small flight path angles ($\phi < 10°$), a constant ballistic coefficient throughout the atmospheric pass, equal atmospheric entry and exit altitudes, and a constant flight path angle from atmospheric entry to perigee and from perigee to atmospheric exit. This perigee solution yields excellent results when compared with numerically simulated three degree of freedom solutions (Desautel, 1984).

The approximate perigee solution (Figure 3.5) provides the following equations:

$$\left(\frac{1+k\phi_i\left(\frac{L}{D}\right)_i}{15k\phi_i} - \frac{1+k\phi_f\left(\frac{L}{D}\right)_f}{15k\phi_f}\right)z_p = 2\ln\left(\frac{V_f}{V_i}\right)$$

$$\ln\left(\frac{V_p}{V_i}\right) = \frac{1}{2}\left(\frac{1 + k\phi_i\left(\frac{L}{D}\right)_i}{15k\phi_i}\right)z_p$$

$$z = \frac{H}{2}\left(\frac{C_DA}{m}\right)\sqrt{\frac{r}{H}}\,\rho$$

| | |
|---|---|
| H = atmospheric scaling factor | Z = Vinh Zeta Function |
| k = angle weighting factor | i = initial (entry) condition |
| r = radial distance | f = final (exit) condition |
| $\rho$ = density | p = perigee condition |
| V = velocity | |

A value of k = 0.35 was found to give the best results when compared to numerically simulated solutions. From these equations, perigee density (altitude) and velocity can be determined. This altitude is plotted versus conic perigee which is a fictitious perigee point through which a drag-free (no atmosphere) trajectory would pass (Figure 3.6).

Given L/D, the ballistic coefficient, stagnation point nose radius ($R_N$), and perigee density and velocity, the stagnation point heating rates can be determined from the following equations (Scott et al, 1984):

$$\dot{q}_{max} = 7.3\sqrt{R_N}\left(\frac{m}{C_DA}\right)^{0.467}\left(\frac{L}{D}\right)^{-0.242}$$

$$q = 18300\sqrt{\frac{\rho}{R_N}}\left(\frac{V}{10^4}\right)^{3.05}$$

A summary of the values obtained from this analytic perigee solution is presented in Table 3.3. Further analysis shows that as conic perigee altitude decreases, total $\Delta V$ budget and stagnation point heating rate increase.

Figure 3.5 Flowchart

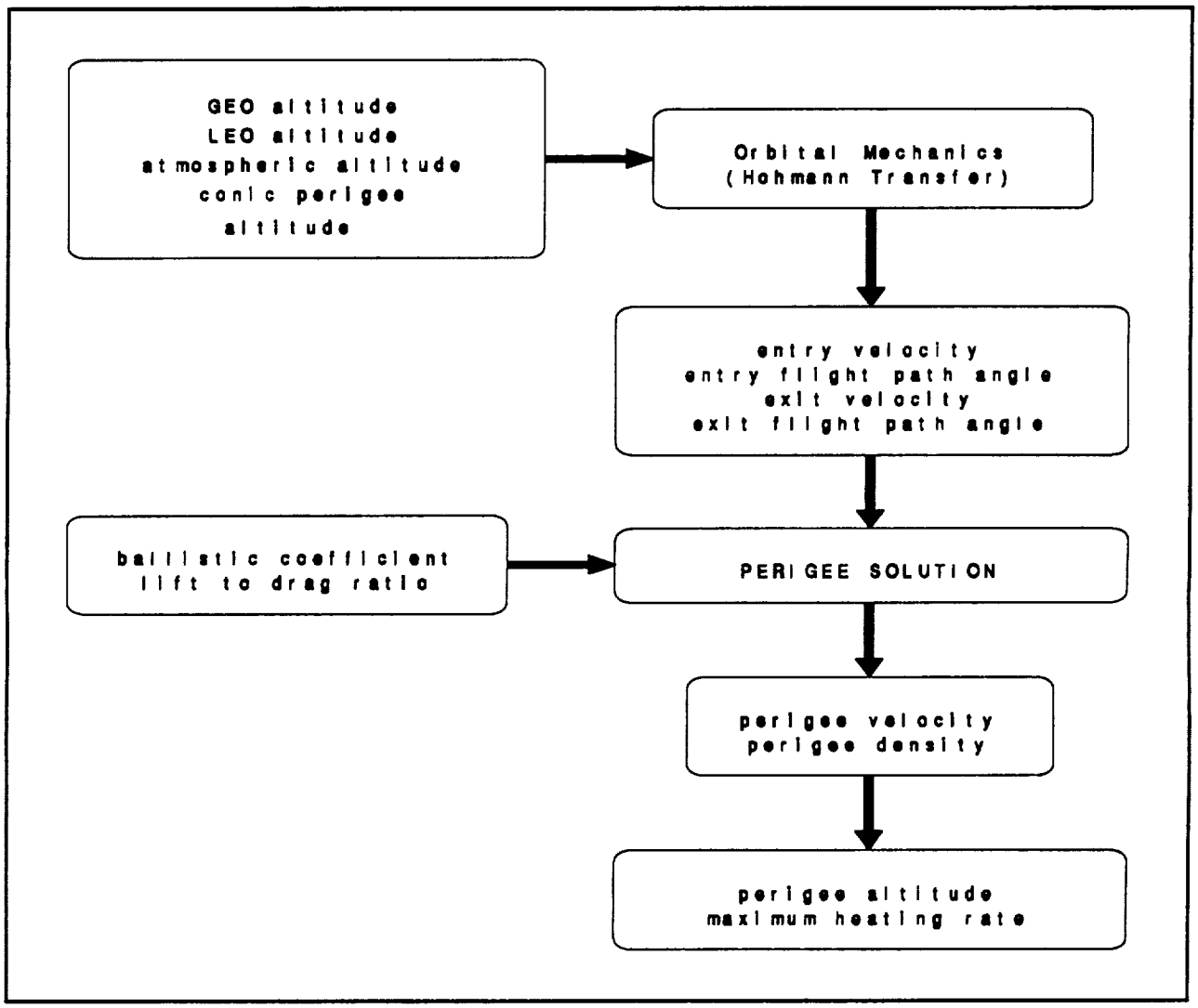


To study the effects of atmospheric drag on the trajectory, the Fortran program, DRAG, was created (Appendix C). DRAG is designed to adjust the energy of the transfer orbit from GEO to LEO by calculating the amount of energy removed due to the drag encountered in the Earth's atmosphere.

Table 3.3 Analytic Perigee Solution Summary

| | 6,000lbm Mission | | | 20,000lbm Mission | | | |
|---|---|---|---|---|---|---|---|
| Mass Entering Atmosphere (lbm) | 29,176 | | | 27,150 | | | |
| Initial Velocity (fps) | 33,811 | | | 33,811 | | | |
| Final Velocity (fps) | 25,885 | | | 25,885 | | | |
| Perigee Velocity (fps) | 32,414 | | | 32,414 | | | |
| Conic Perigee Altitude (ft) | 397,000 | 398,000 | 399,000 | 396,000 | 397,000 | 398,000 | 399,000 |
| Initial Flight Path Angle (rad) | -0.6248 | -0.5101 | -0.3607 | -0.7215 | -0.6248 | -0.5101 | -0.3607 |
| Final Flight Path Angle (rad) | 0.1174 | 0.09585 | 0.06778 | 0.13557 | 0.1174 | 0.09585 | 0.06778 |
| Perigee Altitude (ft) | 265,028 | 268,656 | 274,840 | 263,739 | 266,316 | 269,942 | 276,122 |

The drag on the vehicle is:

$$Drag = \frac{1}{2} C_D \rho V^2 A = F = m a$$

Drag, by definition, will act in a direction opposite that of the vehicle velocity relative to the atmosphere, thus, the perturbative acceleration due to drag is:

$$a = -0.5 \left( \frac{C_D A}{m} \right) \rho V^2$$

$C_D$ = drag coefficient
A = aerobrake planform area
m = vehicle mass entering atmosphere

The atmospheric density, which is dependent on the vehicle altitude (h), is approximated by:

$$\rho = 0.075 \exp(-7.4E\text{-}6\ h^{1.15})$$

During the aeropass, the true anomaly entering the atmosphere is incremented in one degree intervals; for each interval, the force due to atmospheric drag is calculated. The distance travelled along the orbit during one interval is calculated using the average radius over the interval which is approximated assuming the shape of the path to be an arc of a circle.
The change in orbital energy due to atmospheric drag is calculated by:

$$\Delta E = \left( \frac{F}{m} \right) distance = \left( \frac{drag}{unit\ mass} \right) distance$$

The total energy of the orbital transfer during the aeropass is adjusted by adding the change in energy to the previous orbital energy. While keeping the perigee radius ($R_p$) of the transfer orbit constant, the apogee radius ($R_a$) is decreased to satisfy

$$E = \frac{-\mu}{R_a + R_p}$$

$\mu$ = earth gravitational parameter

As the apogee of the transfer orbit is lowered, the velocity of the vehicle near perigee is decreased. As drag is encountered, the vehicle velocity and flight path angle are adjusted in order to achieve the desired perigee altitude.

The true anomaly is incremented until the vehicle exits the atmosphere. The time of flight during one interval is calculated with:

$$TOF = \sqrt{\frac{(a_{i+1})^3}{\mu}} \left[(E_{i+1} - e \sin E_{i+1}) - (E_i - e \sin E_i)\right]$$

a = semi-major axis
e = eccentricity
E = eccentric anomaly

The total time of flight during the aeropass is obtained by summing the time of flights for each interval. The velocity, altitude, heating rate, and accumulated heat are also calculated for each interval.

Though this model simulates the effects of atmospheric drag on the trajectory of the vehicle, it does not take into account the effects of the Earth's oblateness and shocks. These will further alter the total orbital energy and velocity of the vehicle during the aeropass. Also, radiative heating was not considered in the calculations of heating rate and accumulated heat.

To determine the changes in velocity, acceleration, heating, and altitude with respect to time, seven perigee altitudes above 262,467' were chosen from the analytic perigee calculations for input into the DRAG program. All calculations are based on a vehicle mass entering the atmosphere of 291,751 lbm for the 6,000-lbm mission and 271,491 lbm for the 20,000-lbm mission. The program results are shown graphically in Figures 3.7 through 3.16. Critical values are given in Table 3.4.

Figure 3.6 Perigee Altitude vs. Conic Perigee Altitude

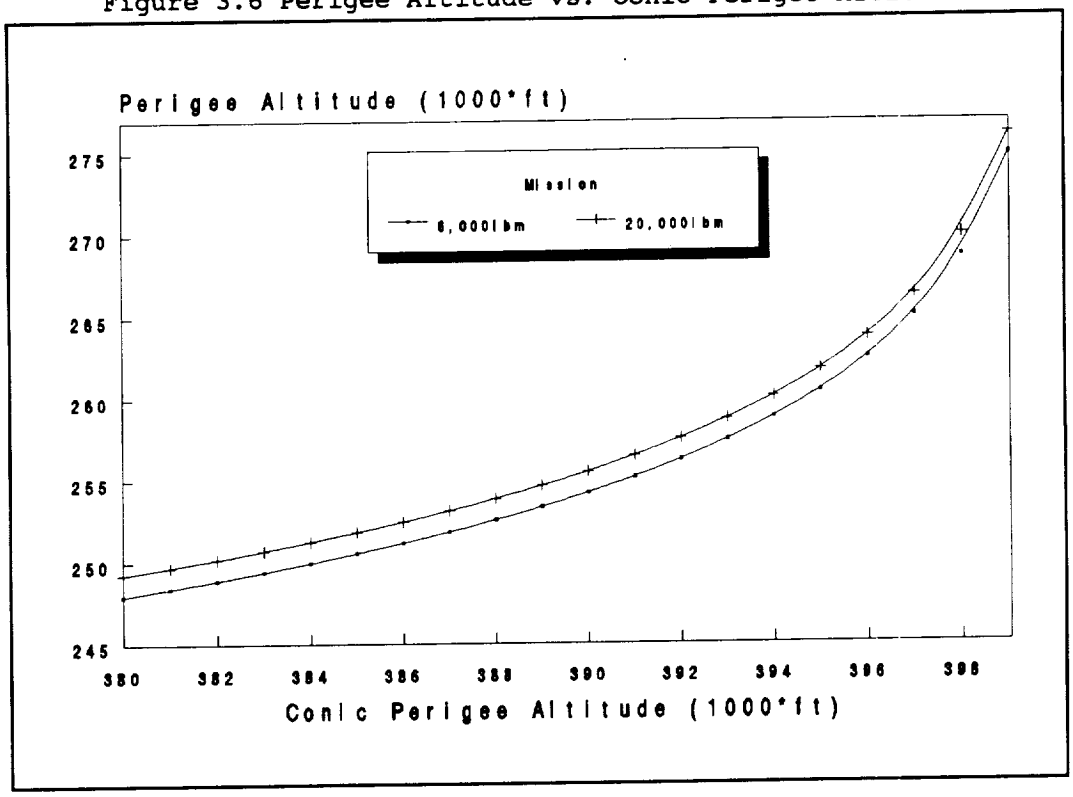


Figure 3.7 Total Heat versus Time (20,000-lbm Mission)

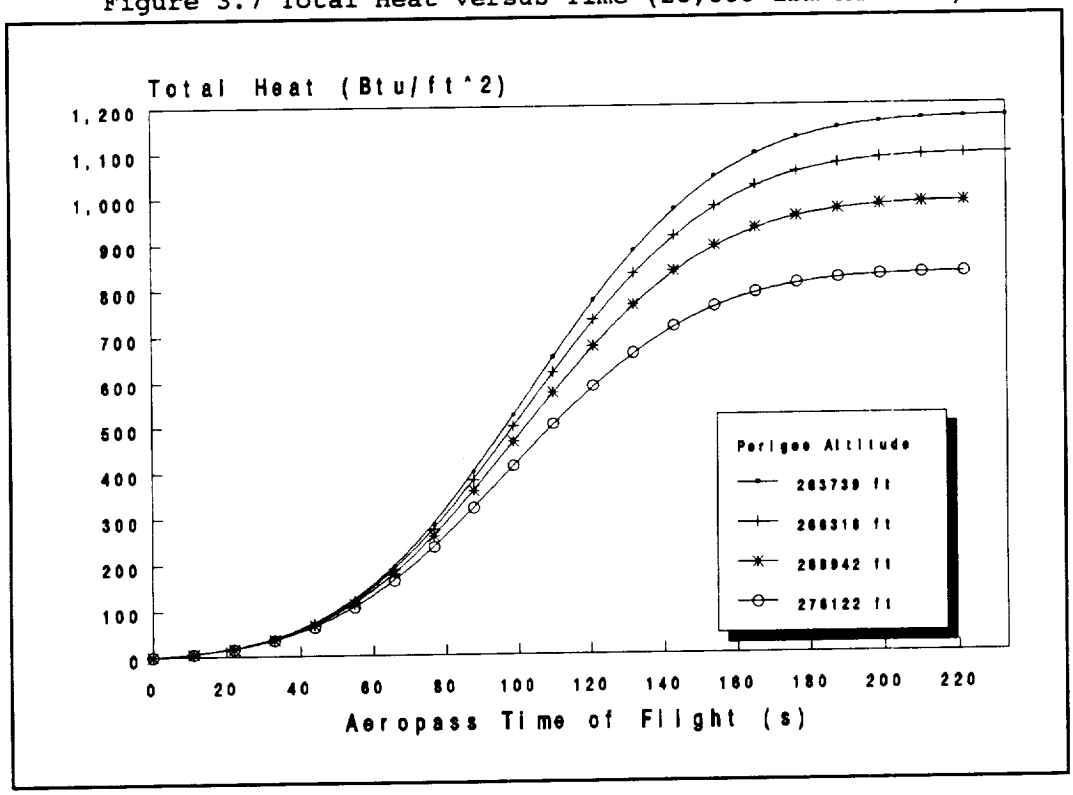

Figure 3.8 Velocity versus Time (20,000-lbm mission)

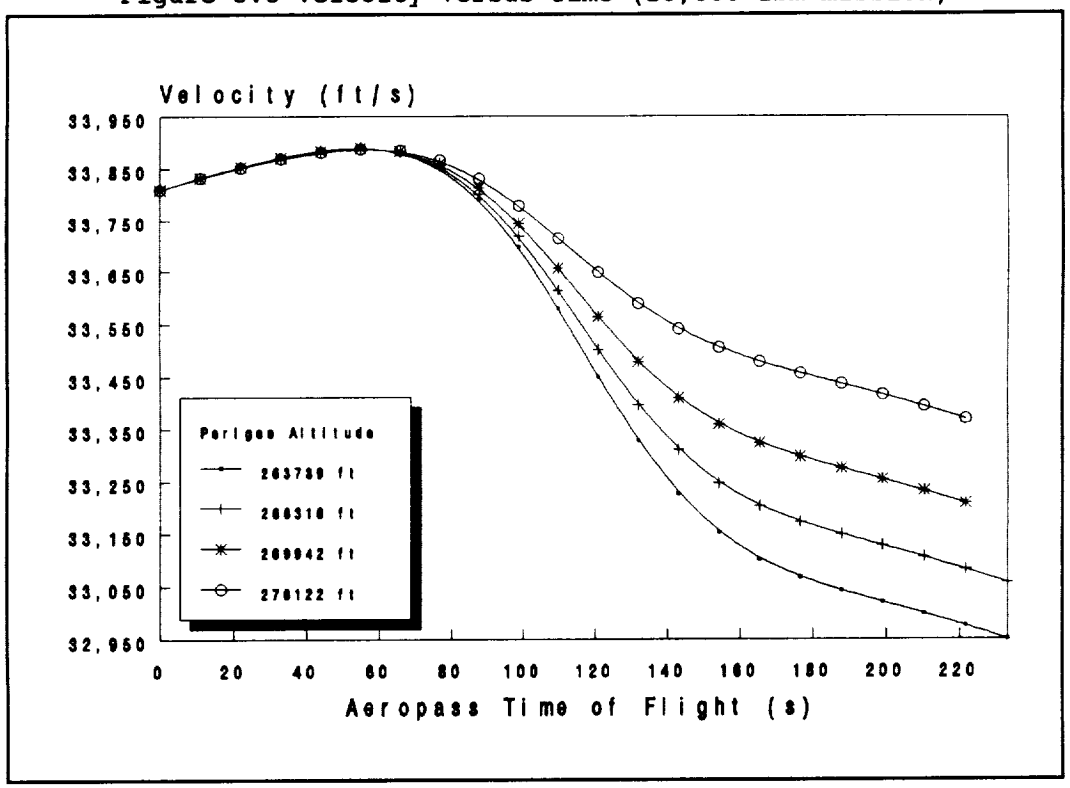


Figure 3.9 Altitude versus Time (20,000-lbm mission)

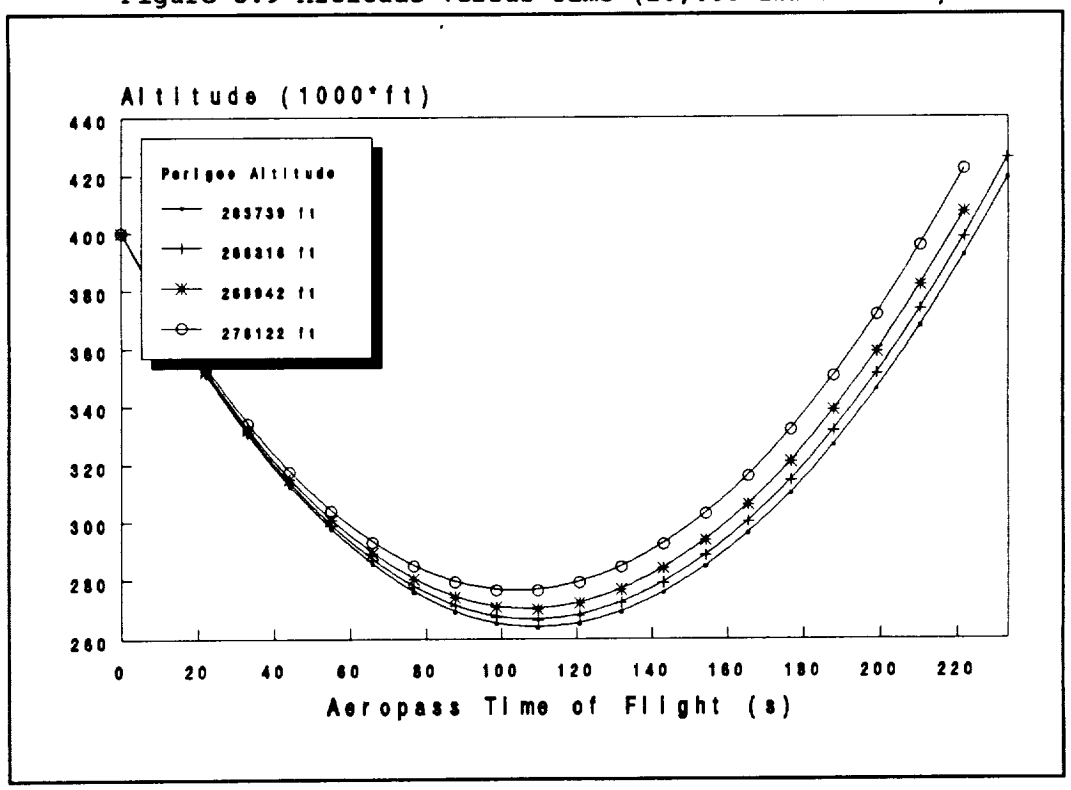

Figure 3.10 Deceleration versus Time (20,000-lbm Mission)

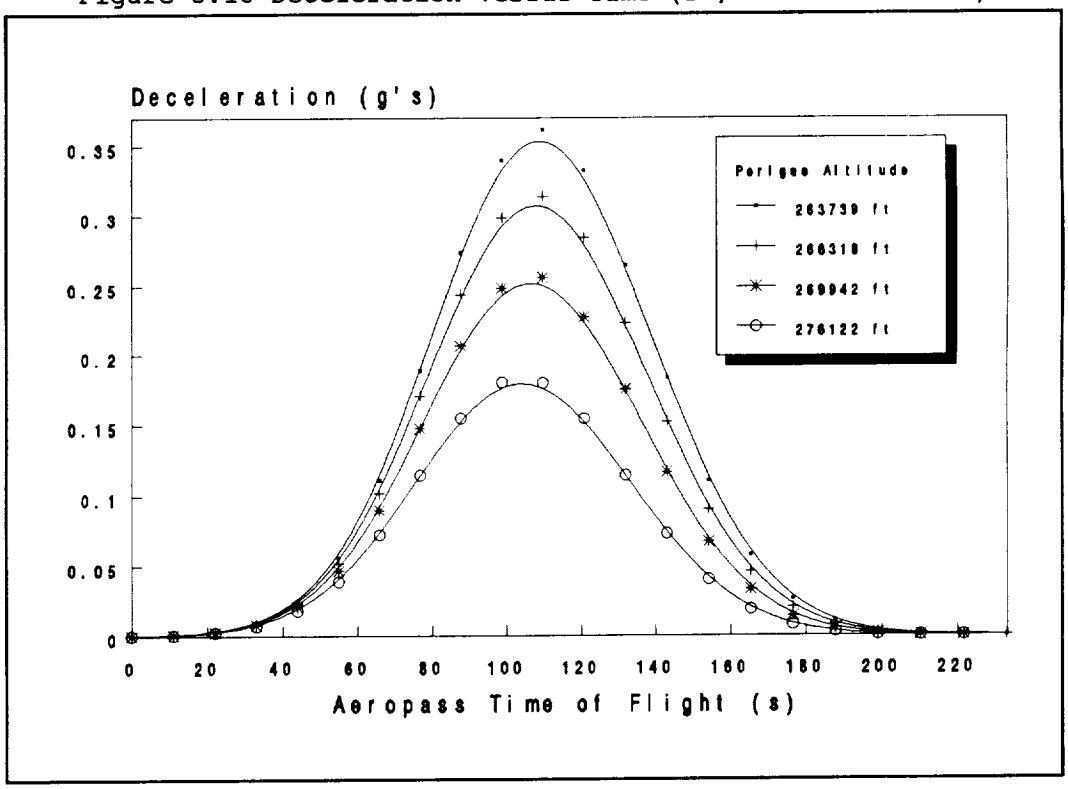


Figure 3.11 Heating Rate versus Time (20,000-lbm Mission)

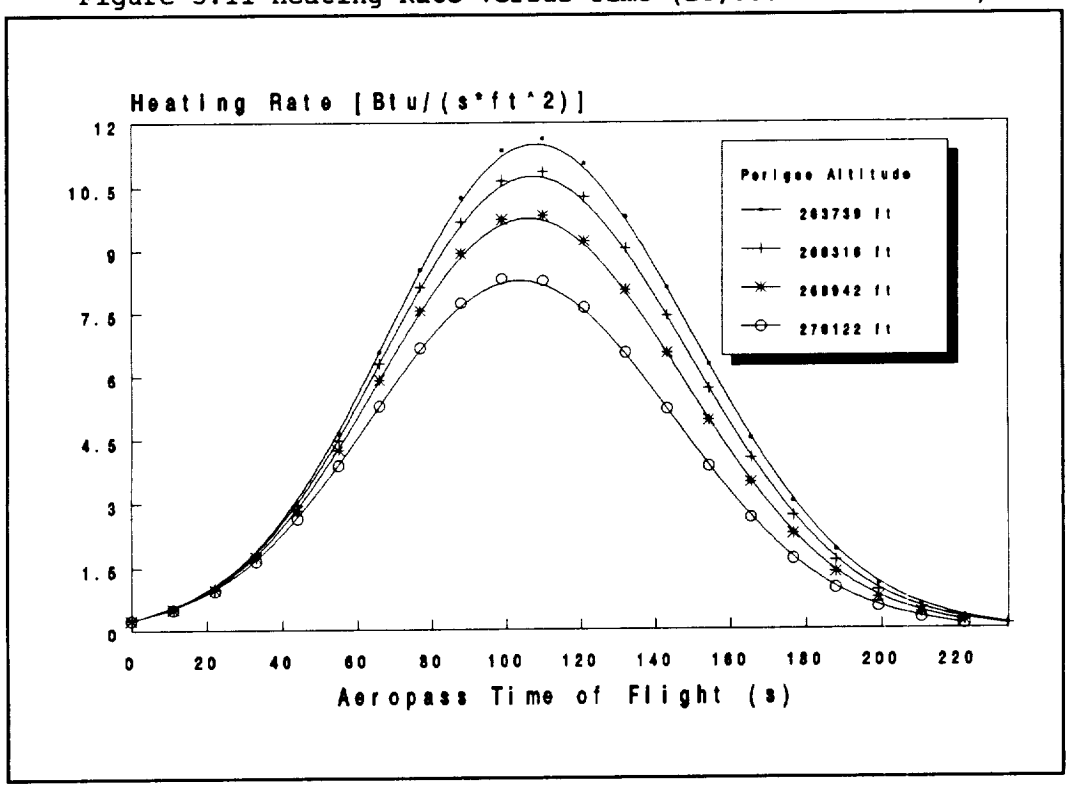

Figure 3.12 Total Heat versus Time (6,000-lbm Mission)

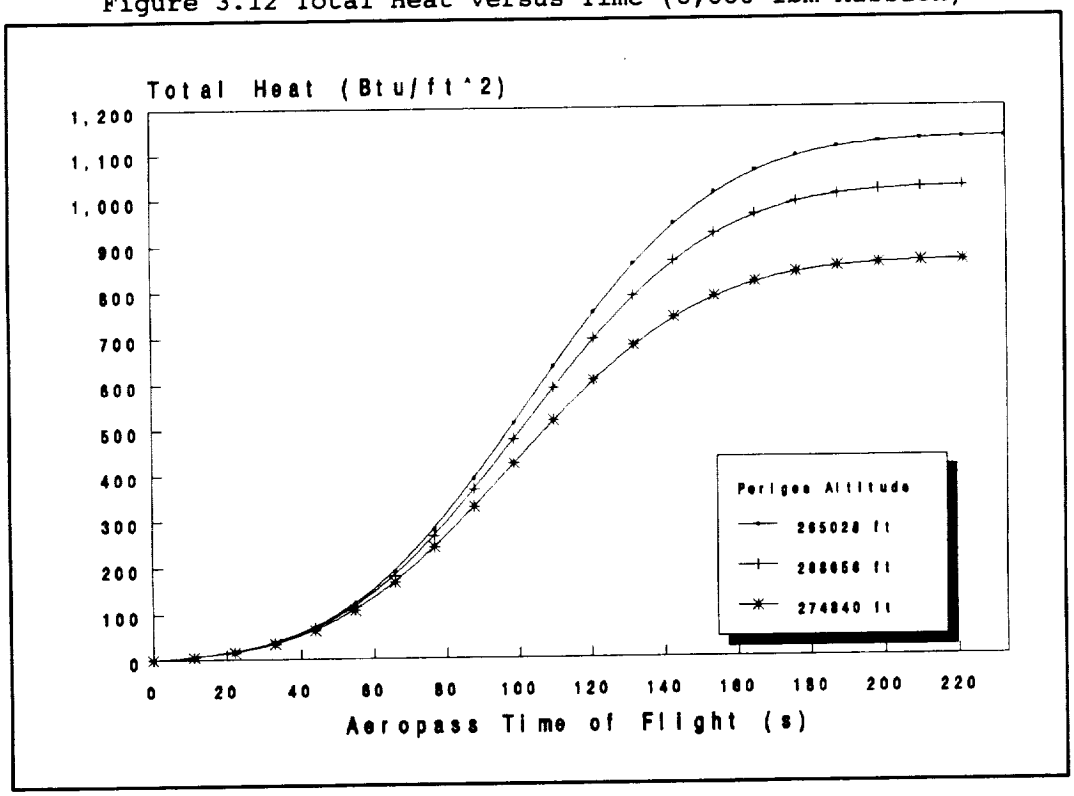


Figure 3.13 Velocity versus Time (6,000-lbm Mission)

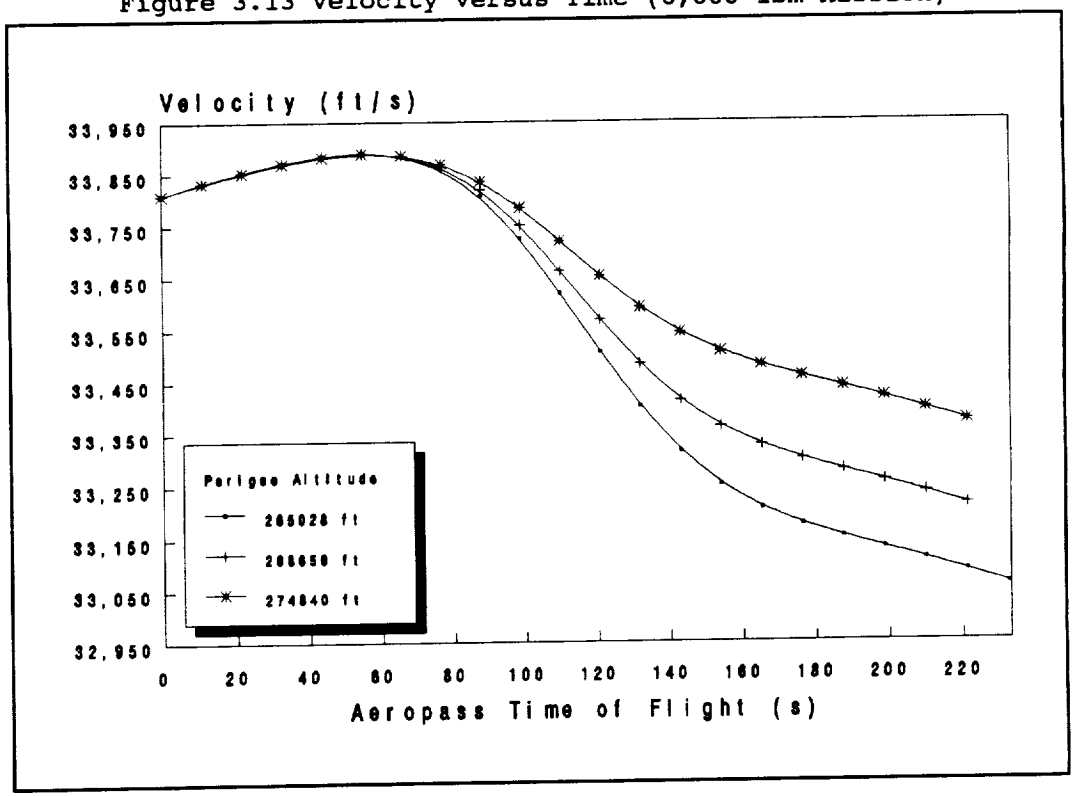

Figure 3.14 Altitude versus Time (6,000-lbm Mission)

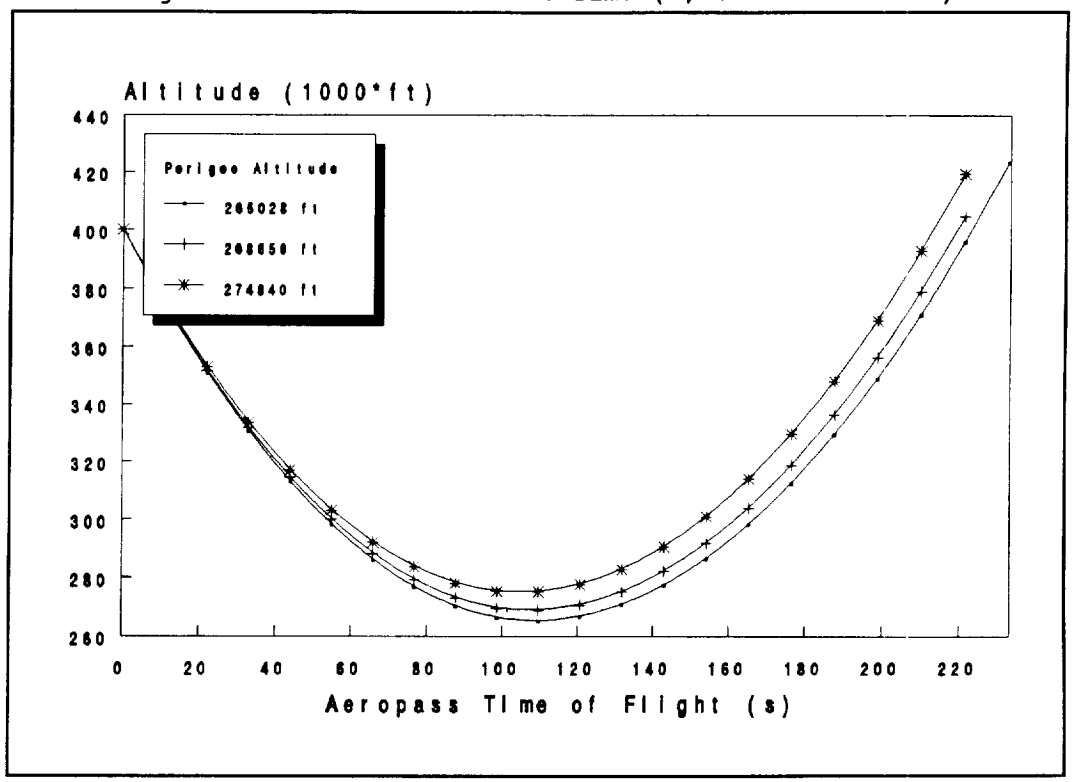


Figure 3.15 Deceleration versus Time (6,000-lbm Mission)

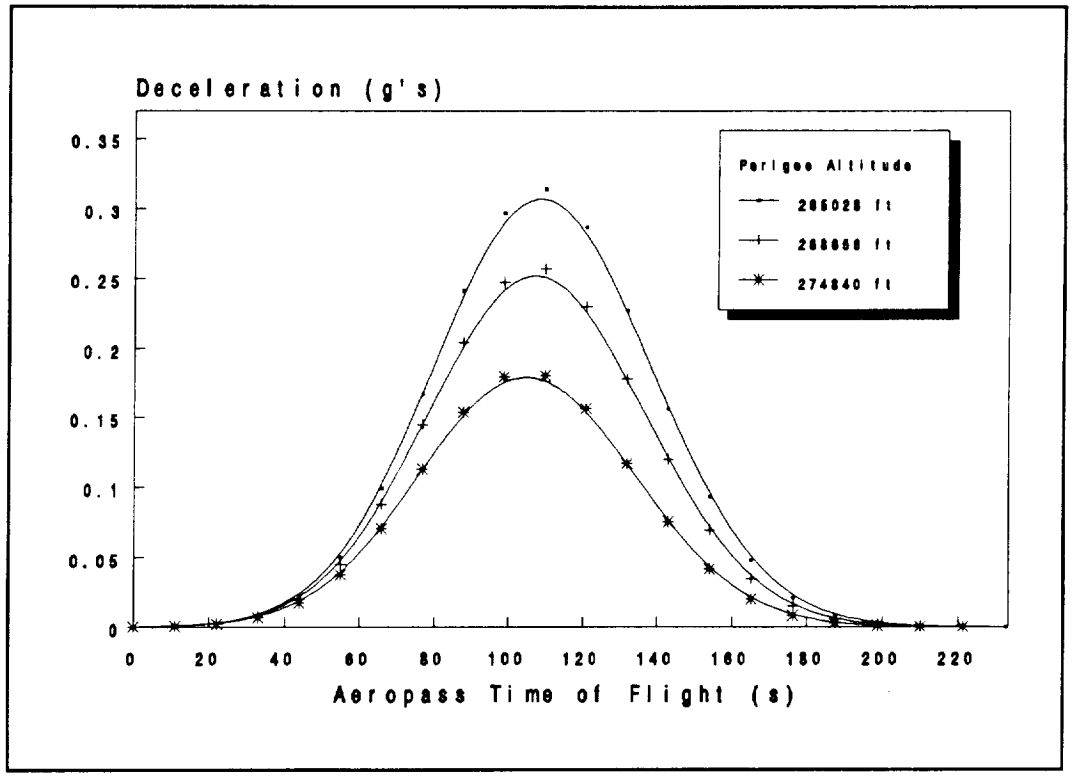

Figure 3.16 Heating Rate versus Time (6,000-lbm Mission)

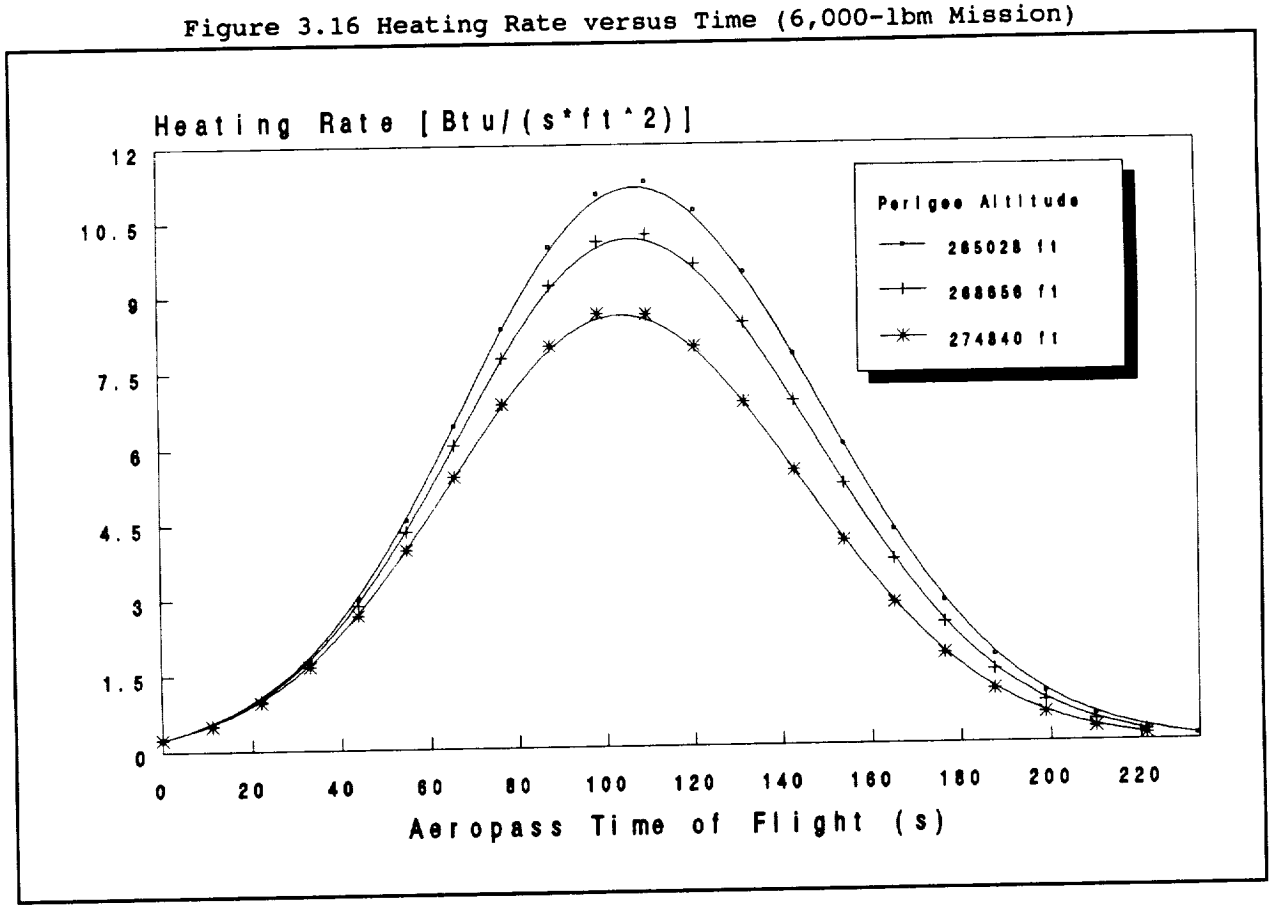


Table 3.4 Critical Values

| Maximum | 6,000-lbm Mission | 20,000-lbm Mission |
|---|---|---|
| Acceleration (g's) | -0.3141 | -0.3617 |
| Heating Rate [Btu/($ft^2$•s)] | 11.26 | 11.63 |
| Total Accumulated Heat (Btu/$ft^2$) | 1,132 | 1,173 |

# Chapter 4

# The Aerobrake

*4.1 Introduction*

*4.2 Geometry and Aerodynamics*

*4.3 Structure and Materials*

*4.4 Thermal Protection System*

## 4.1 Introduction

The possibilities and configurations available in the design of an aerobrake seem limitless; however, adherence to a few primary constraints leads the design toward a sturdy, lightweight, reusable aerobrake that is stable on ascent and employs a flexible, thermal shield. Since the primary difference between an all propulsive mission and an aeroassisted one is the use of an aerobrake, its design must not compromise the aeroassist mission goal of saving propellant and money. Therefore, the limiting mass of the aerobrake is that for which the propellant required for the aeroassisted mission does not exceed the propellant used for an all propulsive mission, and the cost of implementation and maintenance must not exceed the economic benefit.

## 4.2 Geometry and Aerodynamics

The chosen aerobrake configuration is an ellipsoidal nose tangent to an elliptical cone with a toroidal base skirt. The elliptical cone is raked to form a circular base plane which is desirable due to its simplicity as well as its ability to accommodate a bulky payload. A large rake angle ($\delta$) prevents wake impingement on the afterbody by producing a small wake angle. The nose is ellipsoidally blunted to reduce the stagnation point heat flux. The skirt is added to the edge of the aerobrake to reduce trailing edge heat flux and to provide better dynamic stability and rigidity for the aerobrake.

The nomenclature used throughout this design is consistent with that of Cheatwood, et al. whose "Geometrical Description" may be referenced for a more detailed analysis. A cone half angle in the XY plane ($\Theta_{xy}$) of 60° yields a flatter shape, providing surface area efficiency and a lower stagnation point heating than sharper cones (Scott, 1985). Studies have shown that a vehicle with a lift to drag ratio (L/D) in the range of 0.2-0.4 will perform the aeromaneuver most efficiently. Therefore, an L/D of 0.3 was chosen, and from Newtonian theory (L/D = cot $\delta$), the rake angle was determined to be 73°. Given $\delta$ and $\Theta_{xy}$, the cone ellipticity ($\varepsilon_{cone}$) can be determined such that the projection in the rake plane is a circle. $\Theta_{xz}$ can now be defined as 64.9°.

A summary of the aerobrake geometry is provided in Table 4.1. The values for the lift and drag coefficients were obtained from AFE Mach 10 wind tunnel data, the surface area was determined by CADAM, and the reference area was calculated using the nominal aerobrake diameter of 45'.

## 4.3 Structure and Materials

The two main structural components of the aerobrake are the shell and the ribbing. The shell preserves the aerodynamic geometry and provides a rigid base for the thermal protection system (TPS), and the ribbing supports the shell. The primary consideration in the design of these components is that the total aerobrake must be of minimal mass while accommodating a TPS which is sufficient to protect the vehicle from excessive aerodynamic heating. Therefore, the chosen aerobrake structure consists of a rigid shell made of a graphite polyimide honeycomb sandwich construction. During the aeropass, loads are distributed along the length of each rib on the convex side of the shell's curvature. Since buckling is therefore the most likely mode of



PAGE 42 INTENTIONALLY BLANK

PRECEDING PAGE BLANK NOT FILMED

failure, the ribs were designed as L-beams to provide the most efficient strength-to-mass ratio. A network of 45°-rotated parallel ribs reduces the number and size of ribs required, simplifying the arrangement without sacrificing structural integrity (Figure 4.1).

Table 4.1 Aerobrake Characteristics

| | |
|---|---|
| $\theta_{xy} = 60°$ | $\theta_{xz} = 64.9°$ |
| $\delta = 73°$ | $\tau = 60°$ |
| $\varepsilon_{cone} = 0.8112$ | $\varepsilon_b = 2.0$ |
| $C_L = 0.45$ | $C_D = 1.53$ |
| $\left(\frac{L}{D}\right)_{newtonian} = 0.3057$ | $\left(\frac{L}{D}\right)_{experimental} = 0.2941$ |
| $S_{ref} = 1590.43\,ft^2$ | $S_{surf} = 2478.07\,ft^2$ |
| $R = 45\,ft$ | |

### 4.3.1 Shell Structure Design Rationale

Possibilities for the shell structure include a rigid shell on which a rigid or flexible TPS may be mounted, and a flexible structure consisting only of the flexible TPS wrapped tautly over a skeletal support. Due to its low density and simplicity, a flexible TPS was selected, leaving only a choice between the flexible and rigid shell. The greatest drawback of the flexible shell is that it fails to preserve the smooth geometry of the aerobrake. Since the fabric is flat across the support ribs, the resulting surface is only a piecewise linear representation of the true curved surface. This roughness, coupled with the additional deformations encountered during the aeropass, would drastically reduce the quality of flow over the aerobrake, resulting in a turbulent boundary layer and producing undesirable heating. Therefore, the chosen aerobrake structure is a rigid shell on which a flexible or rigid TPS can be mounted.

### 4.3.2 Aerobrake Ribbing Design Rationale

The shell is stiffened using flush mounted beams, or ribs, which are attached to the back of the shell surface. These ribs also provide support for the interface brackets that allow attachment of the aerobrake shell to the vehicle truss structure. In the choice of the rib type or cross-section, several factors were considered: mass, resistance to buckling, and ease of fabrication. Rib cross-sections examined were hollow triangular, hollow rectangular, I-beams and L-beams. On the basis of strength-to-mass ratio, the I-beams and L-beams were considered more closely, and the L-beam was finally chosen since there is no need for the upper horizontal rib surface.

The second strategy in ribbing design is its arrangement; it must be able provide an efficient means of support for the aerobrake surface while preserving the integrity of the aerobrake geometry. As with the rib cross-section, ease of fabrication may exclude certain complex geometries. With these requirements and constraints in mind, the following ribbing arrangements

Figure 4.1 Aerobrake Structure

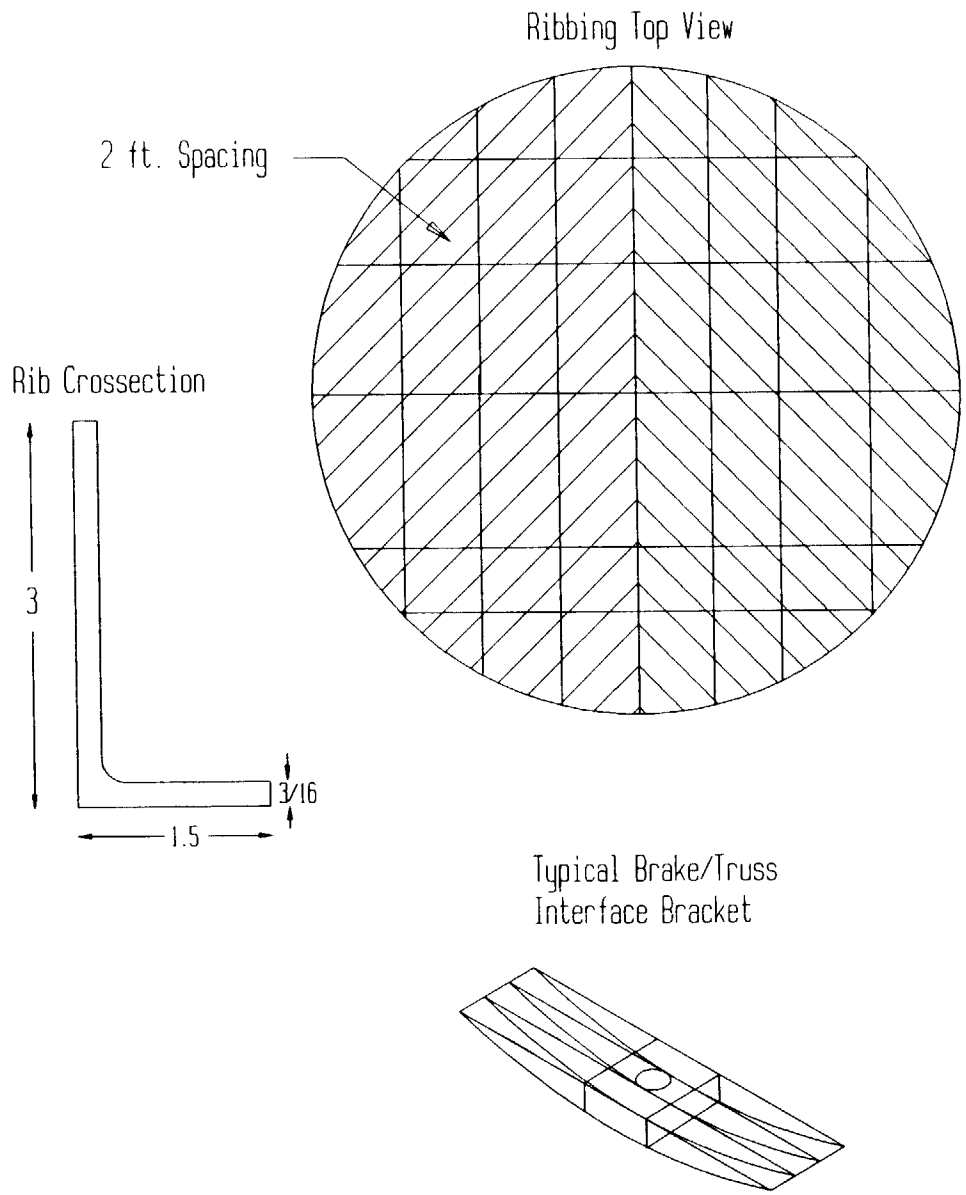

were considered: a radial grid, a rectangular grid, a hexagonal grid, and a rotated parallel rib pattern. The radial pattern is well suited for the conical surface, since only the beams perpendicular to the radial direction are curved. Variation of the grid size allows this kind of "spider web" network to be very efficient.

Unlike the radial pattern, all beams for the rectangular and hexagonal grid patterns are curved, making fabrication potentially difficult. However, this disadvantage is outweighed by the ability of these patterns to provide more evenly distributed support for the rigid shell and TPS. The hexagonal grid, although structurally efficient, results in complex geometries causing obstacles that outweigh its benefits. A compromise between the simplicity of the rectangular pattern and the efficiency of the hexagonal network is the 45° rotated parallel rib pattern. Since each rib is at a 45° angle to the longitudinal axis in the XY, or base plane, there is resistance to buckling longitudinally as well as laterally. For these reasons, the 45° rotated parallel rib pattern was chosen. The actual size of the ribbing beams and spacing was determined after performing an approximate structural analysis based on specific material properties and various loading scenarios.

## 4.4 Thermal Protection System

### 4.4.1 Introduction and Design Rationale

The thermal protection system is the most critical element in any aerobraking vehicle as the entire mission is constrained by the TPS's ability to withstand the intense aerodynamic heating encountered at hypersonic velocities. A reusable TPS is also considered baseline for cost efficiency.

The TPS is designed to reflect as much thermal radiation as possible, while conducting little through the shield. To accomplish this goal, a reflective outer surface coupled with an inner insulating surface and inner reradiating properties is desired. Both rigid and flexible thermal protection systems exhibiting these traits were examined. The rigid system consists of ceramic foam tiles, much like those found on the space shuttle, mounted to the rigid shell surface. However, due to the curved nature of aerobrake, a rigid TPS would require that every tile be individually sculpted to match the aerobrake's surface. The flexible TPS, on the other hand, is a multilayer concept consisting of several ceramic materials, each performing a specific task. Since the flexible TPS is made of fabric, it is easily tailored to fit smoothly over the aerobrake surface without the many seams and gaps that would exist on a tiled surface. Furthermore, the flexible TPS is able to withstand shell flexing, whereas the rigid tiles would be likely to pop off. For these reasons, coupled with the rigid TPS's higher mass, the flexible multilayer ceramic TPS was selected.

The basic idea behind the flexible thermal protection scheme is that the outer layers concentrate and reradiate thermal radiation while supporting the inner insulation, which limits the heat flux though the aerobrake. A reusable flexible quilted multilayer foiled insulation was chosen with a general composition as follows: a thin outer layer of colloidal silica coating ($\alpha/\varepsilon \leq 0.4$, $\varepsilon \geq$

0.8) applied to an outer layer of quilted aluminoborosilicate (ABS) fabric with ABS thread. Following is a layer of silica fiber felt blanket insulation (Q-felt) and ten alternating layers of stainless steel foil/ABS scrim cloth. The innermost layer, which is bonded with RTV sealer to the aerobrake shell, is made of ABS fabric identical to the outer layer (Figure 4.2).

### 4.4.2 TPS Design Rationale

As a first defense against radiative heating, the outermost layer should be highly reflective. Also, since the outermost surface is in contact with the nonequilibrium flow field, it is imperative that it not act as a catalyst to the recombination of dissociated atoms. This would cause all dissociation energy to remain on the surface, further contributing to the heat flux. A silica particulate coating was chosen for this task.

The outer quilted layer serves as a base for the silica particulate and protects and supports the Q-felt insulation. Most importantly, this layer concentrates the intense heat on the outer portion of the Q-felt insulation, allowing reradiation through the outer aerobrake surface. It is therefore desirable that materials considered for this layer have a high emissivity as well as high temperature and heat flux limits. Woven ceramic fabrics considered were Nextel, Nicalon and ABS fabric. The Nextel fabric has a much higher reflectivity than the Nicalon; however, heat flux calculations exclude the use of this material in favor of the silica carbide fabric (Nicalon) and ABS fabric. Recent tests also show that the ABS fabric and threads are better than their Nicalon counterparts; therefore, the ABS material was selected.

The inner insulation layer is a relatively thick layer of high purity silica fiber felt blanket insulation (Q-felt). The primary function of this layer is to insulate the rigid shell structure from extreme temperatures while minimizing the heat flux though the aerobrake, which is accomplished by a material having a low thermal conductivity.

Another important function served by the felt insulation is isolation of the thermal strain between hot outer layers and cooler back surfaces. Ceramic Q-felt is well suited and widely used for these applications and has therefore been selected for this layer.

The final layer is identical to the outer layer, and serves as a backing for the inner layers, as well as providing a quilting surface on which an adhesive may be applied for bonding of the entire TPS blanket to the graphite polyimide shell.

Figure 4.2 Quilted Multilayer TPS Concept

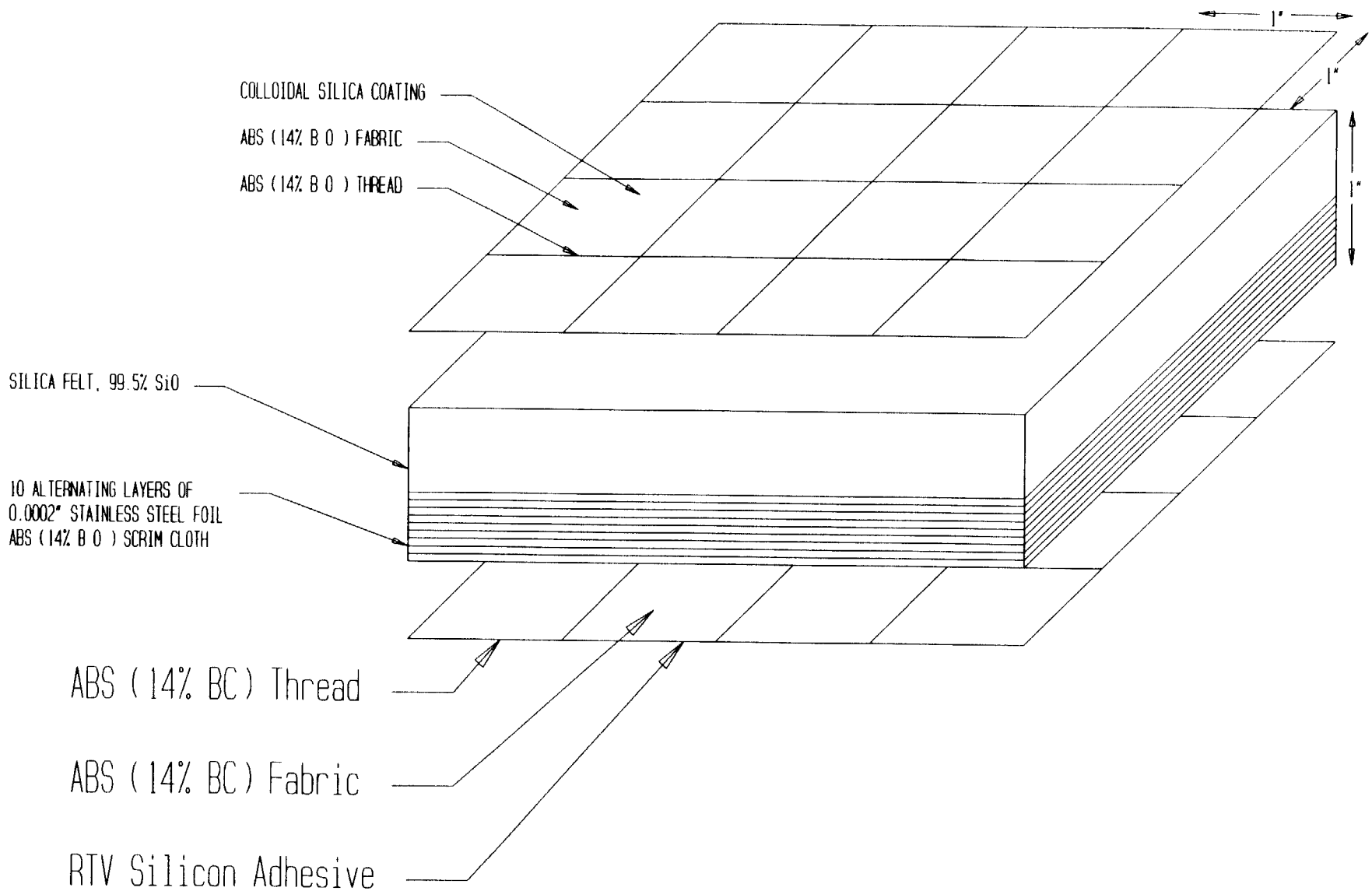

## Aerobrake Configuration and Materials Summary

**Aerobrake Structure**

- Graphite polyimide honeycomb one inch thick sandwich construction
- Reinforced and stiffened via graphite polyimide 3 x 1.5 x 3/16 inch L-beam ribbing
- Graphite polyimide surface mounts for connection of aerobrake to main truss structure

**Reusable Quilted Flexible Multilayer Reflecting TPS:**

- Colloidal silica coating ($\alpha/\varepsilon \leq 0.4$, $\varepsilon \geq 0.8$)
- Aluminoborosilicate (62% $Al_2O_3$, 14% $B_2O_3$, 24% $SiO_2$) outer fabric
- Silica fiber felt blanket insulation (0.5 inch thick)
- 10 Alternating layers of 0.0002 inch thick stainless steel foil and aluminoborosilicate (62% $Al_2O_3$, 14% $B_2O_3$, 24% $SiO_2$) scrim cloth (0.5 inch thick)
- Aluminoborosilicate (62% $Al_2O_3$, 14% $B_2O_3$, 24% $SiO_2$) inner fabric and thread

Table 4.2 Aerobrake Shell and TPS Mass Summary

| Aerobrake Structure | |
|---|---|
| Base Shell | 1,652 |
| Toroidal Skirt | 432 |
| Ribbing | 57 |
| Surface Mounts | 51 |
| Subtotal | 2,192 |
| TPS | |
| Top Surface | 156 |
| Insulation | 780 |
| Spacer/Shield | 42 |
| Bottom Surface | 156 |
| Subtotal | 1,134 |
| Total | 3,326 |

# Chapter 5

# Propulsion Systems

*5.1 Introduction*
*5.2 Propellant*
*5.3 Main Engines*
*5.4 Engine Mounts*
*5.5 Propellant Tank Shape*
*5.6 Main Propellant Tank*
*5.7 Auxiliary Tanks*
*5.8 Insulation*
*5.9 Propellant Lines*
*5.10 Reaction Control System*

## 5.1 Introduction

The propulsion system of the SPARC must fulfill several specific duties: provide efficient transportation between LEO and GEO for the vehicle and its payload, provide full maneuverability, attitude control and docking ability, and operate efficiently so as to minimize the cost of each mission. Out of all candidates for the vehicle propulsion system, liquid chemical propulsion has been selected on the basis of its thoroughly documented advantages: high Isp, high reliability, and a well developed technology. The propulsion system will encompass the main engines, reaction control devices, propellant tanks and propellant feed lines.

## 5.2 Propellant

### 5.2.1 Selection of Propellant

The following propellant characteristics are considered desireable: a low freezing point, a high specific gravity, high content of chemical energy per unit mass, chemical stability, good pumping properties, good availability, low cost, and low molecular weight (Sutton and Ross, 1976). Based on consideration of these characteristics, a liquid oxygen and liquid hydrogen propellant was selected. These particular elements have the highest performance of all well developed engines.

### 5.2.2 Propellant Calculations

Basic propellant relations were combined into a program which calculates the propellant required for each mission (Appendix D). Assumptions inherent in all calculations are as follows: the main tanks can only be filled to 97% capacity, an extra 6% of the total propellant is to be carried for emergency purposes and all burn times are short. The following table gives a partial listing of the program's output.

Table 5.1 Propellant Calculations

| | | **LEO to GEO** | | **GEO to LEO** | | **Propellant Required** | |
|---|---|---|---|---|---|---|---|
| Mission | Vehicle | Payload | $\Delta$ V (fps) | Payload | $\Delta$ V (fps) | $H_2$ (lbm) | $O_2$ (lbm) |
| 1 | 14,555 | 6,000 | 15,345 | 6,000 | 6,810 | 7,703 | 46,225 |
| 2 | 14,716 | 20,000 | 15,345 | 0 | 6,810 | 11,397 | 68,388 |
| 3 | 7,042 | 28,000 | 15,345 | N/A | N/A | 10,278 | 61,672 |

NOTE: Data shown for cylindrical tanks with hemispherical end caps.



PAGE 52 INTENTIONALLY BLANK

PRECEDING PAGE BLANK NOT FILMED

## 5.3 Main Engines

### 5.3.1 Main Engine Selection

The main engines for the vehicle are advanced versions of the existing Advanced Expander Engine (AEE) designed by Pratt and Whitney Aircraft (Pratt & Whitney Aircraft, 1984). This motor is considered superior to all other engine candidates based on the criteria shown in Table 5.2.

Table 5.2 Characteristics of Vehicle Engine Candidates*

| | RL10-IIB | RL10-IIC | RL10-IIIB | RL10-IIIC | AEE |
|---|---|---|---|---|---|
| Full Thrust Vacuum (lbm) | 15,000 | 15,000 | 7,500 | 7,500 | 15,000 |
| Mixture Ratio (O:F nominal) | 6.0 | 6.0 | 6.0 | 6.0 | 6.0 |
| Chamber Pressure (psia) | 400 | 400 | 400 | 400 | 1500 |
| Isp (s) | 460 | 460 | 470 | 470 | 482 |
| Installed Length (in) | 55 | 55 | 55 | 55 | 60 |
| $A_e/A^*$ | 205 | 205 | 400 | 400 | 640 |
| Engine mass (lbm) | 422 | 404 | 431 | 413 | 427 |
| Engine Life (firing/hr) | 190/5 | 20/1.25 | 190/5+ | 20/1.25 | 300/10 |
| Engine Condition | tank-head idle | overboard dump cooldown | tank-head idle | overboard dump cooldown | tank-head idle |

*(Pratt & Whitney Aircraft, 1984; Pratt & Whitney Aircraft, 1985)

### 5.3.2 Engine Modifications

Modifications of the AEE for the SPARC mission include: an increase in chamber pressure of 100 psia, a 1.6% increase in the area ratio, a 5% reduction in mass and a 20% increase in temperature gradient at all heat exchangers. The increased chamber pressure reflects the anticipated use of more durable materials, the mass reduction reflects the anticipated use of lighter materials, and the increased temperature gradient reflects the use of materials with high heat transfer capability. In order for these modifications to be realized, advances in turbomachinery must occur as well as improvements in the areas of cryogenic environment performance, seals, coatings, alloying techniques, and gear geometry.

Materials for the thrust chamber and regeneratively cooled nozzle will also have to be developed. Future materials will need higher strengths to withstand higher combustion pressures, and will need to possess higher thermal conductivity to allow the motor to attain and operate at the assumed temperatures. Many promising alloys have been researched including copper zirconium, copper chromium and several aluminum-bronze alloys. Each of these alloys offer longer life cycles, higher strength, better thermal conductivity and lower strain accumulation (due to heating) than the materials which are presently available, and all are in development stages (Pratt & Whitney Aircraft, 1984). At the time the SPARC construction, these materials, or some of their derivatives, should be sufficiently developed for the modified AEE.

Many characteristics of the AEE were left unchanged. The propellant ratio ($w_o/w_f$) remained at 6.0. Although this ratio does not yield the maximum $I_{sp}$, it does give an impulse which is only 2.0 seconds less than the maximum, a negligible difference (Figure 5.1). Other unmodified characteristics are the pressure drop experienced by the propellant as it travels through the engine and the power required to overcome this drop.

The main pressure drop in the engine occurs at the injector plate. There are additional losses due to friction and joints in the piping, but they are small compared to the injector plate loss. The pressure loss and associated power requirement are calculated using engine geometry and basic procedures (Sutton and Ross, 1976; Bussard, 1965).

NOTS, a computer code developed by the Naval Ordnance Test Station, was used to calculate some of the performance characteristics. Other pertinent characteristics were calculated using basic rocket performance equations (Hill and Peterson, 1970). Modified engine characteristics are listed in Table 5.3.

Table 5.3 Modified AEE Characteristics

| | |
|---|---|
| Oxidizer | liquid oxygen |
| Fuel | liquid hydrogen |
| $W_o/W_f$ | 6.0:1.0 |
| Chamber Pressure | 1,600 psia |
| Chamber Temperature | 6,445 °R |
| $A_e/A^*$ | 650 |
| Isp | 487 sec |
| Thrust | 16,140 lbf |
| Mass Flow Rate | 35.8 lbm/sec |
| Engine mass | 405 lbm |
| Internal Pressure Drops | |
| Oxidizer Stream | 158.808 psia |
| Fuel Stream | 71.09 psia |
| Pump Power Required | 41.4 hp |

Figure 5.1 Engine Performance

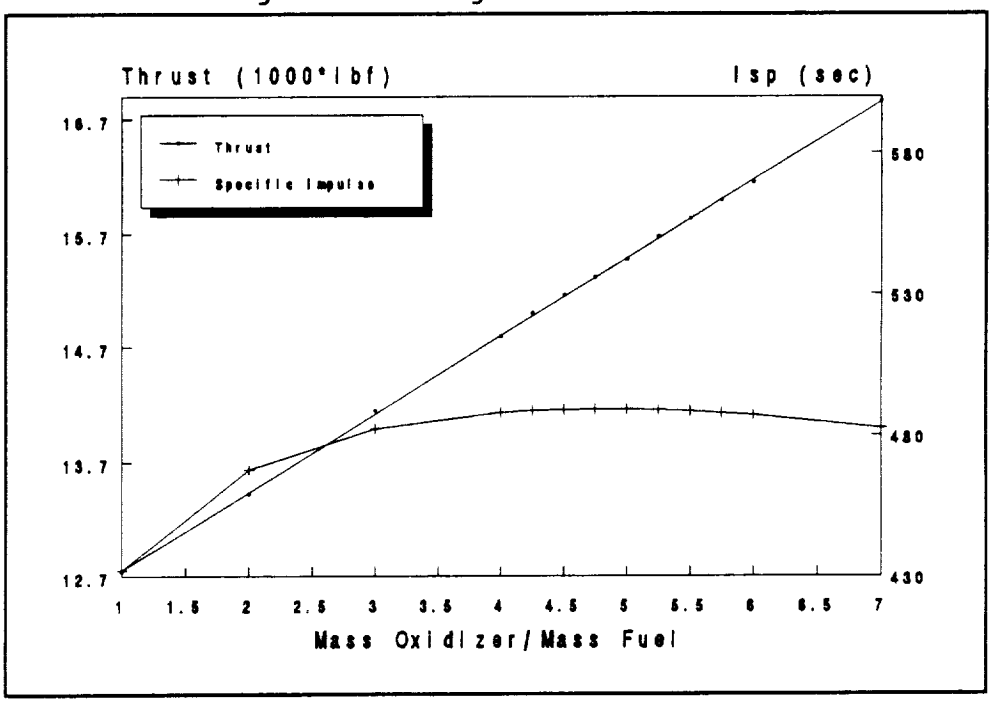

## 5.4 Engine Mount

The purpose of the engine mount is to attach the main engines to the SPARC while allowing engine gimballing and easy engine replacement. All engine supports are attached to a mounting plate, which is then bolted to a structural truss (Figure 5.2). This system allows the engines to be removed from the SPARC without having to individually disconnect all engine supporting members. Only the mounting plate and feed lines must be disconnected. This will greatly reduce turn around time on SPARC missions.

The main support is attached to the engine mounting plate along its centerline by means of a ball and socket joint, allowing for engine gimballing. Three actuators are attached to both the engine and the mounting plate with ball and socket joints, and all can be extended or retracted to impart a positive or negative gimbal angle of 10° on the engine (Figure 5.2). To accommodate the engine gimballing, the feed lines between the mounting plate and the engine must contain bellowed expansion joints.

Two types of actuators were considered. One is a hydraulic extender, and the other is electro-mechanical. The hydraulic actuator is desirable because it can impart a larger force than an electro-mechanical system and become fully extended in a shorter amount of time. However, since hydraulics can be unreliable in space due to the high pressures placed on the seals, and since the electro-mechanical actuation forces and times are reasonable, the latter system was chosen.

The electro-mechanical actuator consists of a motor, a threaded screw, and a two-part support (Figure 5.2). The motor extends the device by rotateing the screw. In order to determine the motor to be used, the required torque was calculated. A force (F) of 100 lbf was assumed necessary to rotate the engine. Assuming a 1" diameter (d) screw with six turns per inch (N), a mean collar diameter of 1.25" (dc), and a friction coefficient of 0.08, the torque (T) required was:

$$T = \frac{F\,dm}{2}\left(\frac{l + \pi\,\mu\,dm}{dm - \mu\,l}\right) + \frac{F\,\mu\,dc}{2}$$

where

$$dm = d - \frac{1}{2}N,\ l = \frac{2}{N}.$$

From this equation, the torque required was calculated to be 14.09 lbf-in. The motor chosen produces a maximum 15 lbf-in torque at 62 RPM, using 1.2 Amps at 36 Volts (Traister, 1983).

The actuators are 24.6" in length in the nominal position. For a 10° angle, one actuator extends to 26" and the other retracts to 21". It can therefore be determined that the screw must turn a maximum of 21.6 revolutions, 6 times (24.6" - 21.0"), requiring a time of 20.9 seconds.

Figure 5.2 Engine Actuation

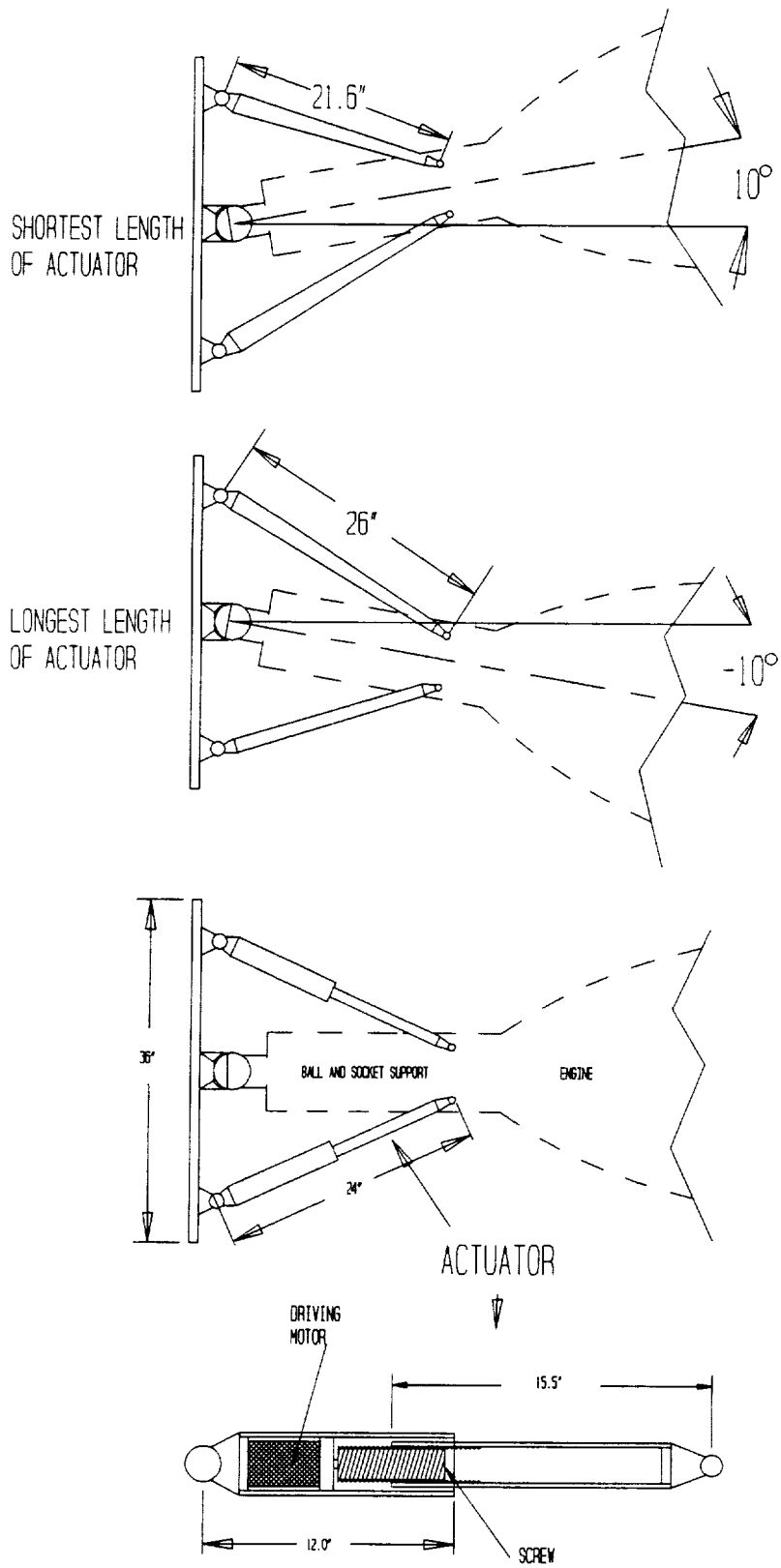

## 5.5 Selection of Fuel Tank Shape

Selection of tank shape from the commonly used pressure vessel shapes is affected by four factors: stress in the tank walls, tank mass, tank surface area, and the amount of radiant heat received by the tank. Tank masses are calculated as intermediate products in the propellant analysis, and surface area is determined using basic geometry. Radiant heat transfer received by each tank during the aeropass is modelled using a gray body approximation. In this analysis, the major heat sources and the tanks are modeled by single, finite rectangular sections. A shape factor could then be generated between each pair of rectangular elements using a specialized procedure (Hsu, 1967). The results of the shape factor analysis are graphed in Figures 5.3 through 5.7, and the results of the mass and surface area comparison are listed in Table 5.4.

Using these results, the cylindrical tank with hemispherical end caps was chosen for both oxidizer and fuel tanks. This configuration had consistently lower shape factors (it received less radiant energy than other shapes), as well as having a relatively low mass. The cylinder with hemispherical ends has a high surface area requiring more insulation and more insulation mass, but the total mass due to the tank shell and its insulation is still better than other designs.

Figure 5.3 Shape Factor - Oxidizer Tank (Front)

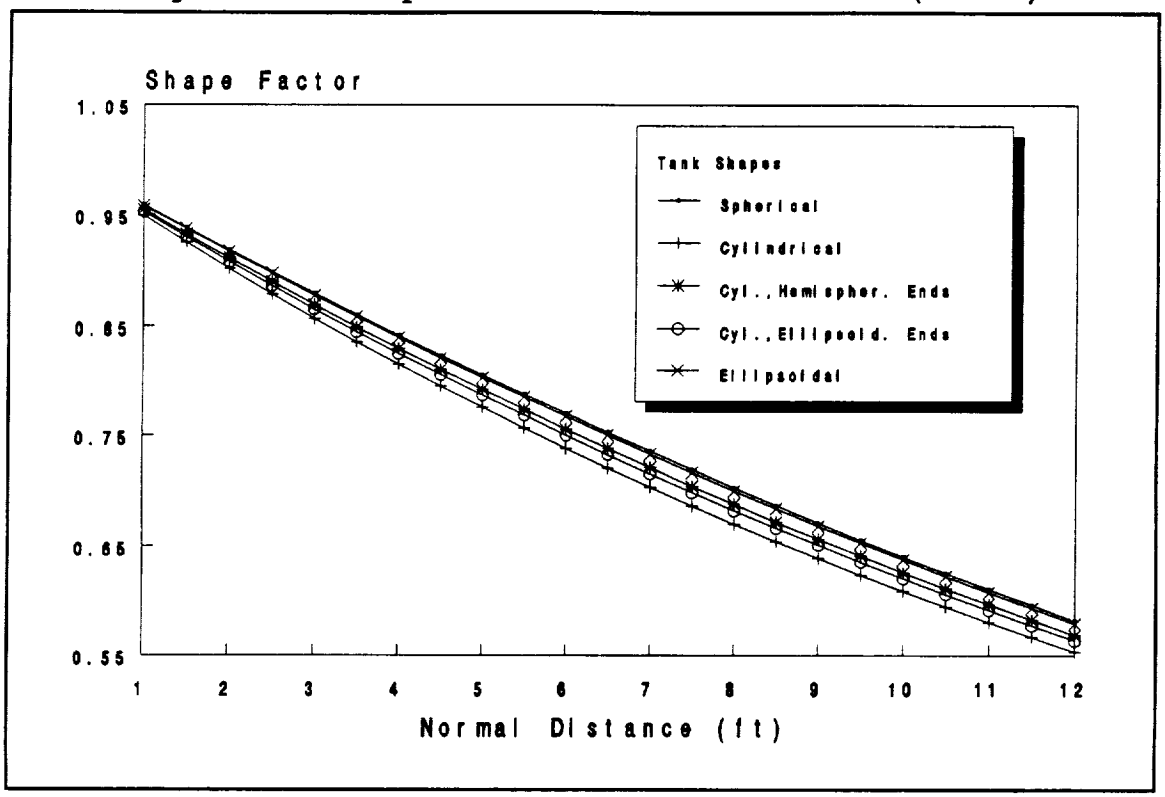


Figure 5.4 Shape Factor - Fuel Tank (Front)

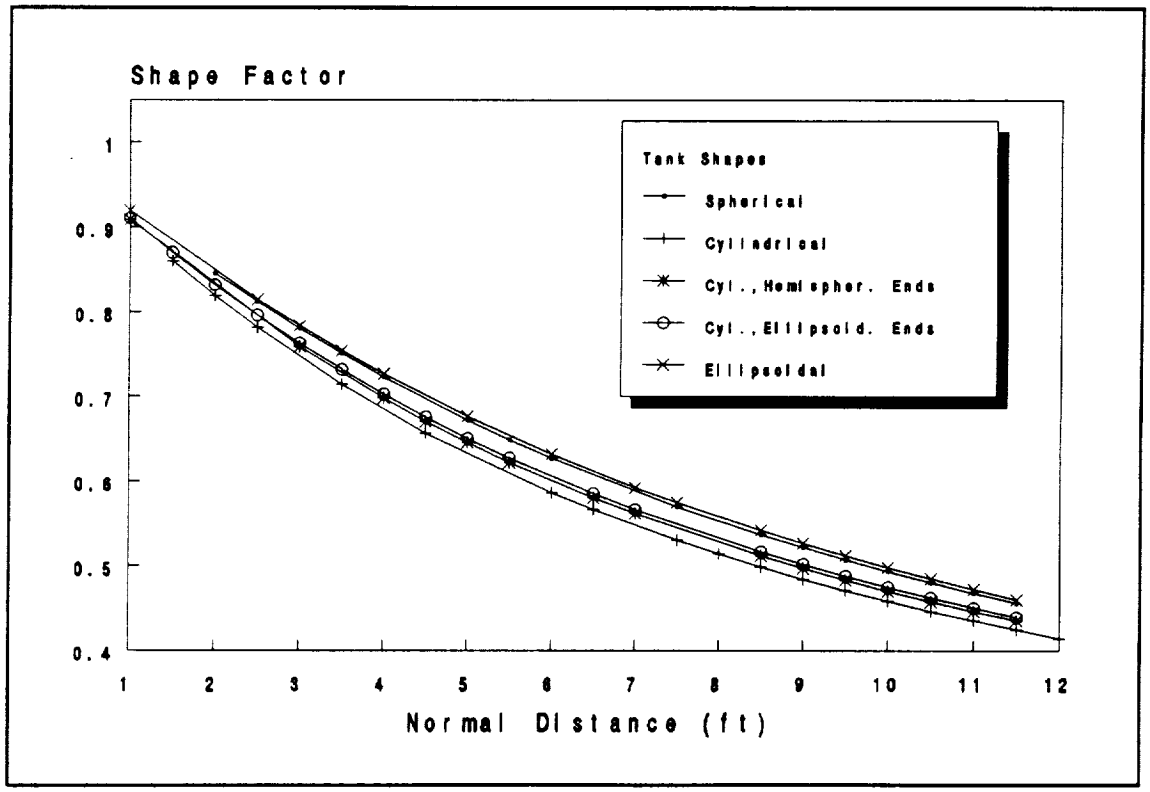

Figure 5.5 Shape Factor - Fuel Tanks (Back)

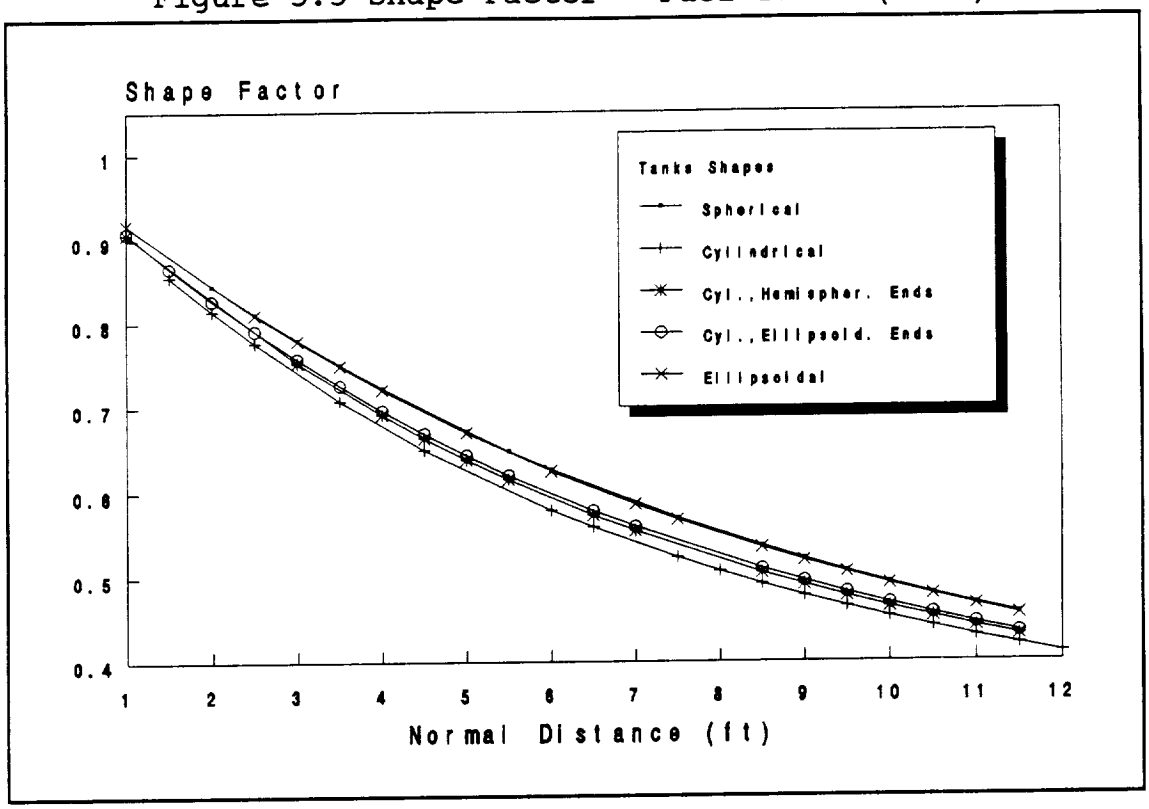


Figure 5.6 Shape Factor - Oxidizer Tank (Profile/Bottom)

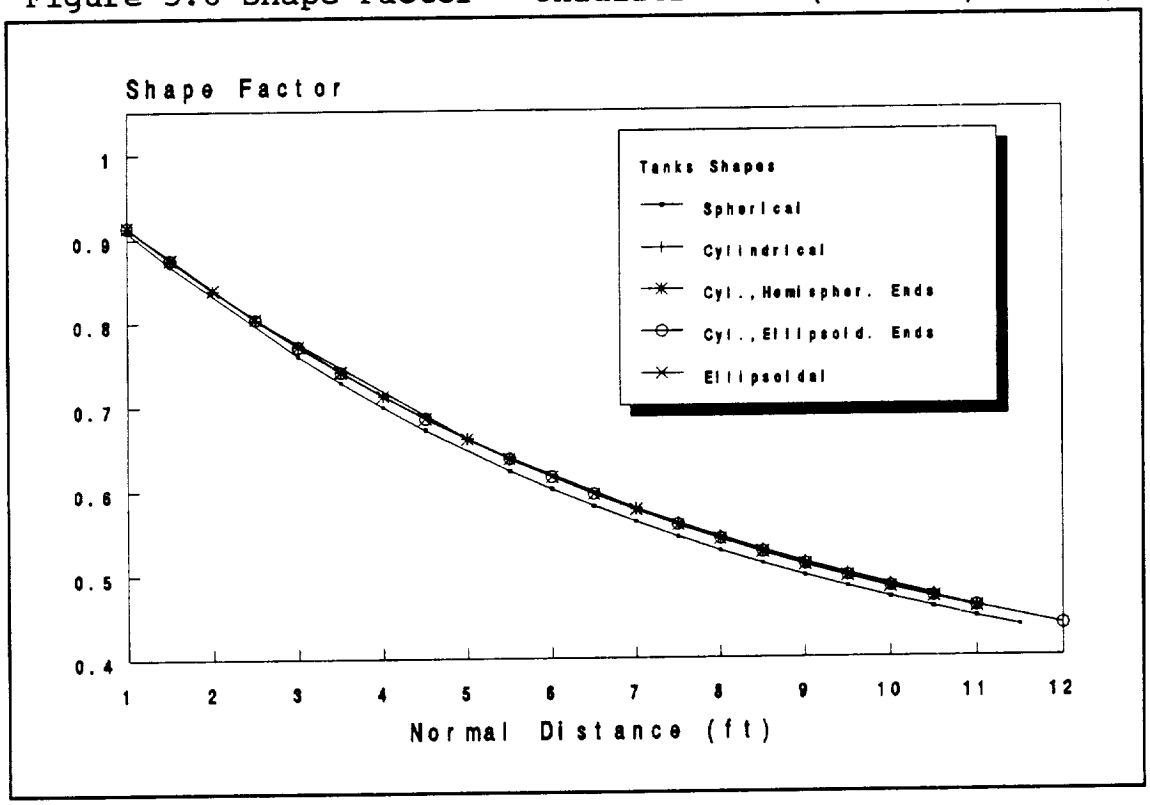

Figure 5.7 Shape Factor - Fuel Tank (Profile/Bottom)

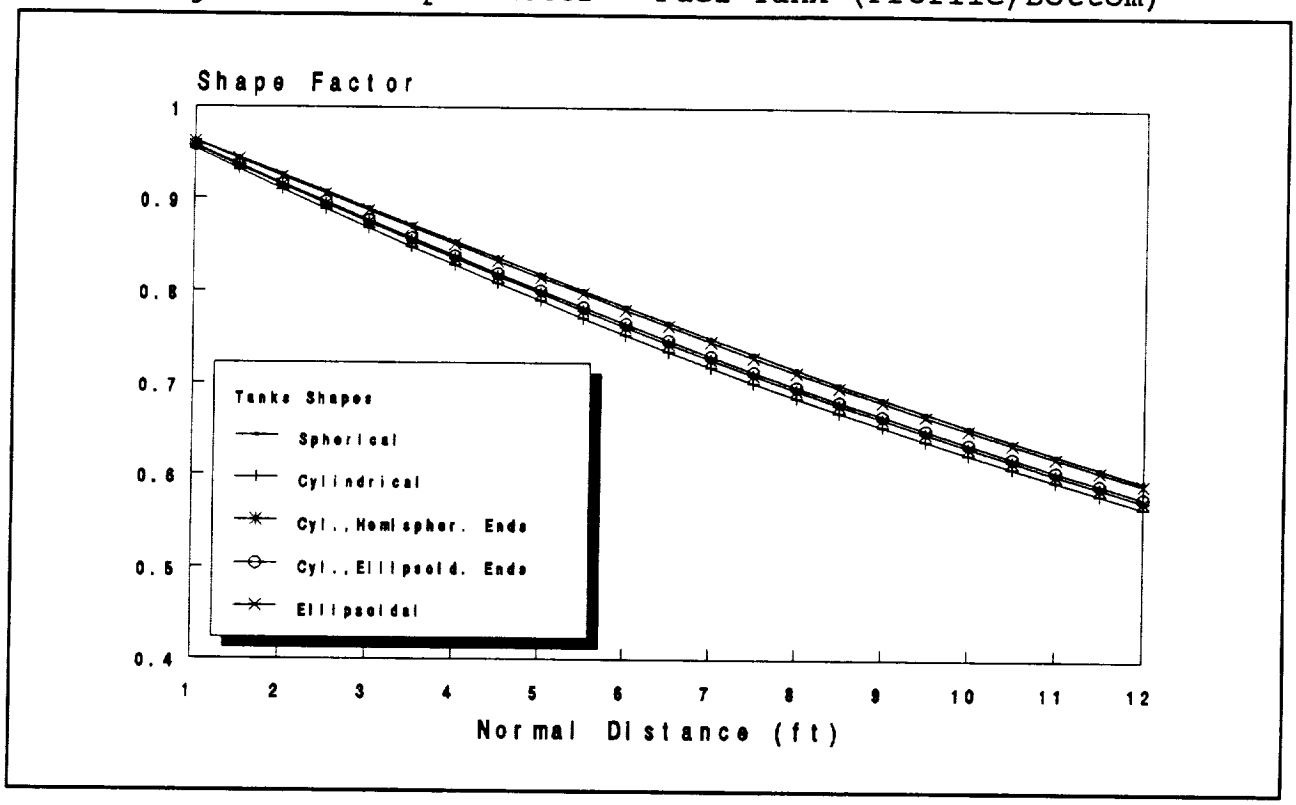


Table 5.4 Tank Characteristics for Tank Shape Selection

| Shape | $H_2$ Tank | | $O_2$ Tank | |
|---|---|---|---|---|
| | Mass (lbm) | Area ($ft^2$) | Mass (lbm) | Area ($ft^2$) |
| Sphere | 153 | 550 | 178 | 440 |
| Cylinder | 235 | 464 | 273 | 406 |
| Cylinder with Hemispherical Ends | 145 | 558 | 181 | 456 |
| Cylinder with Ellipsoidal Ends | 150 | 684 | 174 | 610 |
| Ellipsoid | 202 | 302 | 234 | 450 |

NOTE: These values were generated using an intermediate form of the vehicle. The actual values would be slightly different if the final configuration were used, but the conclusion would be the same.

## 5.6 Main Propellant Tanks

### 5.6.1 Materials

When deciding on a material for the tank shells, several different criteria are taken into account: a high strength-to-mass ratio, availability of the right form and size and thickness, and weldability. Also of concern are the reactions between the material and the propellant, causes and effects of which are as follows:

metal corrosion - material weakening, loss of cross-sectional area
galvanic corrosion - rapid deterioration
steel embrittlement - fracture at low stresses
ingition of material - combustion

The material chosen for the liquid hydrogen tank shells is Ti-5 Al-2.5 Sn ELI. This was selected for its high strength-to-mass ratio and high yield strength, on the order of 1000MPa, at low temperatures. The density of this material is 278.2 $lbm/ft^3$. Titanium alloys are susceptible to contamination and combustion when in contact with liquid oxygen, so several aluminum alloys were considered for the oxidizer tank shells. Al-Mg-Si and Al-Zn-Mg were discarded for low yield strength and low ductility at low temperatures respectively, and two other alloys, 2219-T87 and 2090-T81 were considered. The strength-toughness relationship of both alloys improves with decreasing temperature, as does the tensile elongation and yield strength. 2090-T81 was finally chosen for its lower density, higher yield strength, on the order of 600 MPa, and higher elastic modula. 2090-T81 consists of Al-2.7, Cu-2.2, Li-0.12 by weight and trace amounts of other elements (Glazer, 1987).

### 5.6.2 Cryogenic Storage System

A cryogenic system involves the storage and use of liquid hydrogen and liquid oxygen at less than atmospheric conditions in a low-vapor pressure system. This type of system permits the use of lighter mass shells and higher density fluids, both of which reduce the cost of the system. In order to use cryogenic storage, however, there must be a way to lower the fluids' existing saturation conditions.

Studies show that the most cost-effective method of lowering the saturation conditions is to lower the pressure of the fluid in the tank to 5 psia or below; however, this causes handling problems (Torre). Material fabrication restrictions would exist, and the propellant would have to be continuously resupplied at low vapor pressure. To alleviate these problems, the propellant will be stored at 18 psia without refrigeration, since the relatively short duration of the mission will only allow minimum boiloff to occur (Aydelott, 1990).

### 5.6.3 Tank Shell Thickness

The thickness (t) of the tank shells is based on a stress formula for a cylindrical pressure vessel with hemispherical ends:

$$t = \frac{pr}{\left(\frac{2\alpha}{F.S.}\right)}$$

where

p = pressure in the tanks
r = tank radius
$\alpha$ = material yield stress
F.S. (factor of safety) = 1.5

The thickness of the liquid oxygen tank is 0.0013', and the thickness of the liquid hydrogen tank is 0.00153'.

Table 5.5 Tank Characteristics

| | Main $LH_2$ Tank | Main $LO_2$ Tank | Auxiliary $LH_2$ Tank | Auxiliary $LO_2$ Tank |
|---|---|---|---|---|
| Quantity | 2 | 1 | 2 | 1 |
| Total Length (ft) | 15.1 | 15.0 | - | - |
| Radius (ft) | 5.83 | 4.92 | 3.15 | 2.86 |
| Thickness (ft) | 0.00153 | 0.0013 | 0.001 | 0.0009 |
| Mass (lbm) | 235.5 | 97.5 | 34.6 | 14.9 |

### 5.6.4 Internal Tank Structure

The main component inside the tank structure is the propellant removal system which must be able to function regardless of where the surface level of the liquid is positioned. Three systems were considered: a bladder, propellant settling, and a liquid acquisition device.

A bladder acts similarly to an expanding balloon, pushing the propellant toward the tank outlet. In a saturated system, however, vapor can easily cross to the wrong side of the bladder and enter the lines.

Settling of the propellant uses the reaction control system (RCS) thrusters to position the vehicle so that the propellant settles in the correct position at the time of engine start. This maneuver was found to be undesirable for the SPARC mission for two reasons: total maneuver time would be as long as 30 minutes and each engine restart would require RCS propellant (Blatt, 1980). Since

the SPARC mission is relatively short and since many engine restarts are required, this system was discarded.

The method chosen for propellant removal utilizes a liquid acquisition device: a capillary system which consists of finely woven mesh screens which fit over the tank outlet and are attached to the inner walls of the tank. These screens function as a wick, collecting the propellant and storing it at the tank outlet. Whenever an engine start is required, the propellant is readily available to be pumped into the main lines. This system also acts as a "bubble trap" by not allowing any vapor into the engine. Furthermore, once the engine is started and the vehicle is in a high "g" environment, the propellant is pushed up against the tank outlets, aiding removal (Aydelott, 1990). An internal vent system is included which allows removal of excess vapor to minimize boiloff, and a thermal subcooler is required for the capillary devices to provide net positive suction pressure.

## 5.7 Auxiliary Tanks

For the 20,000-lbm mission, three smaller, spherical tanks will be located directly above the three main tanks and will carry the extra propellant needed for the trip. Propellant lines from the auxiliary tanks will go directly into the main tanks, and capillary lines will extend from the main tanks, through the propellant lines, and into the smaller tanks to access the extra propellant. Auxiliary tank shell material is the same as the main tanks, and other characteristics are listed in Table 5.5.

## 5.8 Insulation

Cryogenic tank insulation can consist of many different materials such as foams, powders, and fiberglass; all of which can be bolted, bonded or sprayed onto the tank surface (NASA SP-8088, 1974). Insulation containing organic constituents will not be used since these will burn if the $O_2$ concentration in the gas permeating from the tank exceeds 25% (Haselden, 1971).

A multi-layered insulation (MLI) was chosen as the most effective (Williamson, 1983). The MLI consists of alternating layers of aluminum coated Mylar and a low conductivity spacer made of a fiberglass net (Figure 5.8). All radiation encountered is reflected by the aluminum. Given the size of the tanks, the maximum allowable heat flux for the insulation is 0.20 Btu/ft$^2$hr (Aydelott, 1990). It was determined that 34 layers of MLI (Figure 5.9) are required on each tank for a total thickness of 0.654" (Stochl, 1974).

## 5.9 Propellant Lines

### 5.9.1 Flow Within the Engine

A brief description of the modified expander cycle and the paths of the propellant as it travels within the engine at full thrust conditions (Figure 5.10) is as follows (Pratt & Whitney Aircraft, 1984). Hydrogen fuel enters the engine through an inlet valve located on a low-pressure pump

Figure 5.8 Propellant Tank and Cross Section

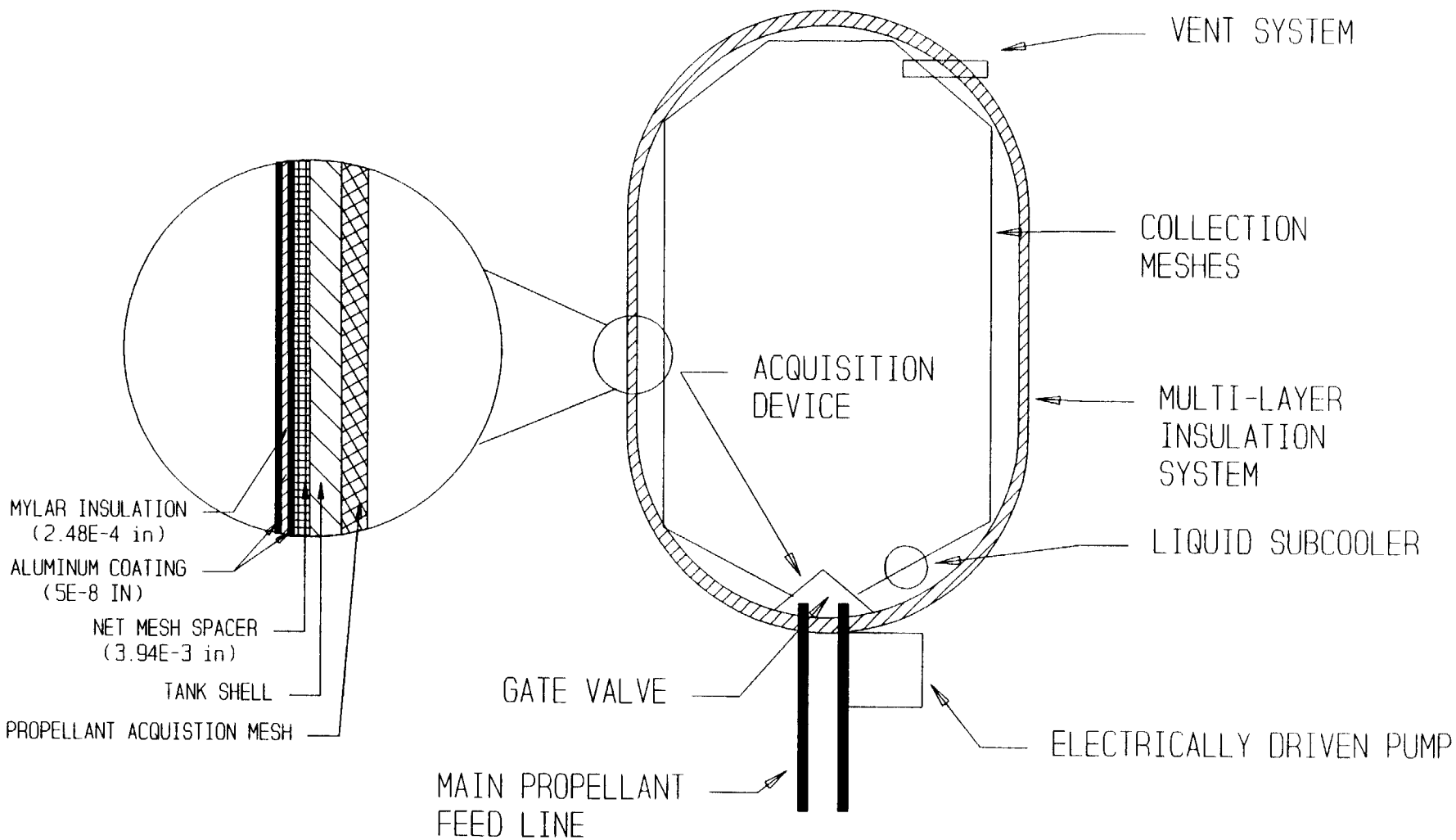

Figure 5.9 Heat Flux versus # of Insulation Layers

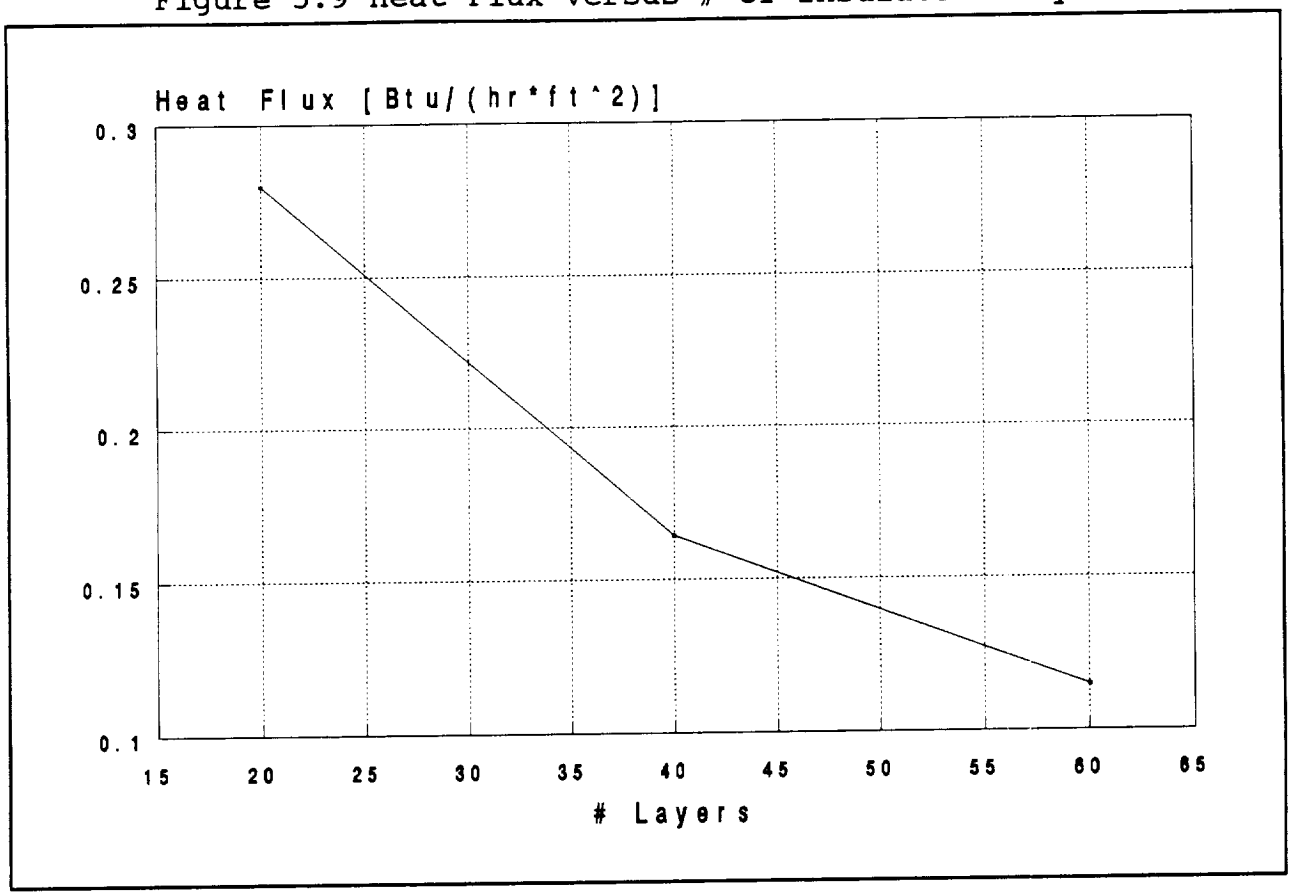

Figure 5.10 Engine Schematic

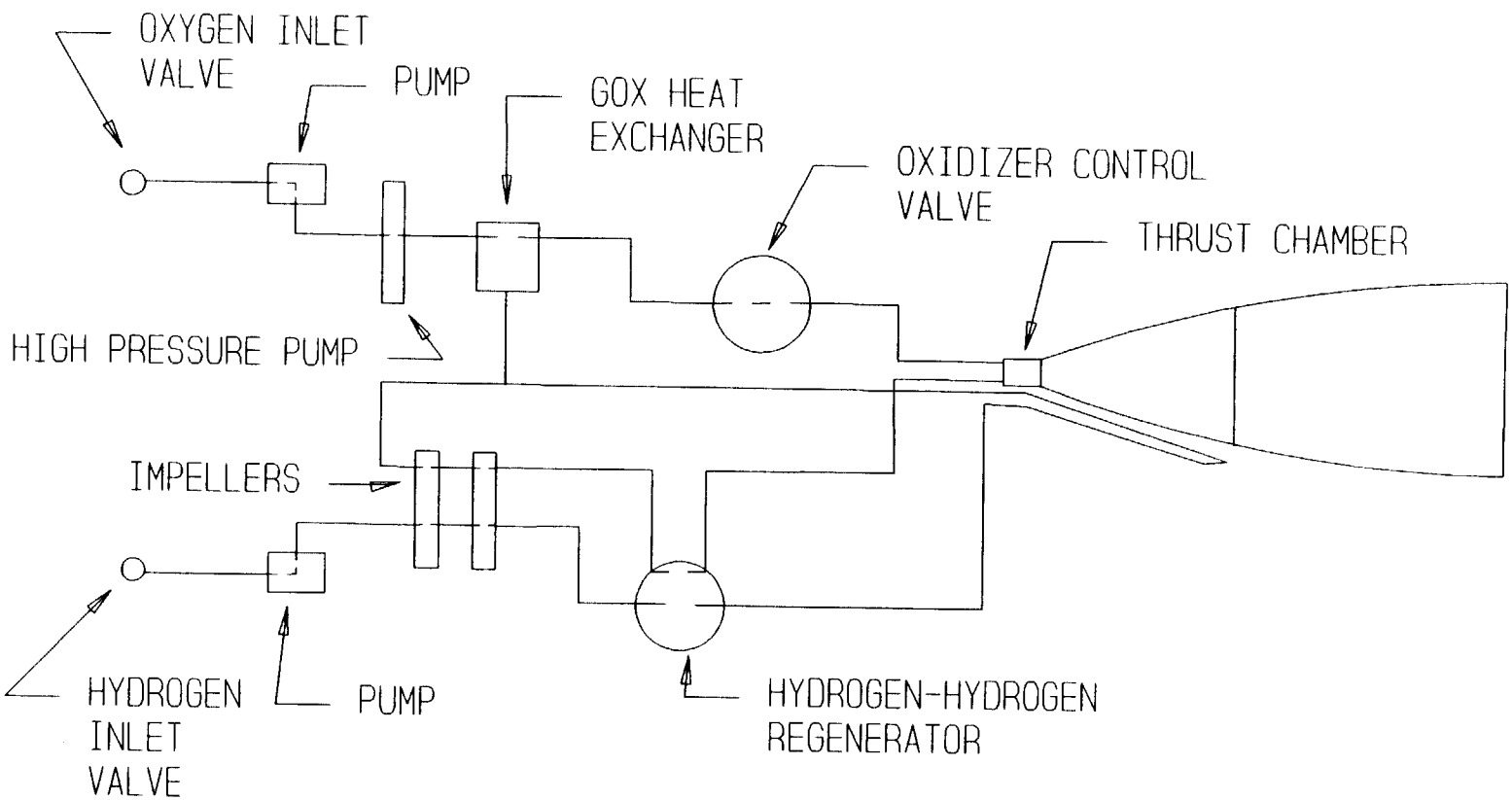

that is driven by the main oxidizer turbopump shaft. Fuel then enters two back-to-back centrifugal impellers mounted on a shaft and driven by a turbine which derives its energy from the hot hydrogen flowing through it. As the fuel exits the high-pressure pump, it enters the hydrogen-hydrogen regenerator which takes energy from the fuel and uses it to preheat the thrust chamber coolant. It also increases the temperature of the fuel enough to change it into a gas to cool the chamber.

The gaseous hydrogen then flows around the thrust chamber which is made of a nickel shell and copper alloy liner. It passes the throat and enters the outside of the nozzle where it cools the nozzle flow, gaining heat which it later uses to drive the turbines. At a point on the nozzle, the flow is turned by a manifold and routed back through the remaining lines. About 3% of this fuel bypasses the turbines and goes through the GOX heat exchanger for use in other areas. The remaining fuel goes through the turbines, which provide the power to drive the turbopumps, and then re-enters the opposite side of the hydrogen-hydrogen regenerator. This removes heat from the fuel before it enters the thrust chamber. The fuel is then recombined with the 3% bleedoff and injected into the thrust chamber.

Oxygen enters the engines through a low-pressure pump driven by the main turbopump, it then enters a centrifugal type, high-pressure pump driven by a turbine. The oxidizer goes to a GOX heat exchanger where it is vaporized by the hot fuel for use later in igniting the thrust chamber. The flow travels to the oxidizer control valve, which is pre-set to give the required mixture ratio (6:1). From here the flow is injected into the combustion chamber. A hydrogen-oxygen torch is used to light the combustion chamber with fuel gathered immediately after it leaves the turbines, and gaseous oxidizer supplied from the GOX heat exchanger.

The engines can be set in two other modes as well: pumped idle operation, and tank head idle operation. During pumped idle operation, the thrust is about 10% of that at full operation; this state is achieved by bypassing 54% of the total hydrogen fuel flow around the turbine. This bypass fuel gives energy to the oxygen that goes through a heat exchanger. Gaseous oxygen is therefore supplied to the injector, giving greater stability at the reduced pressure. During tank head idle operation, used for pump cooldown and propellant settling, the pumps and turbine do not rotate. A thrust level of approximately 70 lbf is obtained. Propellant shutoff is achieved with helium-actuated inlet shutoff valves and main fuel shutoff valves, which prevent fuel from reaching the thrust chamber and extinguishing the flame.

The lines within the engine, the heat regenerators, and the exchangers are all made of aluminum alloys, and the control valves are made of stainless steel and aluminum. The total mass of plumbing, valves and heat exchangers is 170 lbm.

### 5.9.2 Flow from Tank to Engine

Following collection by the acquisition system, the propellant must be pumped through the lines with enough power to reach the injection pump. Several assumptions about the flow are included in the flow calculations:

constant flow velocity, 49.21 fps
constant hydrogen mass flow rate, 4.44 lbm/s
constant oxygen mass flow rate, 31.1 lbm/s
constant hydrogen density, 4.42 lbm/ft$^3$
constant oxygen density, 71.9 lbm/ft$^3$

The propellant leaves the tanks and enters the engine through gate valves at both ends of the lines. The Al-Li lines themselves run underneath the primary truss structure (Figures 5.11 through 5.13). The oxygen line splits into two separate lines after leaving the tank, and in order to keepthe velocity constant, the cross-sectional area after splitting is half of its original value. Line specifications are as follows:

inner diameter of the $H_2$ lines, 1.934"
inner diameter of the $O_2$ lines before split, 1.269"
inner diameter of the $O_2$ lines after split, 0.898"
thickness of all lines, 0.0084"

The thickness is based on stress analysis and manufacturing limitations. Using pipe flow formulas (Shames, 1982), the head loss through all the lines was computed, and a pressure drop was then calculated determining the required strength of the pump at each tank. A pump efficiency of 96% was assumed, and the total mass of the lines was computed (Table 5.6). Refer to Appendix E for equations.

Table 5.6 Propellant Line Characteristics

| | Head Loss (ft) | Pressure Drop (psi) | Mass (lbm) | Power Required (Btu/s) |
|---|---|---|---|---|
| $H_2$ Lines | 511.46 | 17.70 | 3.396 | 3.040 |
| $O_2$ Lines | 327.98 | 163.31 | 1.658 | 13.616 |
| Total | 839.44 | 179.01 | 5.054 | 16.656 |

Figure 5.11 Propellant Lines

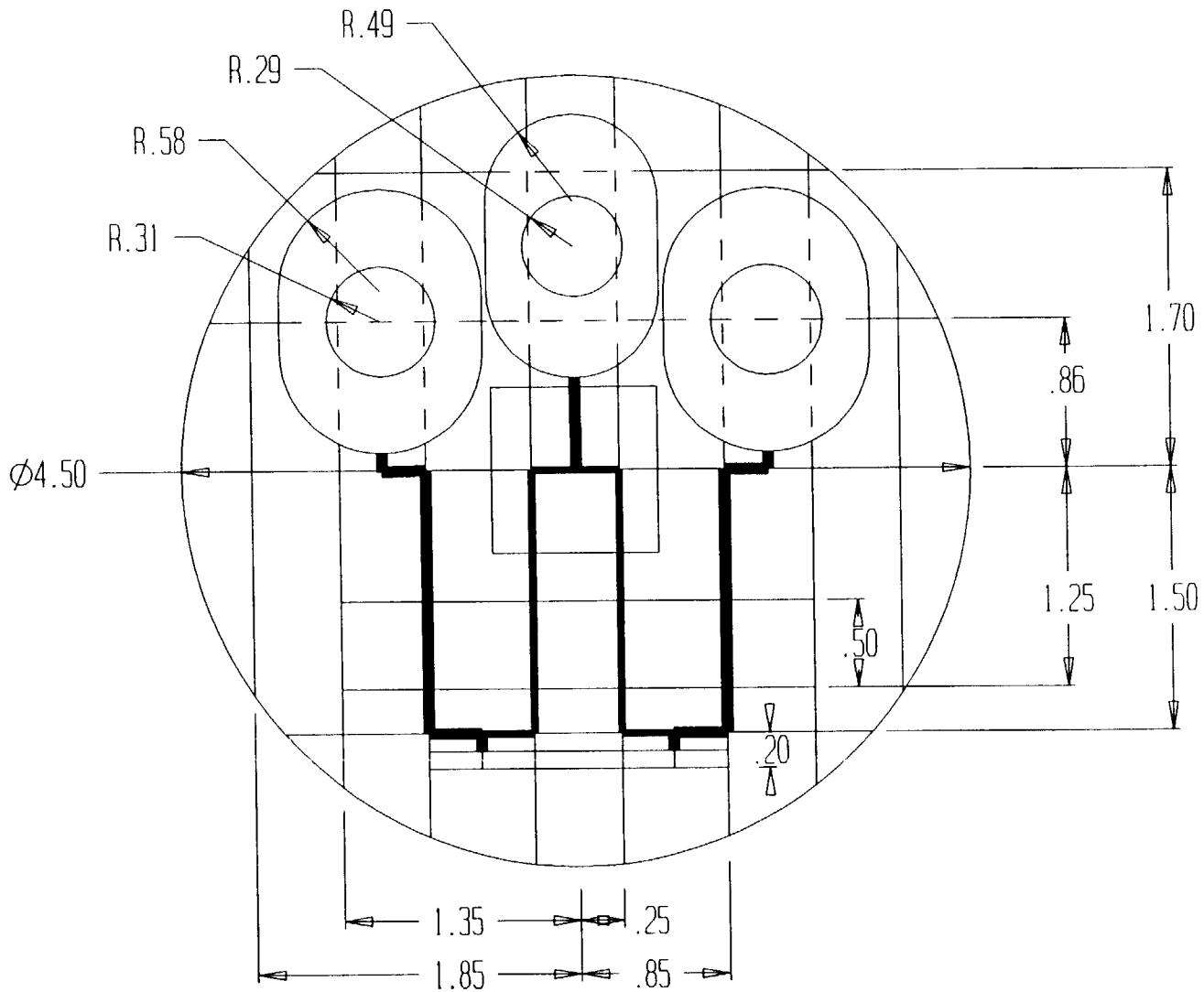

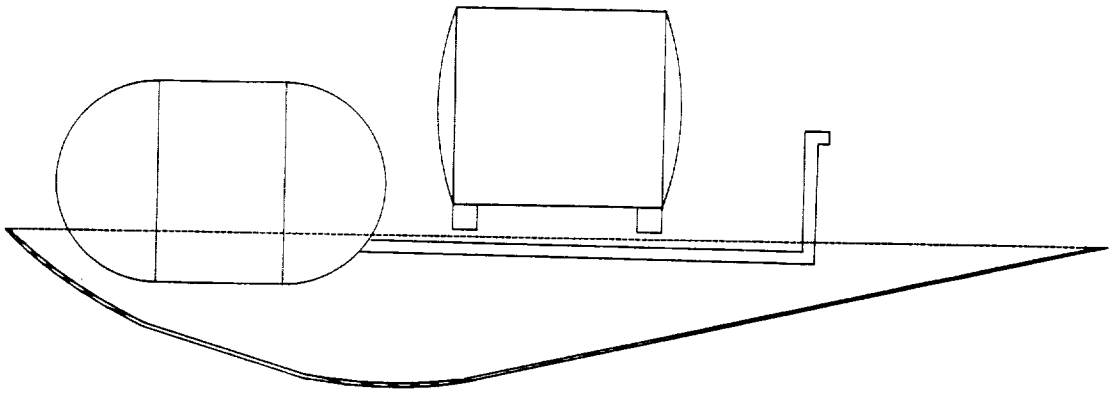

NOTE: PROPELLANT LINE NOT TO SCALE

FIGURE 5.12 OXYGEN LINE LOCATION

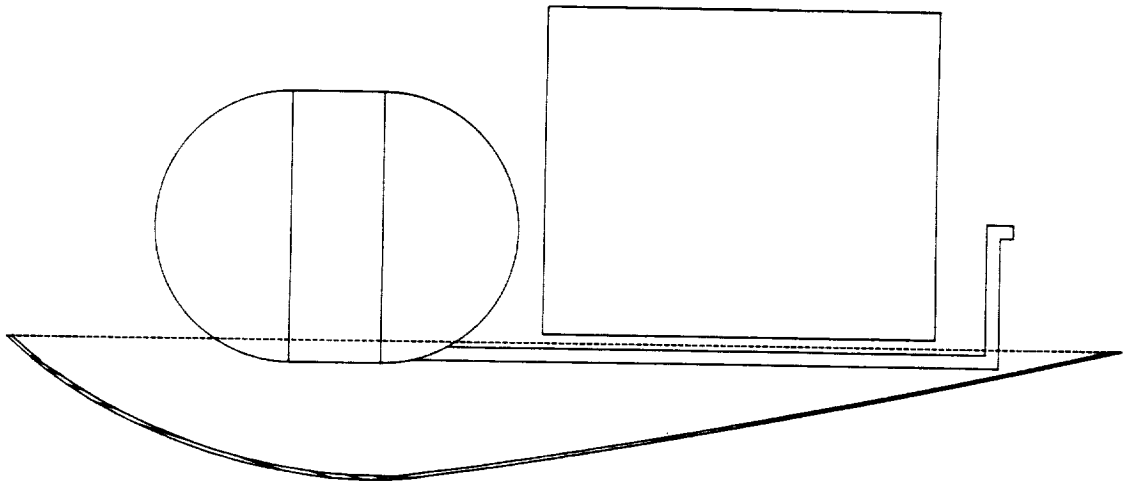

NOTE: PROPELLANT LINE NOT TO SCALE

FIGURE 5.13 HYDROGEN LINE LOCATION

## 5.10 Reaction Control System

### 5.10.1 Requirements

The reaction control system (RCS), required to provide attitude control and short range maneuvering capabilities, has several specific functions and fundamental requirements:

a. control attitude of the craft during initial pointing for main engine start
b. provide orientation control for Space Station or Space Shuttle rendezvous
c. provide thrust for orbital maneuver correction during coasting periods
d. provide attitude control during aerobraking maneuver
e. satisfy manned mission rating requirements

### 5.10.2 RCS Propellant

Initially, two propellant systems were considered: a hydrazine ($N_2H_4$) monopropellant with tank pressurization provided by nitrogen ($N_2$) and an $H_2O_2$ bipropellant. The hydrogen and oxygen system was thought to be preferred to simplify logistics by using the same propellant as the main engines. However, further research showed that this system would be more expensive to develop and build, as well as more complex than a monopropellant system. This created concerns over reliability and mass, and the hydrazine system was chosen.

In the hydrazine system, the propellant is pressurized to 400 psia by the nitrogen gas; to keep the propellant separate from the nitrogen, the tanks contain membrane bladders. The temperature of the hydrazine propellant is kept above the freezing point by an electrical heater, which is positioned around the tank.

### 5.10.3 RCS Thrusters

Three different types of RCS thrusters were considered: a 10 lbf thruster, a 30 lbf thruster, and a 100 lbf thruster. The baseline angular acceleration of the vehicle was determined from the total vehicle moments of inertia to be 0.5 deg/sec, for all axes of rotation. The 10 lbf thruster was discarded since many would be needed to achieve the baseline acceleration, greatly increasing the complexity of the system. The size and high fuel consumption of the 100 lbf thrusters made them undesirable, so the 30 lbf thruster was chosen.

There are four RCS packs. Each pack contains six thrusters for a total of 24 thrusters, each of which produces a maximum thrust of 30 lbf. In order to obtain thrust in the z-direction, through the aerobrake, four of the six thrusters in each pack can be rotated downward at a 45° angle, producing 340 lbf thrust in the z-direction (Figure 5.14). All six degrees of freedom are redundantly satisfied in order to meet man rated mission requirements for dual failure tolerance.

Figure 5.14 Reaction Control System

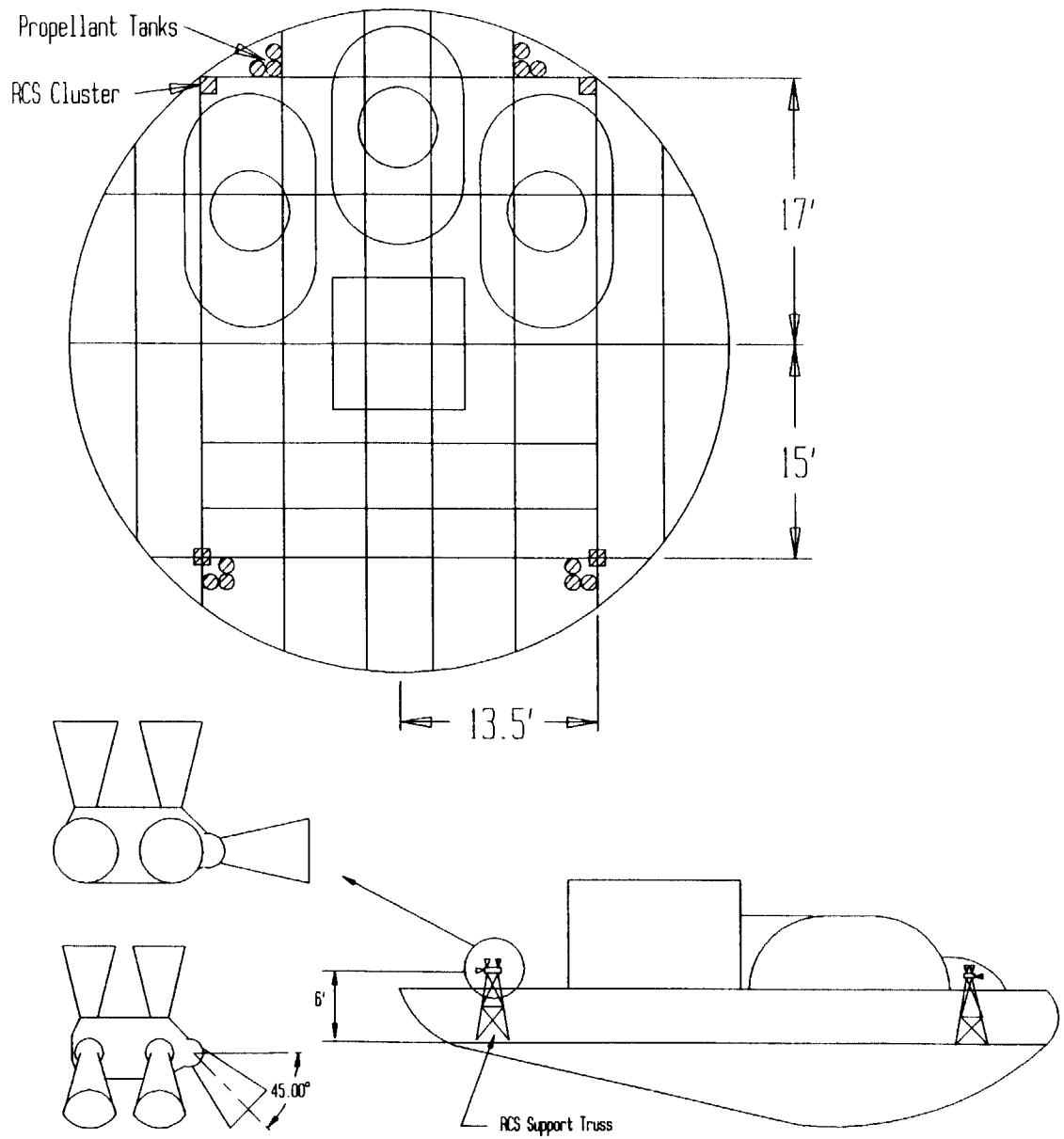

Table 5.7 Thruster Characteristics

| | |
|---|---|
| Maximum Operating Pressure | 380 psia |
| Thrust at Maximum Pressure | 25 lbf |
| $I_{sp}$ | 225 sec |
| Exit Velocity | 7,245 fps |
| $\dot{m}$ | 0.11 lbm/sec |

Table 5.8 RCS Mass Summary

| Mass per Cluster (lbm) | |
|---|---|
| Thrusters | 53 |
| Valves and Regulators | 45 |
| filters | 3 |
| Tanks (1 pressurant, 3 propellant) | 53 |
| Plumbing | 35 |
| Pressurant (usable and residual) | 1 |
| Propellant (usable and residual) | 375 |
| Total Cluster Mass | 565 |

### 5.10.4 RCS Propellant Feed System

A schematic arrangement of an RCS cluster is shown in Figure 5.15. The line between the pressurization tank and the propellant tank is 0.25" stainless steel tubing. Double isolation valves keep $N_2$ pressure from the propellant tank during docking and Shuttle delivery, and double regulators direct the pressure to the propellant tank. The propellant is stored in three 19" diameter tanks instead of one large tank to facilitate placement of the tanks on the SPARC truss structure. All propellant feed lines are 0.5" stainless steel and are kept above the hydrazine freezing point with electrical heaters.

### 5.10.5 RCS Location

The RCS clusters are positioned on trusses mounted to the SPARC main structure at the perimeter of the aerobrake (Figure 5.14). This placement allows for the largest possible moment arms to be created around all three axes, decreasing the impact of center of gravity travel during the mission. The support trusses place each cluster six feet above the aerobrake structure so that the RCS plumes do not interfere with aerobrake skirt and there is minimum contamination from

RCS exhaust. The total moments created by the thrusters and the associated angular accelerations for the heaviest mission at the first burn, are as follows:

| | |
|---|---|
| $Mz_{max}$ = 3540.0 lbf-ft | $\alpha_z$ = 0.7059 deg/sec |
| $My_{max}$ = 1982.8 lbf-ft | $\alpha_y$ = 0.4557 deg/sec |
| $Mx_{max}$ = 3001.0 lbf-ft | $\alpha_x$ = 1.1240 deg/sec |

### 5.10.6 RCS Operation

All RCS packs are left in an inert condition during vehicle delivery to the Space Station and remain inert while the vehicle is docked. Upon leaving the Space Station, all isolation valves are opened to fill the system with propellant. Regulator valves maintain the correct nitrogen pressure, and thruster valves maintain correct thruster pressure. After a mission, the isolation valves are closed and the thruster valves are opened to flush the feed lines and thrusters of any residual propellant.

Figure 5.15 Reaction Control System Schematic

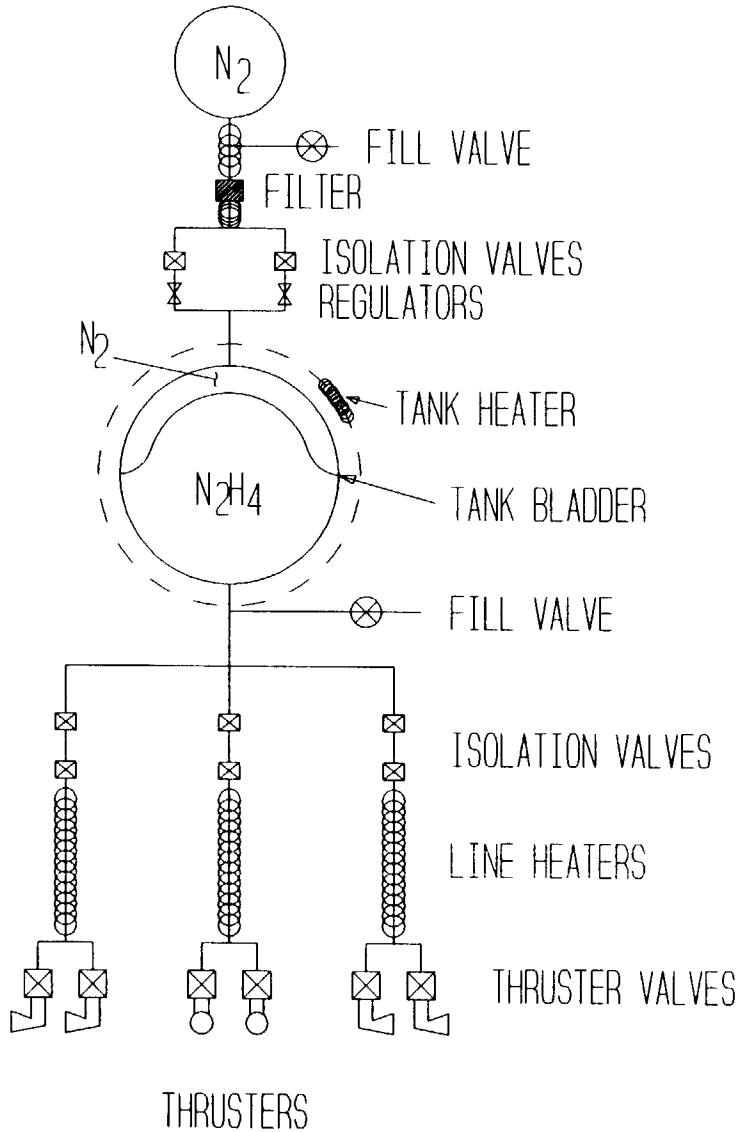

# Chapter 6

# Structures

*6.1 Introduction*
*6.2 Materials*
*6.3 Main Truss Structure*
*6.4 Structural Analysis*
*6.5 Payload Accommodation*
*6.6 Tank Support*
*6.7 Docking*

PAGE 78 INTENTIONALLY BLANK

PRECEDING PAGE BLANK NOT FILMED

## 6.1 Introduction

The vehicle structure includes the design of the truss support structure, payload bays, tank support, and crew module. The structure is self-supporting and independent of the aerobrake. Truss support design considers high strength-to-mass requirements, the shape of the aerobrake, and the orientation and position of all vehicle components. Design of the payload bays includes consideration of volumetric requirements, attachment to the vehicle structure and removal when the vehicle is docked. Tank support design considers space restrictions and applied loads, and design of the crew module considers protection of crew and equipment, life support, guidance, and communication. All components were analyzed to ensure that loads and deflections were within the material limits.

## 6.2 Materials

In the design of the truss support structure, three materials were considered: boron-aluminum, graphite-polyimide, and boron-epoxy. All three of these are fiber-reinforced composites, superior to the now obsolete whisker composites and monolithic aluminum materials that have been prominently used in the aerospace industry. Specifically, boron-aluminum is a metal matrix (aluminum) composite with a metal reinforcer or fiber (boron). Graphite-polyimide is a thermoplastic matrix (polyimide) composite with a carbon (graphite) reinforcer, and boron-epoxy is a thermoplastic matrix (epoxy) composite with a metal (boron) reinforcer. All three of these materials have high specific strengths and relatively low thermal coefficients.

Several factors were taken into account when deciding what material to select. The truss structure material must posses high ultimate specific strengths in both the longitudinal and transverse directions, as well as high ultimate specific shear strength. Also, thermal expansion is critical where the truss members attach to the aerobrake since the aerobrake backwall temperature is approximately 600° F. These material properties are listed in Table 6.1.

In performing the stress analysis using Static Structural Analysis for Microcomputers (SSAM), all three materials were considered and graphite polyimide produced the smallest mass while ensuring a sound structure. It was therefore chosen for use on the SPARC. It should be noted that SSAM is configured for monolithic materials so that the transverse properties of the composites could not be considered. Boron-aluminum does have higher transverse properties than graphite polyimide, but this is neglected since the structure is designed such that the largest load components are directed in the longitudinal direction.

Graphite polyimide has two other significant advantages over boron aluminum. It has a much lower coefficient of thermal expansion, and there is a continuous material boundary between the aerobrake and the main structure since the aerobrake is also made of graphite polyimide. If boron aluminum is used large thermal stresses would occur at the brake-structure interface due to the discontinuity in thermal coefficients between the two materials.



PAGE 80 INTENTIONALLY BLANK

PRECEDING PAGE BLANK NOT FILMED

Table 6.1 Material Properties

| Property (at 200 °F) | Bo/Al | Graphite Polyimide | Boron/Epoxy |
|---|---|---|---|
| Coefficient of Thermal Expansion (per °F) | 3.2E-6 | 1.0E-6 | 2.0E-6 |
| Specific (Young's) Modulus | | | |
| Tensile | | | |
| $E(1)/\rho$ | 1.348E11 | 1.319E11 | 1.588E11 |
| $E(2)/\rho$ | 8.986E10 | 0.890E10 | 1.429E10 |
| Compressive | | | |
| $E(1)/\rho$ | 1.348E11 | 1.180E11 | 1.588E11 |
| $E(2)/\rho$ | 4.900E10 | 0.923E10 | 1.429E10 |
| Ultimate Specific Strength (Tensile-Compressive) | | | |
| Tensile | | | |
| $FTu(1)/\rho$ | 8.087E8 | 12.858E8 | 10.798E8 |
| $FTu(2)/\rho$ | 8.169E7 | 3.198E7 | 5.500E7 |
| Compressive | | | |
| $FTu(1)/\rho$ | 7.965E8 | 11.200E8 | 18.600E8 |
| $FTu(2)/\rho$ | - | - | 21.173E7 |
| Specific Modulus (Shear) | | | |
| $G_{12}/\rho$ | 3.472E10 | 0.554E10 | 0.371E10 |
| Ultimate Specific Strength (Shear) | | | |
| $T_{12}/\rho$ | 7.761E8 | 9.891E8 | 7.940E8 |

(1) Denotes the given property in the longitudinal direction
(2) Denotes the given property in the transverse direction
(3) All numbers are in units of ($in^2/sec^2$) except coefficient of thermal expansion and density which are in units as stated

## 6.3 Main Truss Structure

### 6.3.1 Design Considerations

In designing the truss support structure, there were four areas of consideration: the strength of the structure, the mass of the structure, the simplicity of the frame, and the adaptability of the structure to mission changes. Graphite-polyimide was chosen for the truss structure to meet the high strength and low mass requirements of the design; to further reduce the mass of the structure, it was decided that the truss members be hollow cylinders. For simplicity, all members except for those at the engine mounts have the same cross-section.

### 6.3.2 Truss Frame

To facilitate analysis of the truss structure, as well as assembly and maintenance of the vehicle, the structure must be as simple as possible. Furthermore, since one of the missions does not require an aeropass, considerable thought was given to a removable aerobrake. This requires that the truss structure be self-supporting and stable with or without the aerobrake ribbing and thermal protection structure. The truss structure is designed with the exact shape of the aerobrake to facilitate the connection of the two.

The main structure consists of eight truss networks running the length of the vehicle in the thrust direction and four running perpendicular to the thrust direction (Figure 6.1). Section views of the aerobrake at each truss network are shown in Figure 6.2. The structure is fitted to the shape of the aerobrake, and the members on the vehicle plane are connected to the members on the inner aerobrake surface by vertical members (indicated by vertical dimensions in Figure 6.2B and 6.2C). Truss networks are placed to provide maximum support of the tanks and payload.

Additional support for the payload is provided by two transverse trusses in the vehicle plane located 7.5' and 12.5' behind the centerline of the aerobrake. There are also two additional transverse trusses to support the engine mount structure, located 16' and 17' behind the aerobrake centerline. The engine mount structure is a pyramid configuration consisting of 5 members. The point at which they connect is 6.7' above the vehicle plane and is where the engine mount plate is bolted to the structure. The total mass of the truss structure is 1095 lbm.

## 6.4 Structural Analysis

The structural analysis performed on the main truss structure was done with the aid of the software system SSAM. This software, written by B.J. Korites, is based on the direct stiffness method, or displacement method, which involves writing an equilibrium equation for each of the degrees of freedom. Specifically, this method produces a set of linear algebraic equations that are symbolized in general matrix form as follows: [k][x]=[f], where [k] represents the stiffness matrix, [x] the degrees of freedom, and [f] the applied loads. In general, three major assumptions are employed by this theory. First, the geometry of the structure is essentially the same after deformation takes place, implying small structural displacements. Second, stress levels cannot

exceed the elastic limit, so only linearly elastic materials were used. Lastly, inertial forces are absent, so only static problems are considered. Though the aerobrake is a dynamic vehicle, this method is reasonable for a simplified analysis of the structure as a whole. Two further assumptions are required for the stiffness matrix [k]. First, shear distortions of each element are small compared to bending, axial, and torsional distortions; second, the elements are prismatic and only simple beam theory applies.

In designing the structure using SSAM, thrust, drag and thermal loadings were taken into account. The thrust loading was modeled using the 20,000-lbm scenario with a maximum g-loading of 1.32. A 10° gimball angle was assumed and added to the 8.4° mount angle to determine the vertical and horizontal components of the load which was applied to the engine mount structure. The drag loading was modeled using the Cp distribution and distributing the maximum atmospheric drag across the aerobrake surface. Thermal loads were also modeled, and the results were combined with the thrust and drag into two additional models: thrust-thermal and drag-thermal.

There are 105 nodes (joints) present, creating a possible 630 degrees of freedom (6x105). If all degrees of freedom (DOFs) are free, however, the program produces singularities in the matrix and is unable to run. In order to avoid this problem and decrease computer time, it is necessary to reasonably restrict the total number of DOFs to 159. The restrictions on the DOFs are as follows: the rotation of all 105 nodes was fixed and the displacements in each coordinate direction for the 52 nodes which attach the structure to the aerobrake were fixed. Rotation is not permitted since truss elements are not capable of transmitting or resisting moments, but they are capable of transmitting and resisting axial tension and compression.

It was found that the combined thrust-thermal model produced the largest deflections. Several runs were completed with varying member thicknesses in an attempt to optimize the thickness, and using a factor of safety of 1.5, the maximum deflection of any node was 0.04" (occurring at the engine mounts).

### 6.4.1 Truss Element Description

The final truss structure consists of 215 graphite polyimide hollow cylindrical members and 105 joiners. Due to the greater loadings present at the engine location, the 18 engine mount members have a thickness about four times that of the other members, which ensures adequate structural strength. A typical truss member is shown in Figure 6.3 with its corresponding cross section. The engine mount members are similar to the one shown except the thickness is 0.89" producing almost a solid cylinder.

### 6.4.2 Joint Description

Each truss member is fitted to a titanium silicon carbide (Ti-SiC) joiner which connects several members. The most common connection consists of a five member connection and is shown in Figure 6.3. Each member is connected to the joiner by two Ti-SiC shear pins which are oriented

Figure 6.1 Truss Support Structure (Top VIew)

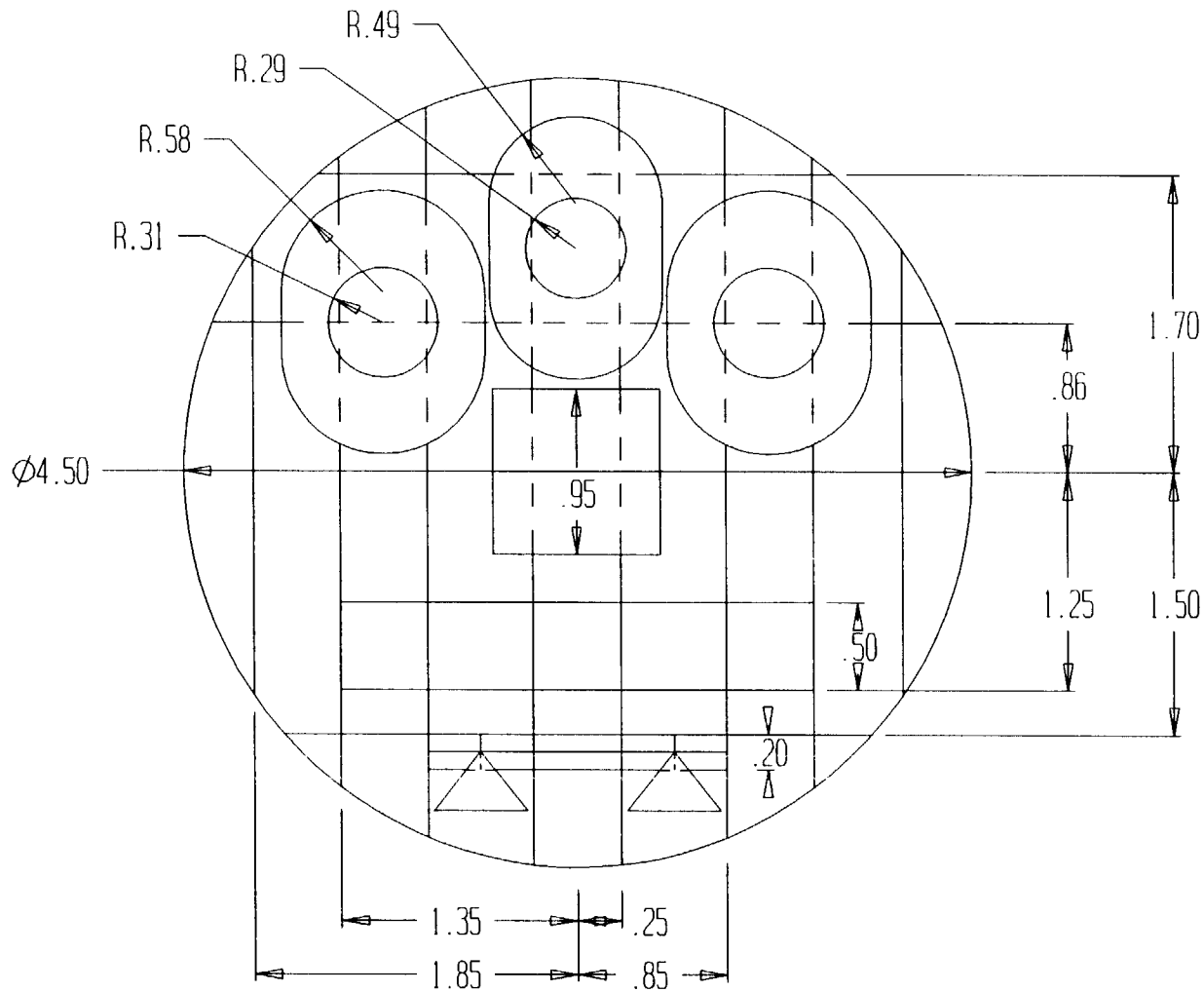

# LOCATIONS OF SECTION VIEWS

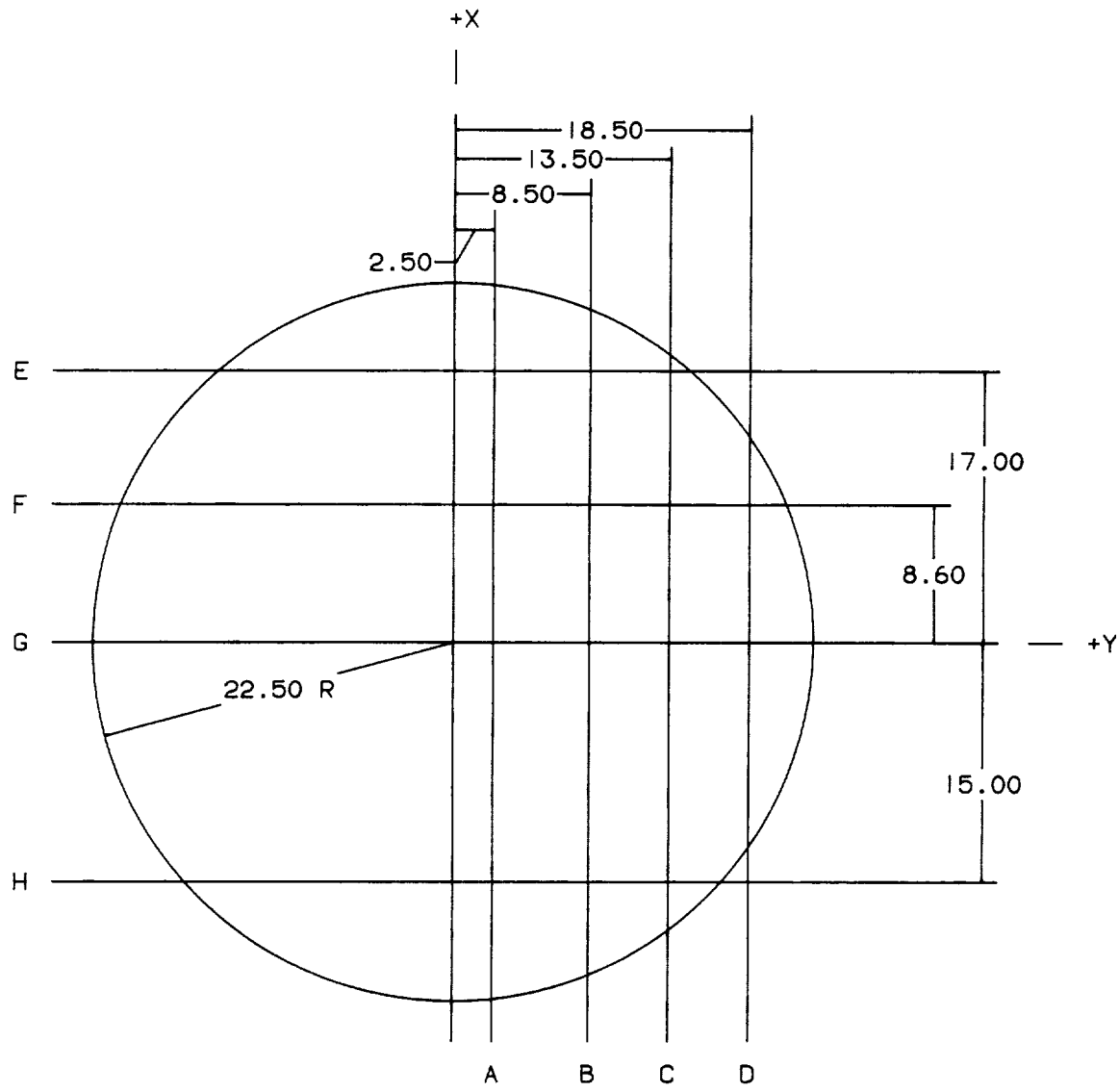


ALL DIMENSIONS IN FEET

SECTION A

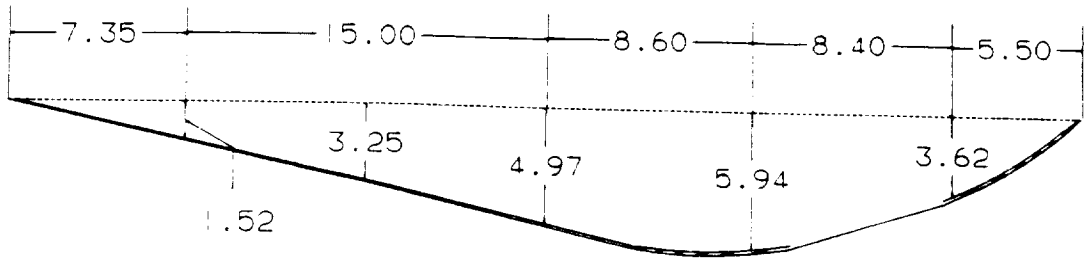


SECTION B

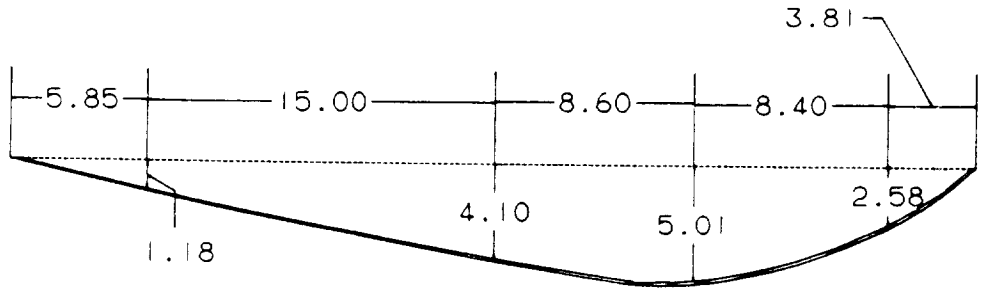


SECTION C

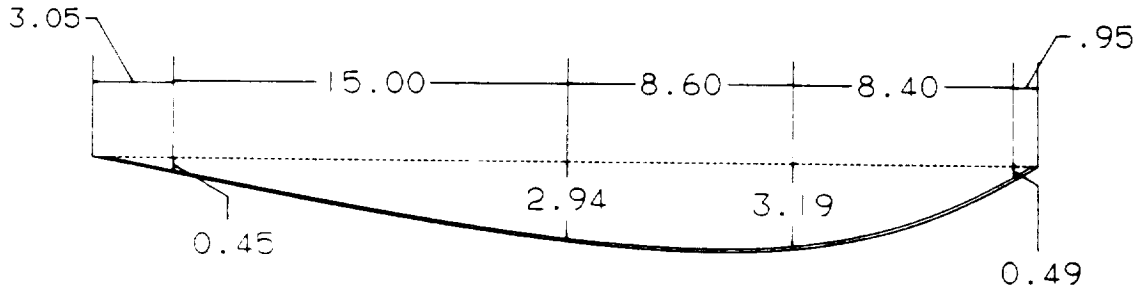


SECTION D

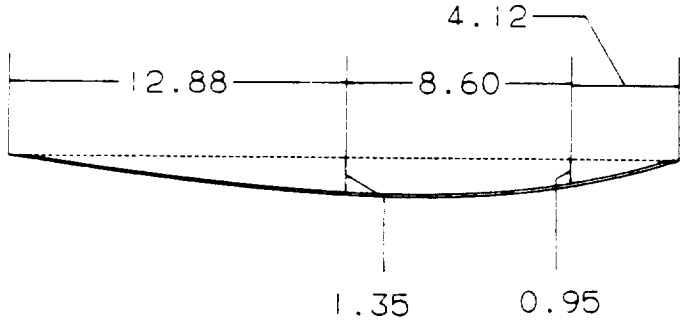




ALL DIMENSIONS IN FEET

SECTION E

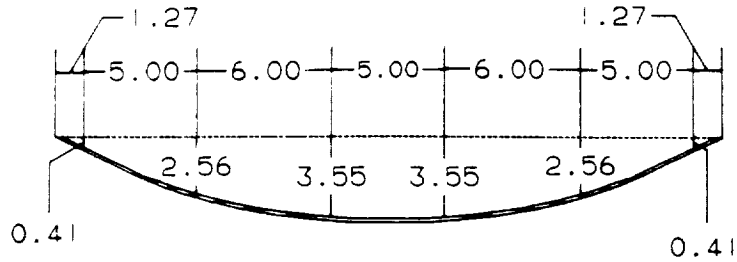


SECTION F

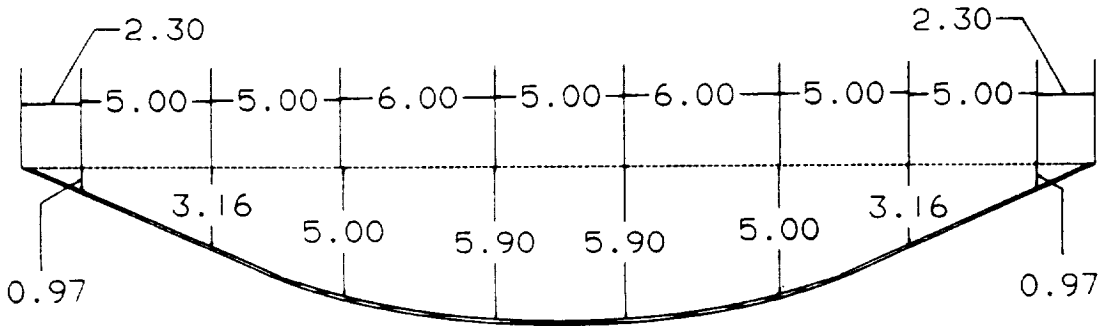


SECTION G

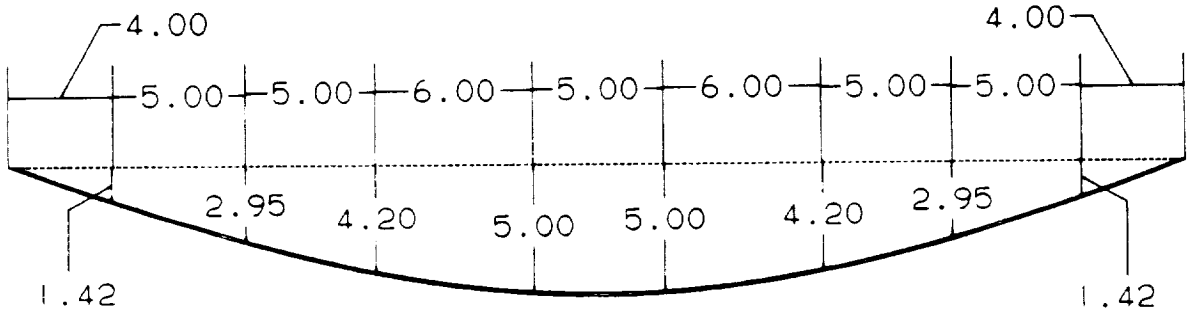


SECTION H

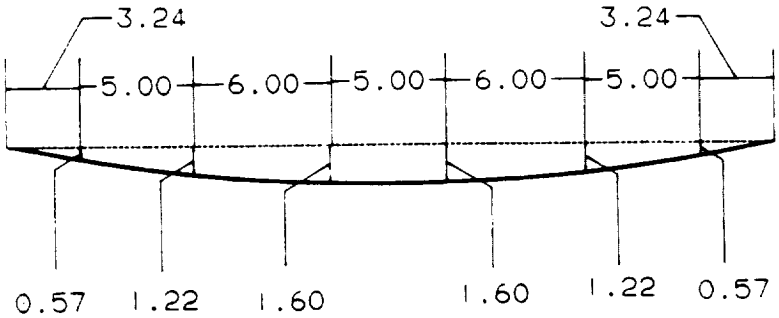




ALL DIMENSIONS IN FEET

Figure 6.3 Typical 5-Member Joiner

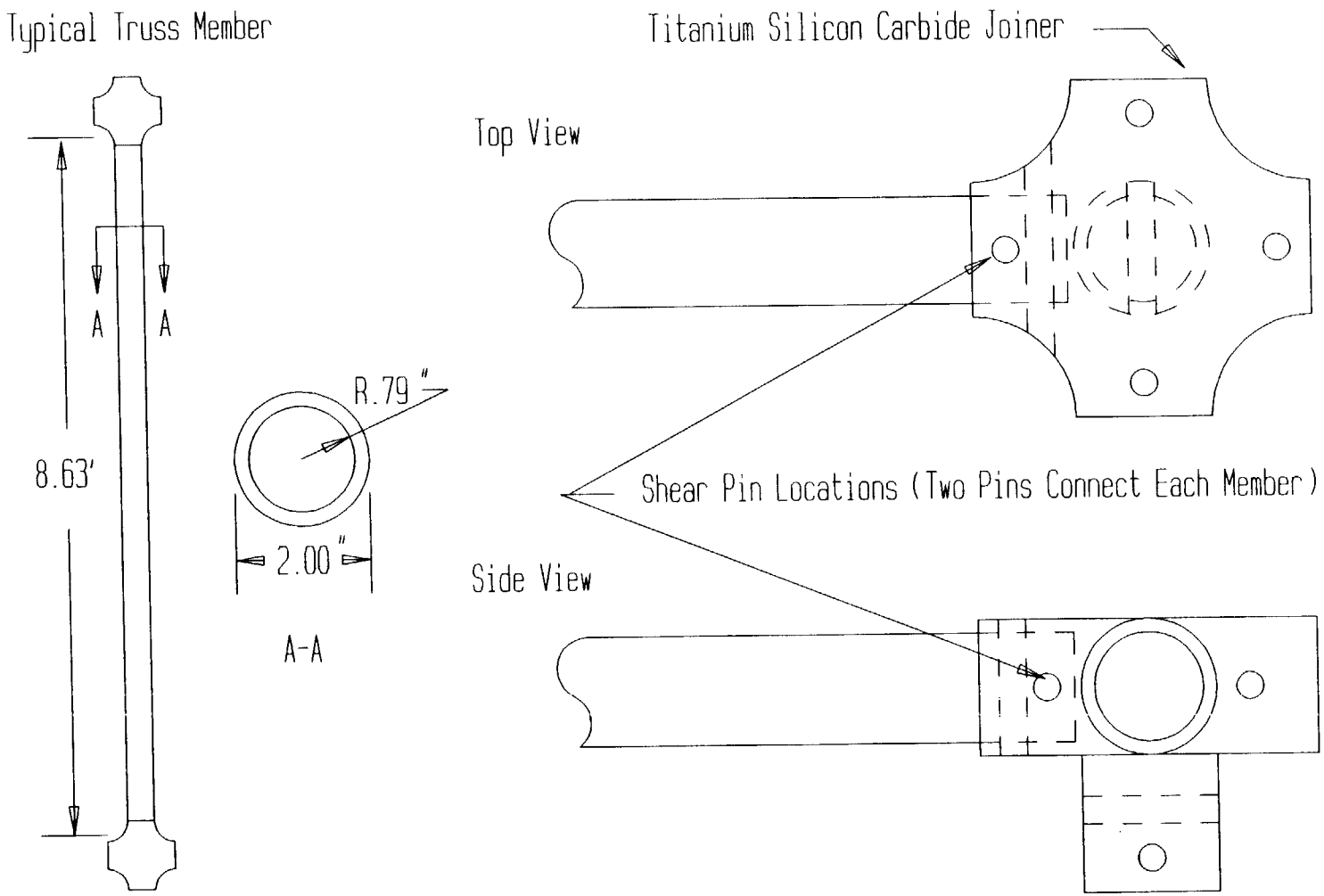

perpendicular to each other or at angles, if needed. Since other node points have their own unique geometries, other joiners similar to the 5-member joiner were made for the 3 and 7-member conjunctions.

### 6.5 Payload Accommodation

The three payload requirements are: 6,000 lbm, 20,000 lbm, and 28,000 lbm, and it is desirable that the same vehicle be able to accommodate all three missions. Initially, the payload was "strapped on" to the truss structure; however, it was determined that without adequate protection, the payload might be damaged by space debris or docking maneuvers. Therefore, a payload bay was designed with a standard size such that one would be necessary for the 6,000-lbm mission, two for the 20,000-lbm mission, and three for the 28,000-lbm mission. The maximum mass that one bay must accommodate is therefore 10,000 lbm.

The volume of the bays was determined using the mass-to-volume ratio of the Space Shuttle payload bay: 6.13 lbm/ft$^3$; therefore a 10,000-lbm payload requires a volume of 1,631 ft$^3$. A circular cylindrical shape was initially considered because of its high resistance to stress and deformation; however, when three bays are used for the 28,000-lbm mission, their length exceeds space limitations. A rectangular bay satisfies spacial requirements, and was therefore chosen with the outer dimensions being 14.67' long x 10' wide x 13.15' high.

Two different designs were considered for meteoroid protection: a single layer and two separated layers. It was determined that to adequately protect the payload, a single layer would require more material and therefore more mass than two layers, so the latter design was implemented. Each layer is made of aluminum-boron; the outer layer is 0.04", and the inner layer is 0.037". The total skin mass is 929.5 lbm.

Structural support was designed for a 10,000-lbm payload at the maximum loading condition of 1.32 g's during thrusting and using a factor of safety of 1.5. A standard I-beam graphite polyimide stringer arrangement was analyzed with SSAM, and based on the results, the optimum size and placement of the stringers were determined (Figure 6.4). Total stringer mass is 726 lbm, and total payload bay mass (empty) is 1,655.6 lbm. The maximum normal stress calculated by SSAM is 1.27 x 10$^7$ lbf/ft$^2$, well within material limits.

The payload can be attached at any node along the middle stringer that spans the 14.67'x 10' section. This allows for adjustable placement of the payload center of gravity to accommodate the stability requirements during aerobraking. Attachment points will be placed at every node on the middle stringer.

The payload bays are attached to the vehicle truss structure at four points with a ratchet-type connection. Similarly, four ratchet connections are located on top for payload bay removal and positioning when the vehicle is docked (Figure 6.4).

Figure 6.4 Payload Structure

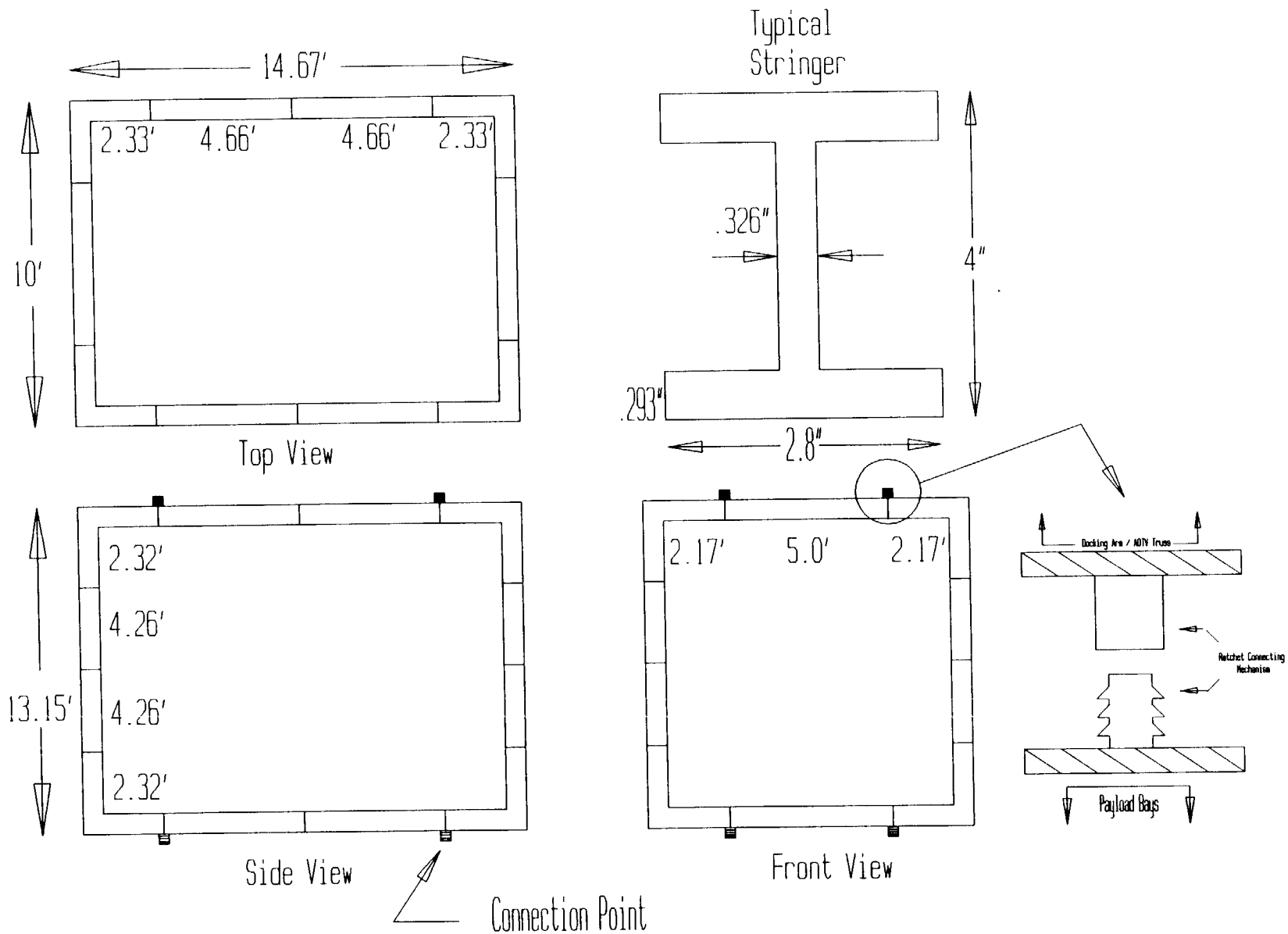

## 6.6 Tank Support

The propellant tank support structure must provide rigid support for the main and auxiliary tanks while being simple and compact due to space limitations between neighboring tanks. To reduce the complexity of the tank support design, it is assumed that all support members of the frame will be of the same cross-section. The main tank support structures consist of several transverse octagonal sections held together by eight longitudinal beams that run down the length of the tank (Figures 6.5 and 6.6). Placement of the transverse sections is limited by the location of the vehicle's underlying truss network, and points of attachment to the vehicle are shown. All beams are hollow circular cylindrical rods made of graphite polyimide. This material was chosen for its high strength-to-mass and rigidity-to-mass ratios.

Structural analysis on each support was performed using SSAM. The cross-sectional area of the members was initially estimated, and using the results of the stress analysis in conjunction with the axial and buckling failure criteria for graphite polyimide, adjustments were made to the support structure design and the cross-sectional area. This iterative process continued using a factor of safety of 1.5 until a minimum cross-sectional area was found. The support structure was designed for the maximum loading of 1.32 g's during thrusting for the 20,000-lbm mission, and results of the stress analysis are given in Table 6.2.

Figure 6.5a Oxygen Main Tank Support

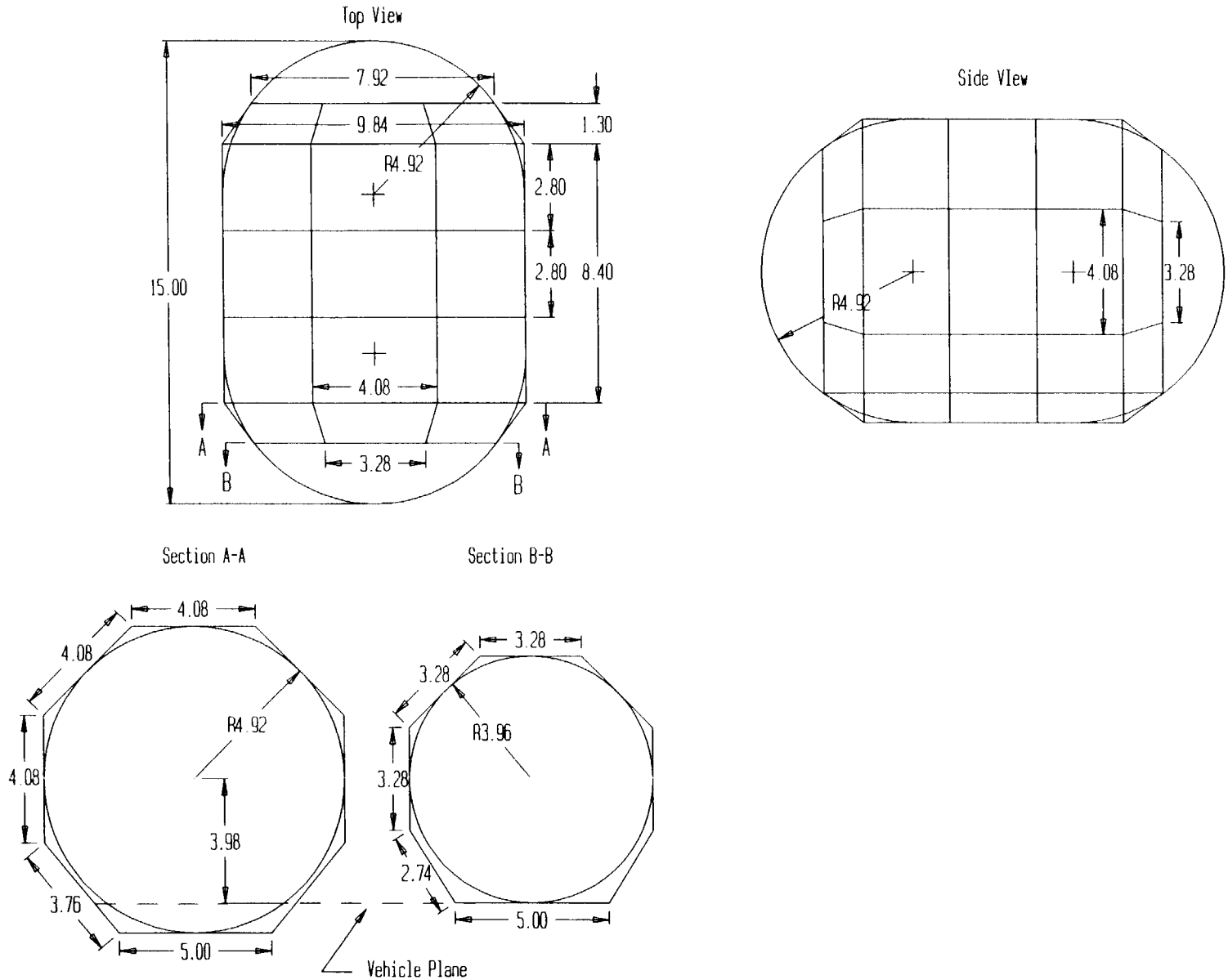

# Figure 6.5b Oxygen Auxiliary Tank Support

Tank Support: LO2 Auxiliary Tank

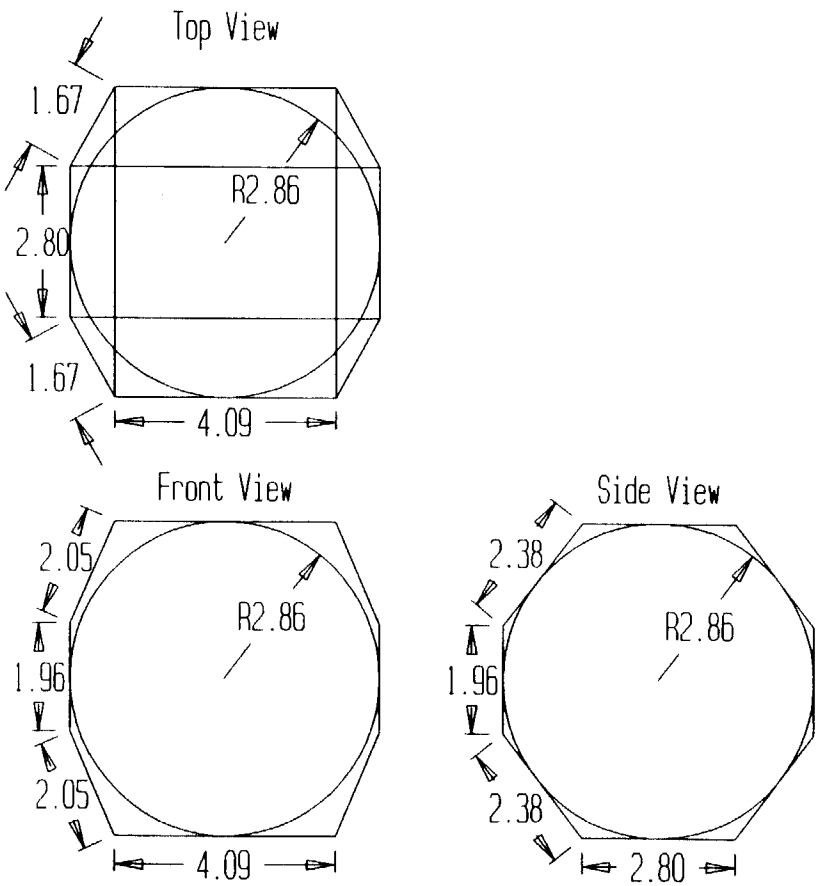


Main-Auxiliary Tank Assembly

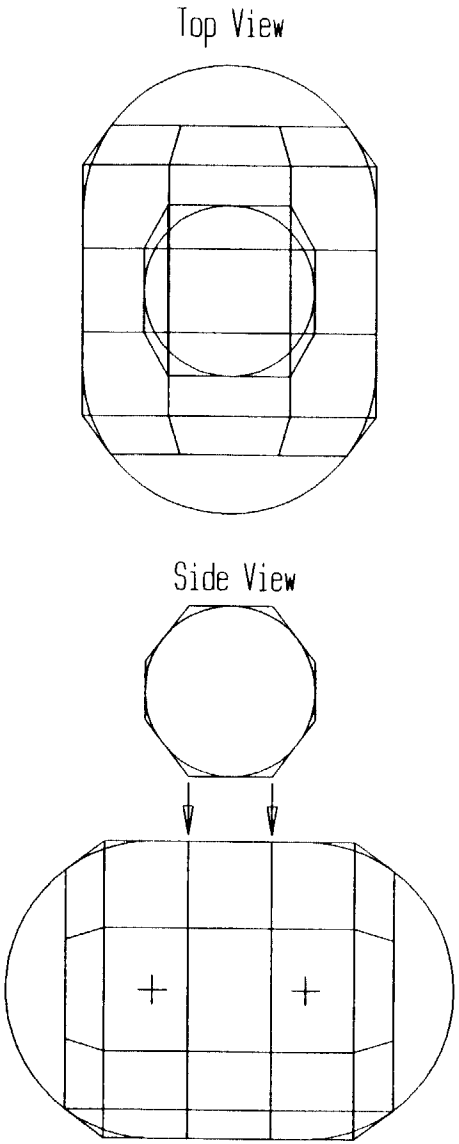

Figure 6.6a Hydrogen Main Tank Support

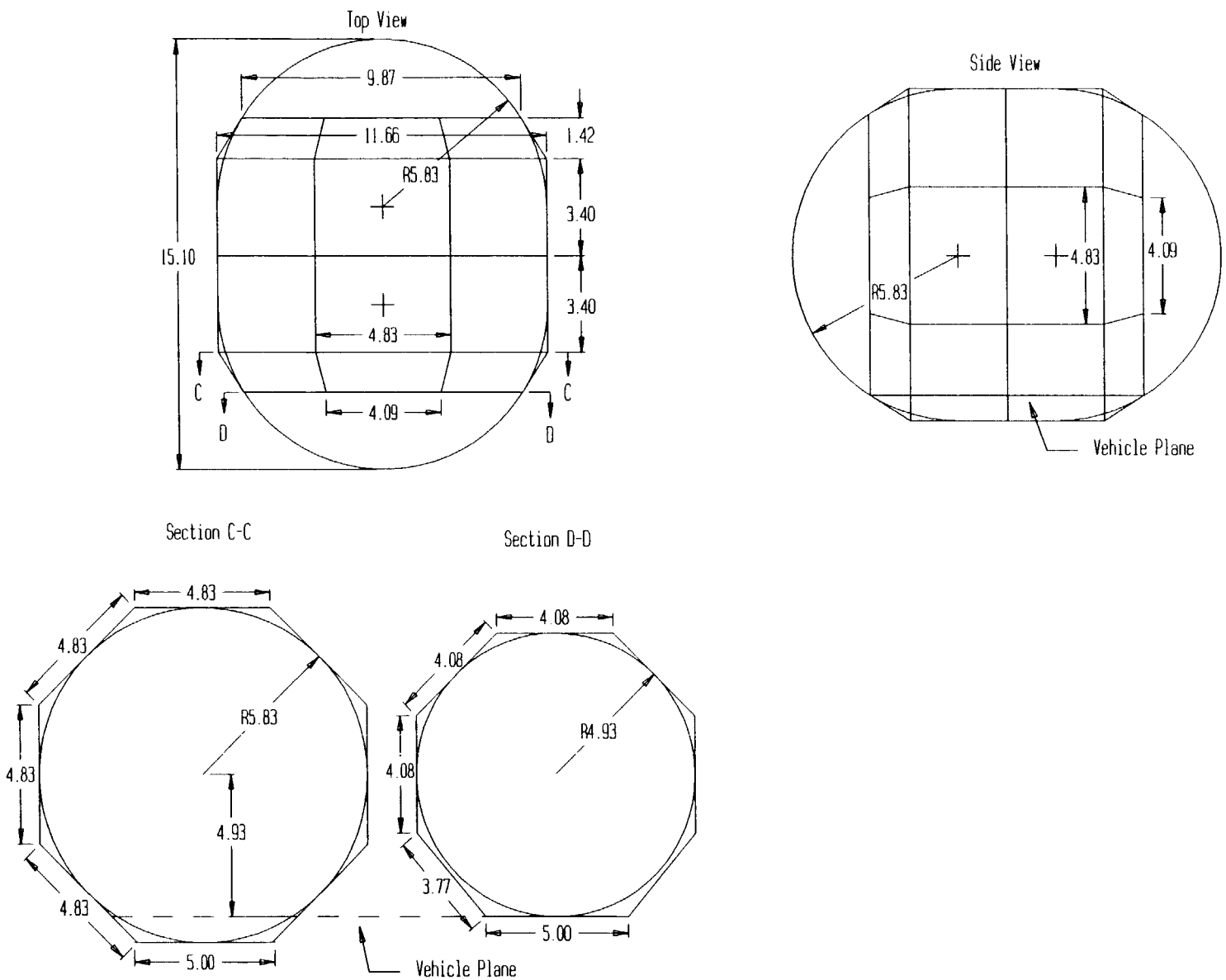


C-2

# Figure 6.6b Hydrogen Auxiliary Tank Support

Tank Support: LH2 Auxiliary Tank

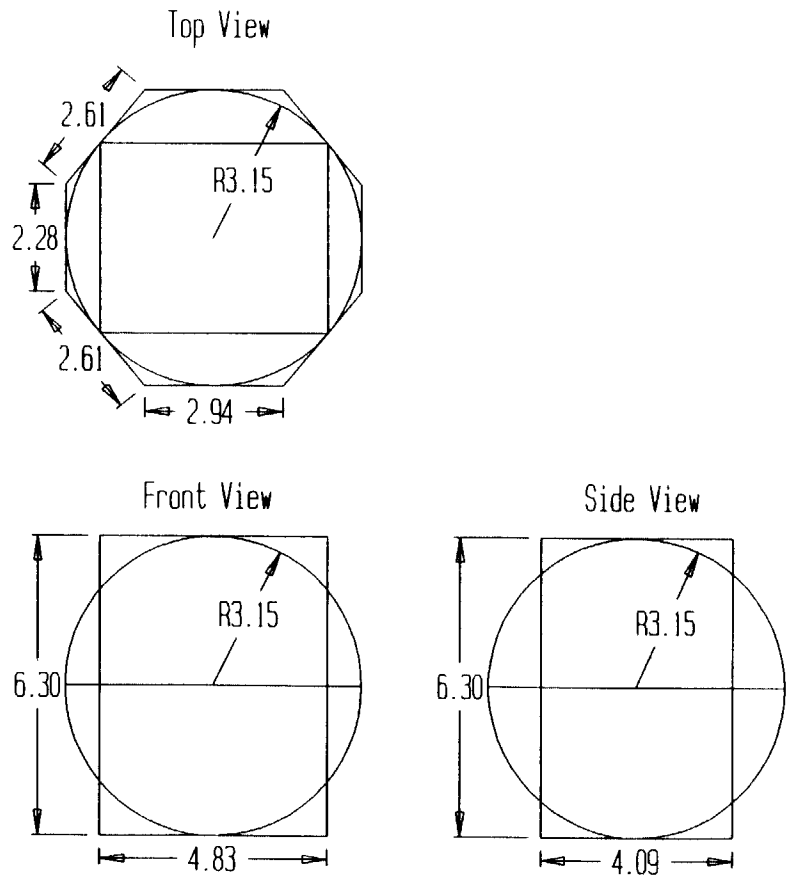


Main-Auxiliary Tank Assembly

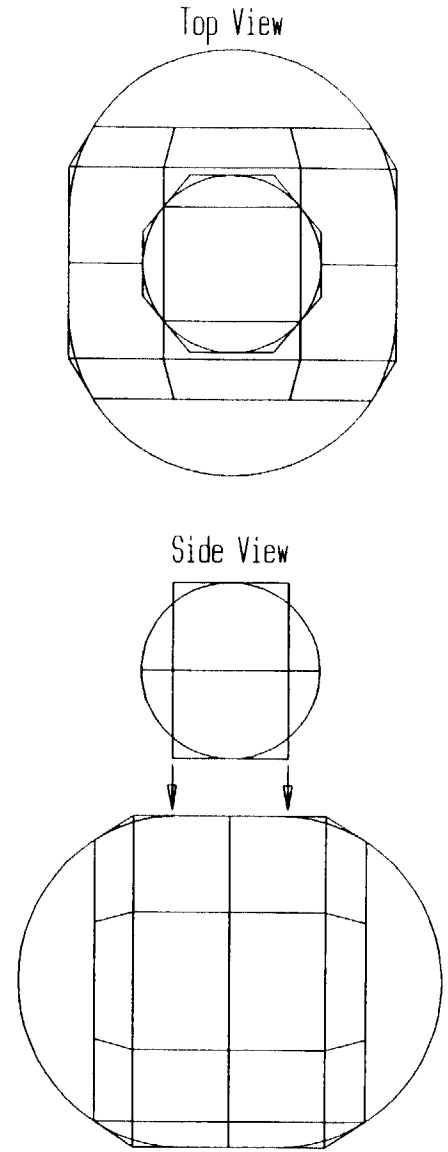

Table 6.2 Propellant Tank Characteristics

| Thrusting (1.32 g, 1.5 F.S.) | | |
|---|---|---|
| $LH_2$ Tank | Tank Support Maximum Deflection | Tank Support Maximum Stress |
| | 0.019031 in | 190.95 kip/in$^2$ |
| Main | Outer Radius | 1.00 in |
| Main | Inner Radius | 0.90 in |
| Main | Area | 0.5969 in$^2$ |
| Main | Total Structural Mass | 116.86 lbm |
| Auxiliary | Outer Radius | 0.50 in |
| Auxiliary | Inner Radius | 0.41 in |
| Auxiliary | Area | 0.2573 in$^2$ |
| Auxiliary | Total Structural Mass | 14.576 lbm |
| $LO_2$ Tank | Tank Support Maximum Deflection | Tank Support Maximum Stress |
| | 0.018656 in | 193.33 kip/in$^2$ |
| Main | Outer Radius | 1.25 in |
| Main | Inner Radius | 0.71 in |
| Main | Area | 3.325 in$^2$ |
| Main | Total Structural Mass | 830.27 lbm |
| Auxiliary | Outer Radius | 1.00 in |
| Auxiliary | Inner Radius | 0.895 in |
| Auxiliary | Area | 0.6251 in$^2$ |
| Auxiliary | Total Structural Mass | 28.63 lbm |

## 6.7 Docking

The purpose of this section is to describe a feasible docking scenario which will provide for safe removal of the crew and payload while remaining compatible with the Space Station. Further design constraints include allowance for vehicle maneuverability and the of serviceability of all components. Adaptability to future space missions is also desired.

Assumptions inherent in the design are the presence of an airlock on the Space Station and on GeoShack for crew removal and a hangar on the Space Station to store and protect the vehicle from material degradation. Further assumptions based on structural limitations include a maximum moment on the docking arms of 1000 ft-lbf torque, a maximum impact velocity of 0.38 fps, and zero angular velocity. Zero angular velocity will also greatly decrease the fuel requirements of the RCS.

The general scenario consists of the maneuvering of the vehicle into the docking area, attachment to a structural support arm(s), removal of payload and crew, detachment of the aerobrake when necessary, and vehicle storage. Maneuvering of the vehicle is accomplished by the use of the RCS which was designed to provide movement in the negative z-direction.

Three configurations were initially considered, the primary difference being the direction from which the structural support arms attach to the vehicle: from the bottom, side, and top. In each configuration, the support arms attach at three points, equally spaced around the aerobrake perimeter to ensure adequate support.

The bottom orientation consists of a fixed arm which is attached to the front of the vehicle structure and two retractable arms which attach toward the rear. The payload and crew module are removed from the top with the use of a retractable, offloading arm which then transports its cargo to a desired location by way of an electrical track system. The scenario for the top orientation is the same with the exception that both the structural support arms and the offloading arm access the vehicle from above. The side orientation consists of a single arm that attaches at three points and has the ability to rotate and retract. The payload and crew module are removed in a manner similar to the other scenarios.

The bottom orientation was discarded primarily due to the fact that truss structure is required above, beside and below the vehicle, whereas the top and side configurations only require truss structure above the craft to support the entire operation. The side orientation was discarded due to the weakness of the structural support arm. Too much movement and too many joints were required for the arm to be designed efficiently. Due to these and additional considerations, the top orientation was adopted.

### 6.7.1 Final Docking Scenario

The final configuration, (Figure 6.7), consists of a 29' fixed structural support arm and two retractable arms. The fixed arm locks to the truss structure directly in front of the $LO_2$ tank, and the retractable arms attach to the rear of the vehicle at an 18° angle from the vertical allowing adequate room to remove the payload and crew module. Component removal and vehicle servicing is accomplished with a retractable offloading arm which moves on an electrical track along the vehicle y-axis, situated on a truss section that moves along the vehicle x-axis (Figure 6.8).

Figure 6.7 Docking (Side View)

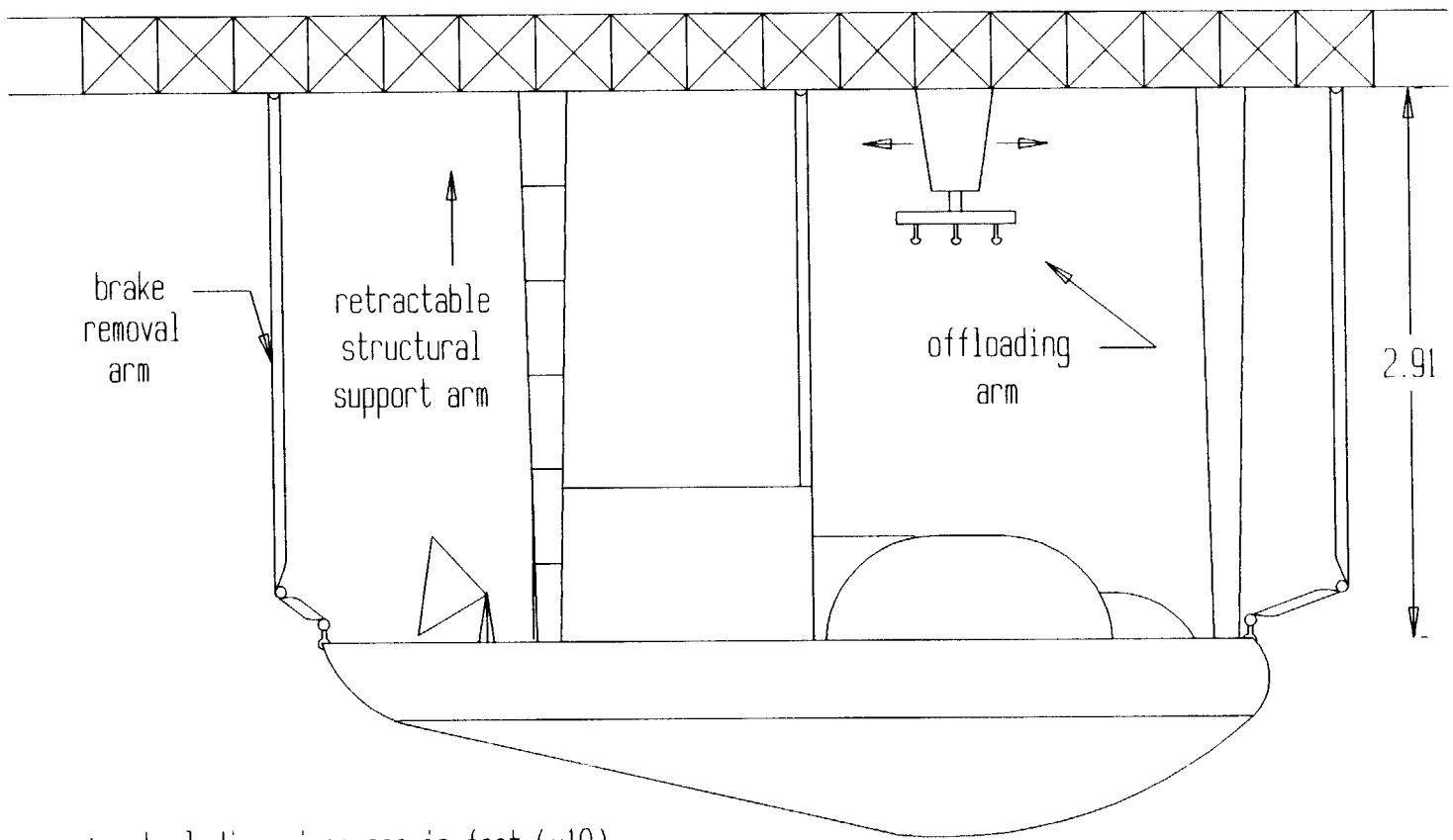


* actual dimensions are in feet (x10)

Figure 6.8 Docking (Top View)

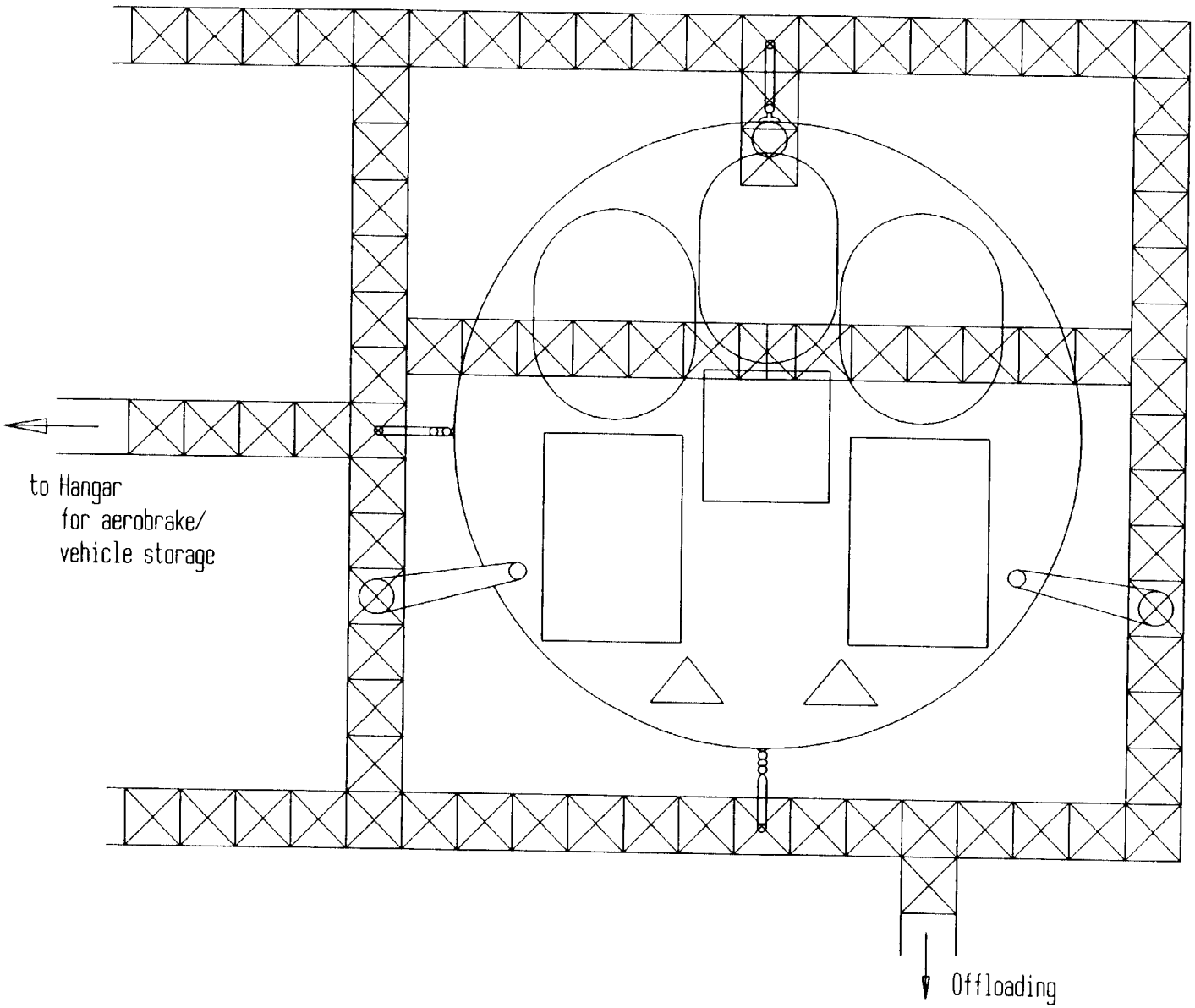

The offloading arm is also capable of maneuvering the airlock, stored on the Space Station and on GeoShack, into position over the crew module. The airlock seals to the crew module providing for crew exit without removal of the module itself, and it is sealed with a double-ring system for redundancy. Rubber seals on both the airlock and crew module connect, and an inflatable ring is released which conforms to all surfaces. Similar seals are present in the hatch doors on both the crew module and the airlock, and the vacuum remaining between the hatch doors is vented into the airlock prior to crew exit.

In the event of an expendable mission, or if servicing is necessary, the aerobrake can be removed by four small attachment arms. Three are initially attached to the skirt of the aerobrake in the front, rear, and on one side of the vehicle. The aerobrake is then released, moved toward the hangar; once it has cleared the vehicle, the fourth attachment arm is connected to the unsupported side. These same arms can also transport the entire vehicle to the hangar if removal of the aerobrake is not required (Figure 6.9).

Figure 6.9 Docking (Rear View)

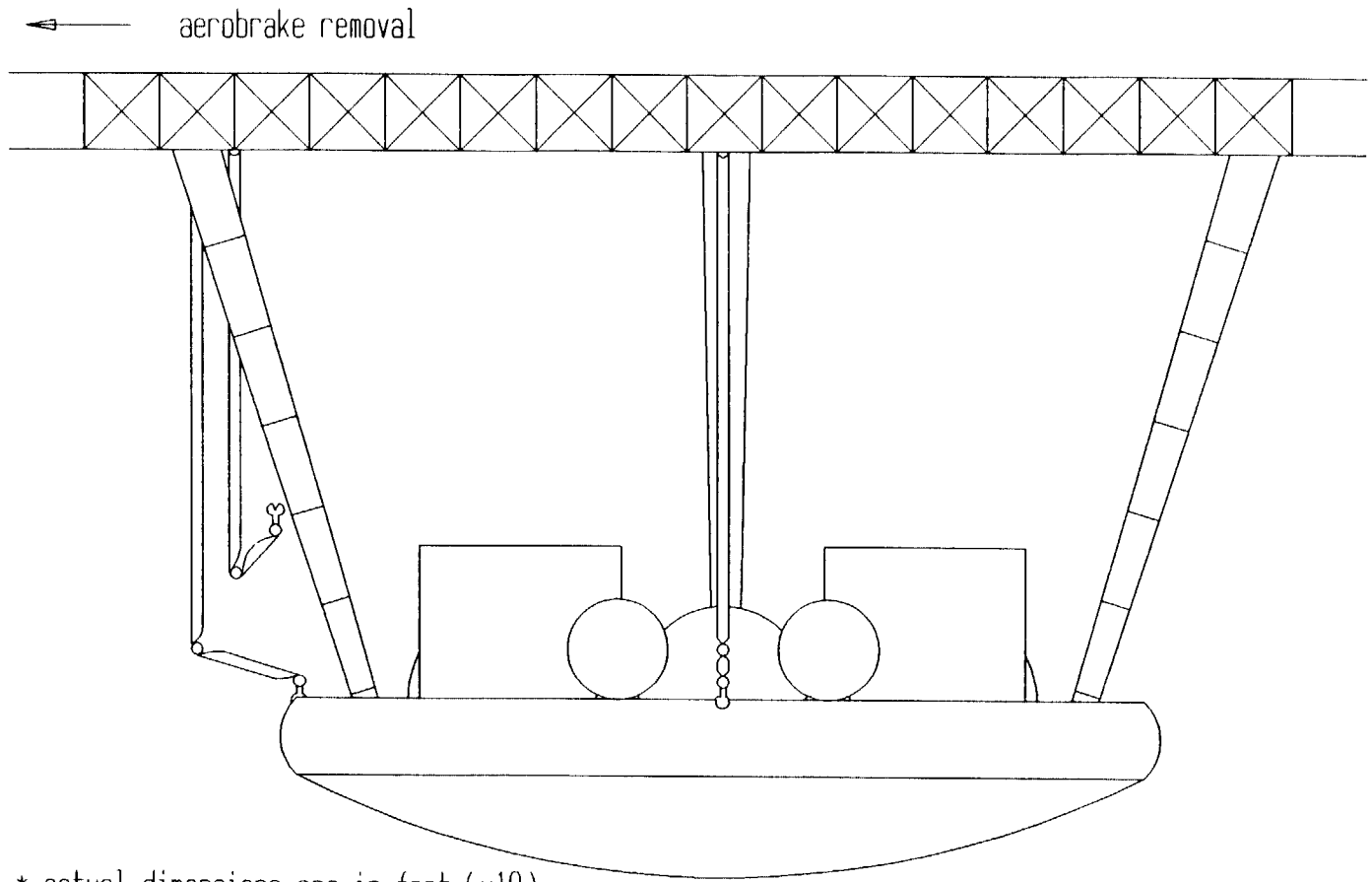


* actual dimensions are in feet (x10)

# Chapter 7

# Crew Module

*7.1 Introduction*
*7.2 Cabin Environment*
*7.3 Atmospheric Control System*
*7.4 Interior Design*
*7.5 Extravehicular Activity*
*7.6 Hull Structure*
*7.7 Pressure Shell*
*7.8 Insulation*
*7.9 Radiation Protection*

## 7.1 Introduction

Success of manned space flight requires that the crew be protected from potential environmental hazards as well as being provided with the materials required for life support. The crew cabin must also be sized, equipped and arranged to allow for necessary crew functions both inside and outside the cabin. The nominal manned mission requirements for the vehicle consist of a 5-crew, 2-day mission to and from GEO with a 2-day emergency reserve. A separate mission, called the extended mission, will be able to provide for three crew members over a 4-day mission to and from GEO with a 2-day emergency reserve. The total cabin mass is approximately the same for both the nominal and the extended missions, which is achieved by adjusting the life support and crew function requirements. The life support system is designed to accommodate the largest mission requirement, eliminating the need for two different systems.

## 7.2 Cabin Environment

The cabin conditions are the same for both the nominal and extended missions. The artificial environment consists of: pressurization, atmospheric composition, temperature, and relative humidity. Crew comfort and a safe livable environment must be provided for the duration of the mission. The nominal cabin environment is as follows:

| | |
|---|---|
| Total pressure: | 14.7 psia |
| Atmosphere: | 80% nitrogen and 20% oxygen |
| Temperature: | 70° F |
| Humidity: | 50% |

The two-gas environment of 80% nitrogen, 20% oxygen at standard sea-level conditions was selected to simulate conditions of both the Earth and the Space Station.

## 7.3 Atmospheric Control System

The Atmospheric Control System (ACS) meets demands for life support, thermal control, $CO_2$ and trace contaminant control, humidity control and pressurization. The ACS is an open system, meaning that none of the life support systems are regenerative. Due to the short length of both missions, a partially or completely regenerative system was not practical.

### 7.3.1 Cabin Atmospheric Pressurization

Due to the absence of an airlock on the crew module, oxygen requirements are greater due to the need for cabin repressurization. For the nominal 5-crew, 2-day mission, the system must provide two repressurizations and one reserve; for the extended mission, the system must provide six chamber repressurizations plus one reserve. The ACS is therefore designed for the limiting pressurization requirements of the extended mission.



PAGE 104 INTENTIONALLY BLANK PRECEDING PAGE BLANK NOT FILMED

Each crew member consumes a maximum of 2.2 lbm $O_2$ per day, so for the extended, 3-crew, 4-day mission with 3-day emergency reserve, a total 46.2 lbm of oxygen is required. The oxygen needed for seven recompressions (10.05 lbm $O_2$ each) with a leakage rate of four lbm/day increases the oxygen required to 144.5 lbm for the entire mission. Similarly, the nitrogen requirements for the extended mission cabin atmosphere come to 432.7 lbm.

The oxygen and nitrogen used by the ACS are stored cryogenically. Operating pressures for the oxygen tank are between 100 and 294 psia, while nitrogen is kept between 124 and 327 psia. For the extended mission requirements, the vehicle carries one oxygen tank and two nitrogen tanks. The cryogenic storage vessels consist of an inner shell and an outer shell lined with superinsulation. The inner shell is a filament wound composite pressure vessel consisting of a thin Al-6061 liner wrapped with Kevlar fibers in an epoxy resin. A simple outer shell of Al-6061 and insulation liner helps insulate the inner vessel as well as protect it from radiation. The dry mass summary estimates for the atmospheric storage tanks are as follows:

Table 7.1 Mass Summary of Atmospheric Storage Tanks

| | Oxygen (lbm) | Nitrogen (lbm) |
|---|---|---|
| Inner Shell | 6.0 | 8.5 |
| Insulation | 18.6 | 27.4 |
| External Shell | 7.0 | 9.0 |
| Internal Plumbing | 15.5 | 15.5 |
| External Plumbing | 3.8 | 3.8 |
| Support | 17.0 | 21.5 |
| Total Dry Mass | 67.9 | 85.7 |

### 7.3.2 Contaminant Removal

Each crew member produces about 2.2 lbm $CO_2$ per day, and since $CO_2$ tends to cause adverse physiological and biochemical effects at high concentrations, it is necessary to keep the partial pressure below 0.0735 psia (1/2% total pressure). Typically, the problem caused by carbon dioxide contamination is solved by chemical absorption. Anhydrous lithium hydroxide, LiOH, was chosen as the $CO_2$ absorbing agent due to its mass advantage over other absorbents.

Trace contaminants such as ammonia, carbon monoxide, ethanol, freon, and methane are emitted by many types of materials, and metabolic contaminants may also be present. For the trace contaminant control system, the cabin implements a combination of chemical absorption and

filtration. The chemisorbent consists of a bed of activated charcoal and one of lead dioxide, backed with a filtration system.

A schematic of the entire ACS is shown in Figure 7.1 and a mass summary is given on Table 7.2. Cabin airflow rate will vary between 45 fpm and 75 fpm with a nominal air flow rate of 60 fpm.

Table 7.2 ACS Mass Summary

| Component | Dry gas flow rate (lbm/hr) | Mass of component (lbm) |
|---|---|---|
| Heat Exchanger | 30 | 37.5 |
| Chemisorbent | 60 | 5.2 |
| Charcoal | 10 | 3.5 |
| Lithium Hydroxide | 60 | 12.5 |

7.3.3 Thermal Management and Control

The metabolic heat rate generated by each crew member is about 0.13 Btu/sec. Additional heat is generated by fans, motors, and control systems; so to maintain a comfortable environment, heat must be removed from the cabin atmosphere. Thermal management involves four main processes: heat transport, heat rejection, thermal storage, and temperature control. Heat transport is be accomplished with pumped liquids and with liquid metal (sodium) heat pipes that operate on a fluid change phase. Heat rejection will be performed by panels which radiate to space the heat that is transported to them, and thermal storage is achieved by transferring the sensible heat to substances contained within a heat exchanger. The heat exchanger is typically a plate-fin, liquid cooled device that transfers the heat of the environment to the cooling liquid. Finally, temperature control is achieved with a valve that governs the control of the thermal fluid in the heat pipe.

## 7.4 Interior Design

The major cabin components (Figure 7.2) consist of: control and display panels, thrusting seats, a commode-urinal / personal hygiene system, a utility storage area that serves also as a safe haven during solar flares, and a whole-body shower system (extended mission). The volumetric allocations for each of these devices are shown in Table 7.3.

Figure 7.1 Atmospheric Control System Schematic

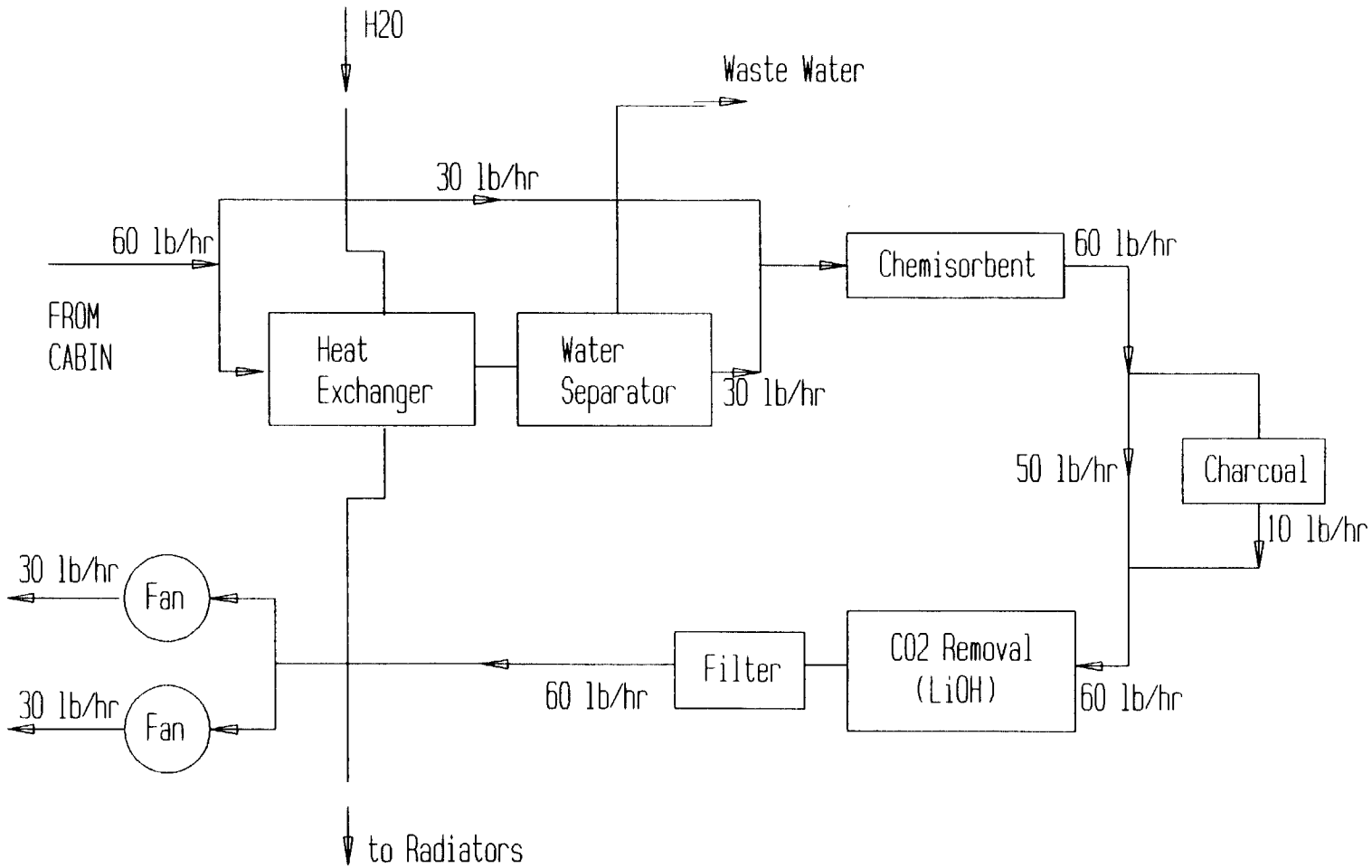

Figure 7.2 Crew Module Interior Floor Plan

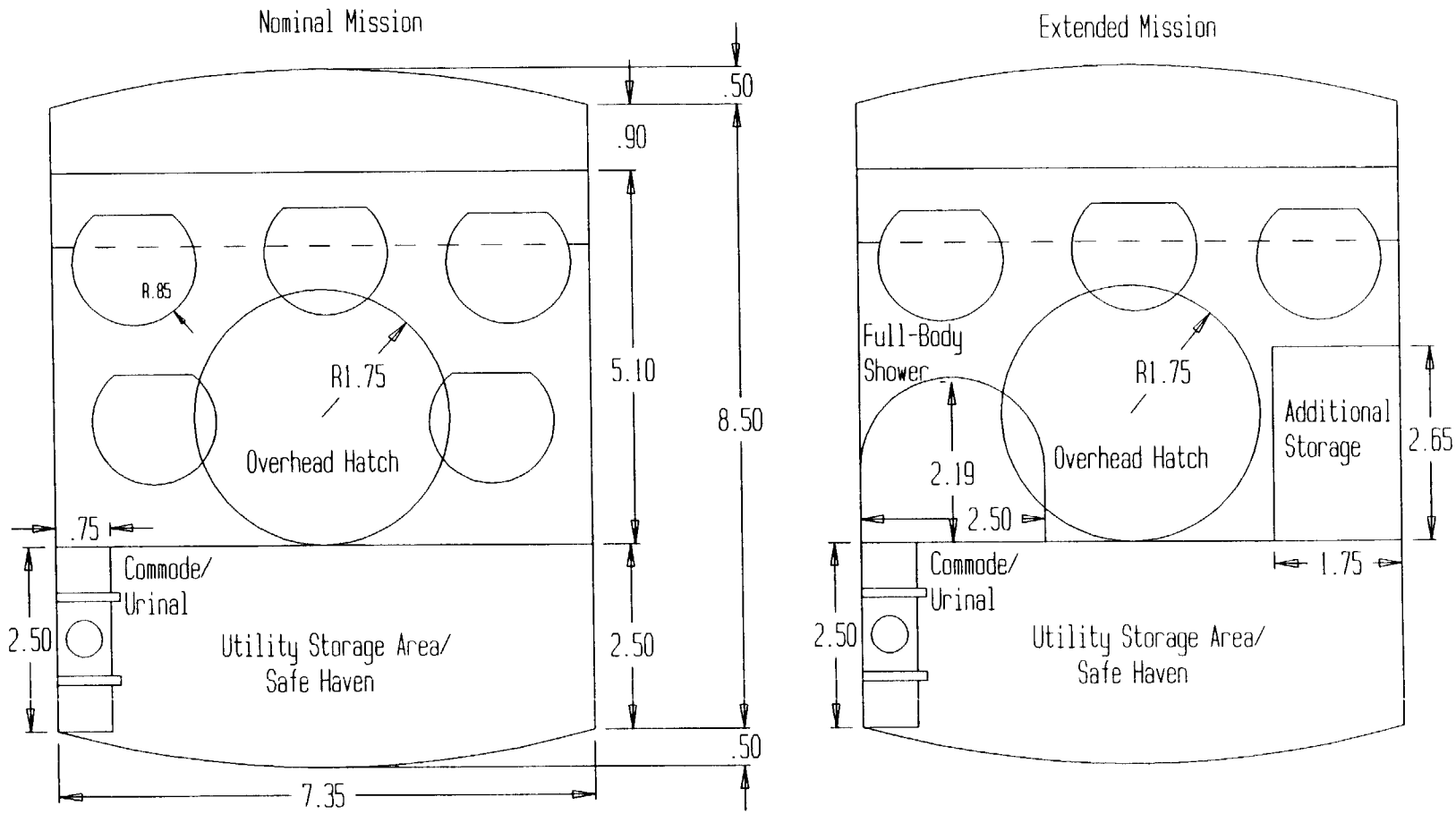

Table 7.3 Volumetric Allocations ($ft^3$)

| | |
|---|---|
| Total Cabin Space | 700.0 |
| Controls / Displays | 70.0 |
| Storage Area / Safe Haven | 160.0 |
| Full Body Shower | 42.7 |
| Commode | 50.7 |
| Personal Hygiene | 36.3 |

## 7.5 Extravehicular Activity

### 7.5.1 Mission Requirements

For SPARC missions, extravehicular activity (EVA) encompasses the servicing and repair of satellites and carrying out of rescue missions in space. EVA has both disadvantages and advantages. Disadvantages include the impaired mobility and visibility of the EVA suits which add to the inherent safety risks of space activity. One advantage of EVA is that it provides physical, mental and sensory adaptability at the work site. It also provides competence when frequent problems and malfunctions arise or when delicate operations are required.

### 7.5.2 Extravehicular Mobility Units (EMU's)

EMU's are designed to provide a completely integrated extravehicular protection system along with maximum astronaut mobility to incorporate the needs of extended EVA. Currently, portable life support systems provide the same support as that of the crew cabin: thermal control, contaminant control, humidity control, pressurization, and communication.

Previous EMU's have required a 5.0-psia atmosphere, but the 14.7 psia mixed gas atmosphere of the crew cabin will require the use of a 8.0-psia hard pressure suit for EVA. Due to the higher levels of radiation at GEO, future EMU's will also require additional shielding. The vehicle will carry one EMU for each crew member on both the nominal and extended missions. The mass of each unit is approximately 40 lbm with an expendable mass of 21 lbm (1-person, 7-hr). The expendable mass consists mostly of the water sublimator/heat exchanger for thermal control and a LiOH canister for $CO_2$ control.

### 7.5.3 Manned Maneuvering Unit (MMU)

The manned maneuvering unit (MMU) provides astronaut mobility and altitude control away from the space vehicle. Propelled by cold-gas jets, these units allows the EVA astronaut to maneuver up to any distant object or satellite for repair and/or retrieval. The mobility of such a

unit makes the device ideal for EVA repair and rescue operations. The SPARC carries two MMU's on the nominal and extended missions.

A device called the MMU Servicer is to be carried on the vehicle for the extended mission only. The MMU Servicer is a tele-robotic manipulator system that has the capability to mate with the MMU for delicate operations, as well as provide a means for performing remote space operations such as satellite retrieval, servicing and maintenance.

### 7.6 Crew Module Hull Structure

The crew module hull structure consists of twelve longitudinal members and four ribs (Figure 7.3). The cross-section of the stringer was designed using SSAM. Both the stringers and ribs were made of graphite-polyimide, due to its plastic properties and high specific strength.

The hull structure consists of 50 stringers: 20 (5x4) that lie on the bottom region of the rib located where the structure attaches to the crew-module support bracket (Figure 7.4). The end caps extend 0.5' out from the cylinder and are each reinforced by two stringers. The other 28 (7x4) stringers lie along the four ribs outside the support bracket region.

The hull was designed using SSAM with a factor of safety of 1.5 at the maximum loading condition of 1.5 g's at an angle of 20° relative to the cylinder's longitudinal axis (10° engine offset plus 10° gimbal angle). The 20° case was the worst case scenario since severe combined loadings in both the transverse and longitudinal directions would occur at this angle. Thermal loading was taken into account in one of the runs, but it was insignificant since the inner skin is insulated from the outer portion of the structure. The maximum deflection of just 0.07" was found to occur at the nodes lying on the top of the structure.

The entire structure consists of 98 nodes and 588 (98x6) degrees of freedom (DOF). However, the number of DOF were reduced to 124 for the SSAM analysis by imposing the following constraints: all nodal rotations were restrained and displacement and rotation of the 20 nodes where the crew module attaches to the support bracket and displacement of the two end cap nodes were restrained. The remaining 76 (98-22) nodes were restrained in the x-direction and the 28 nodes (7x4) on each of the four ribs were restrained in the y-direction. The final run on SSAM demonstrated that the structure was sound and within the ultimate material limits of graphite polyimide for both shear and normal stresses.

### 7.7 Pressure Shell

Materials considered for the pressure shell which houses the crew were: boron-aluminum, graphite-polyimide, and boron-epoxy. A thin-walled pressure vessel analysis using a factor of safety of 1.5 was performed using each of these materials. Boron-aluminum, the chosen material, has the highest density of the three. Yet it still provided the smallest mass because its critical thickness was much smaller than the other two materials.

Figure 7.3 Crew Module 3-D Wireframe

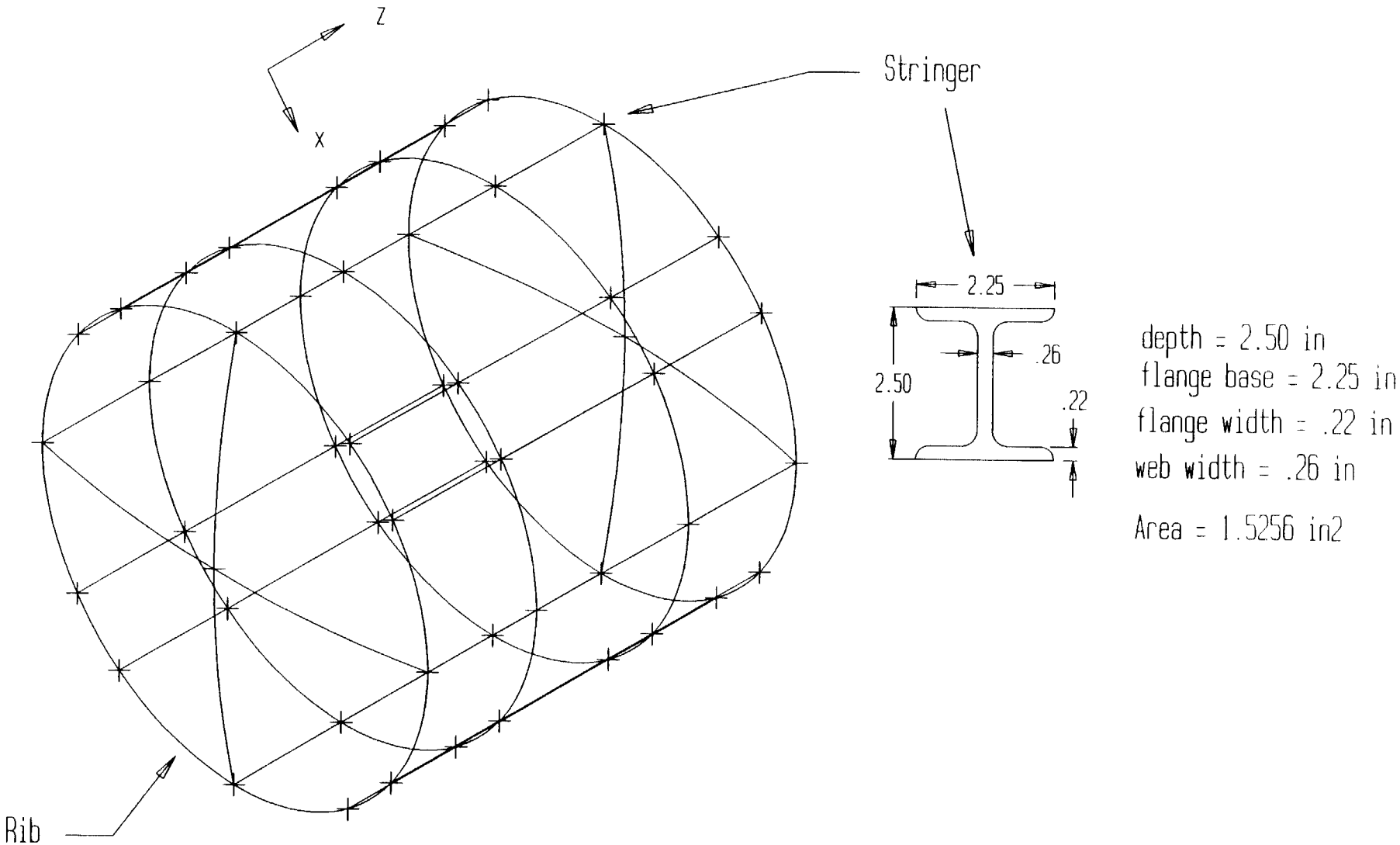

Figure 7.4 Support Bracket

+ denotes crew module attachment location

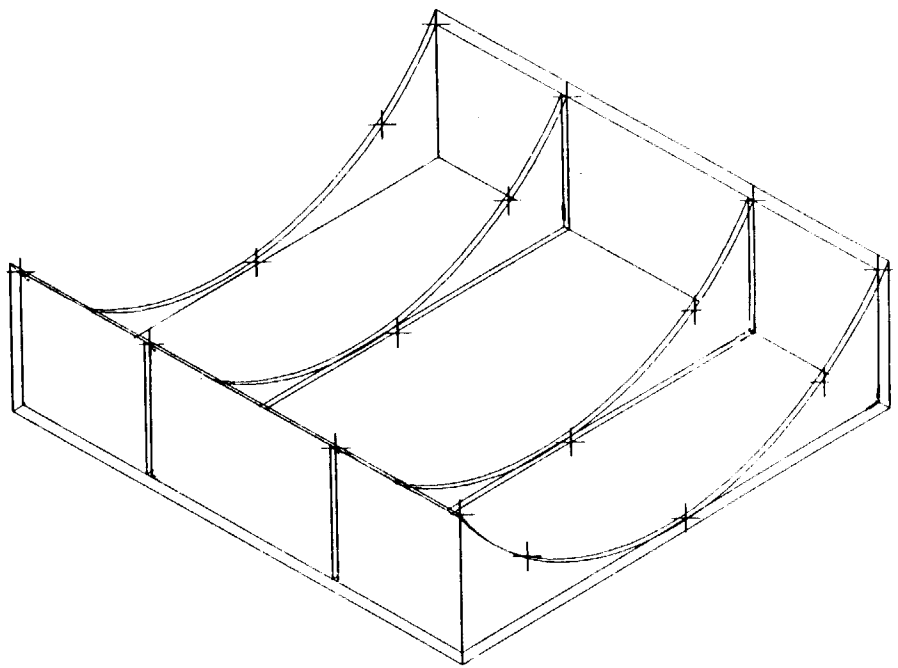

Table 7.4 Crew Module Mass Summary

| | Nominal Mission (lbm) | Extended Mission (lbm) |
|---|---|---|
| **I. Structures** | | |
| Pressure Shell | 124.0 | 124.0 |
| Safe Haven | 951.0 | 951.0 |
| Insulation | 95.0 | 95.0 |
| Outer Shell | 789.0 | 789.0 |
| Stringers / Ribs | 280.0 | 280.0 |
| Support Bracket | 120.0 | 120.0 |
| **II. Life Support** | | |
| $O_2$ Vessel (dry mass) | 67.9 | 67.9 |
| $N_2$ Vessel (dry mass) | 85.7 | 85.7 |
| $O_2$ Requirements | 105.2 | 144.6 |
| $N_2$ Requirements | 217.5 | 423.7 |
| Thermal Heat Control | | |
| Heat Exchanger | 37.5 | 37.5 |
| Radiators (x2) | 19.0 | 19.0 |
| Contamination Control | 33.2 | 33.2 |
| Water Requirement | 68.3 | 152.5 |
| **III. Interior Design** | | |
| Commode Collection | 160.7 | 160.7 |
| Whole Body Shower | ---- | 105.5 |
| Space Suits | 200.0 (x5) | 120.0 (x3) |
| MMU | 640.0 (x1) | 640.0 (x2) |
| MMU Servicer | ---- | 130.0 |
| Seats | 250.0 (x5) | 150.0 (x3) |
| Crew | 850.0 | 510.0 |
| **TOTAL MASS** | 5094.0 | 5139.3 |

## 7.8 Insulation

Within the pressure shell and the outer shell lies a 2.5" gap where the insulation is located (Figure 7.5). This insulation consists of foam backed layers of Kevlar and Multi-Layer insulation and works in connection with the thermal control system to provide standard sea level conditions inside the cabin. The insulation also provides an added protection against meteoroid impact.

## 7.9 Radiation

The two strategies for protecting the crew from radiation are: the light shielding of the entire crew module for protection from moderate radiation and the heavy shielding of a safe haven within the module for protection from more intense radiation. The outer shell and safe haven were designed for the three main sources of radiation that could be encountered during a mission: galactic cosmic rays, the Van Allen Belts, and solar flare radiation.

From cosmic rays, the minimum aluminum shell thickness was calculated using the equation:

$$t = 2.7E\text{-}6\left(\frac{AT}{P}\right)^{1/3}$$

where

A = surface area of the shell
T = mission duration
P = probability of no penetration.

Using a probability of 0.95, the thickness was determined to be 0.0136".

Van Allen radiation involves three particles: protons, electrons, and Bremsstrahlung photons, high energy particles mainly produced from electrons. Three equations corresponding to each of these particles were used. Each of these equations are based on the most intense regions of the Van Allen belts which occur from 540 nmi to 16,200 nmi above the Earth with peaks at 1,620 nmi and 11,880 nmi. The mission trajectory never dips to 1,620 nmi, yet 11,880 nmi is within the trajectory. Protection against this peak region had to be taken into account. The three equations based on aluminum are as follows:

$$Dp = \frac{3.38}{g^{1.3}} - \frac{1.73}{g^{1.2}} + 7.0E\text{-}4\,g^{0.45} - 1.9E\text{-}3\,g^{0.35} + 5.8E\text{-}3$$

$$De = \frac{1.93}{g^{1.4}} - \frac{2.08}{g^{1.3}} + \frac{32}{g^{0.35}} - \frac{44.8}{g^{0.25}} + 12.95$$

$$Dr = 2.0e^{\frac{-x}{4.2}}$$

Figure 7.5 Crew Module Cross Section

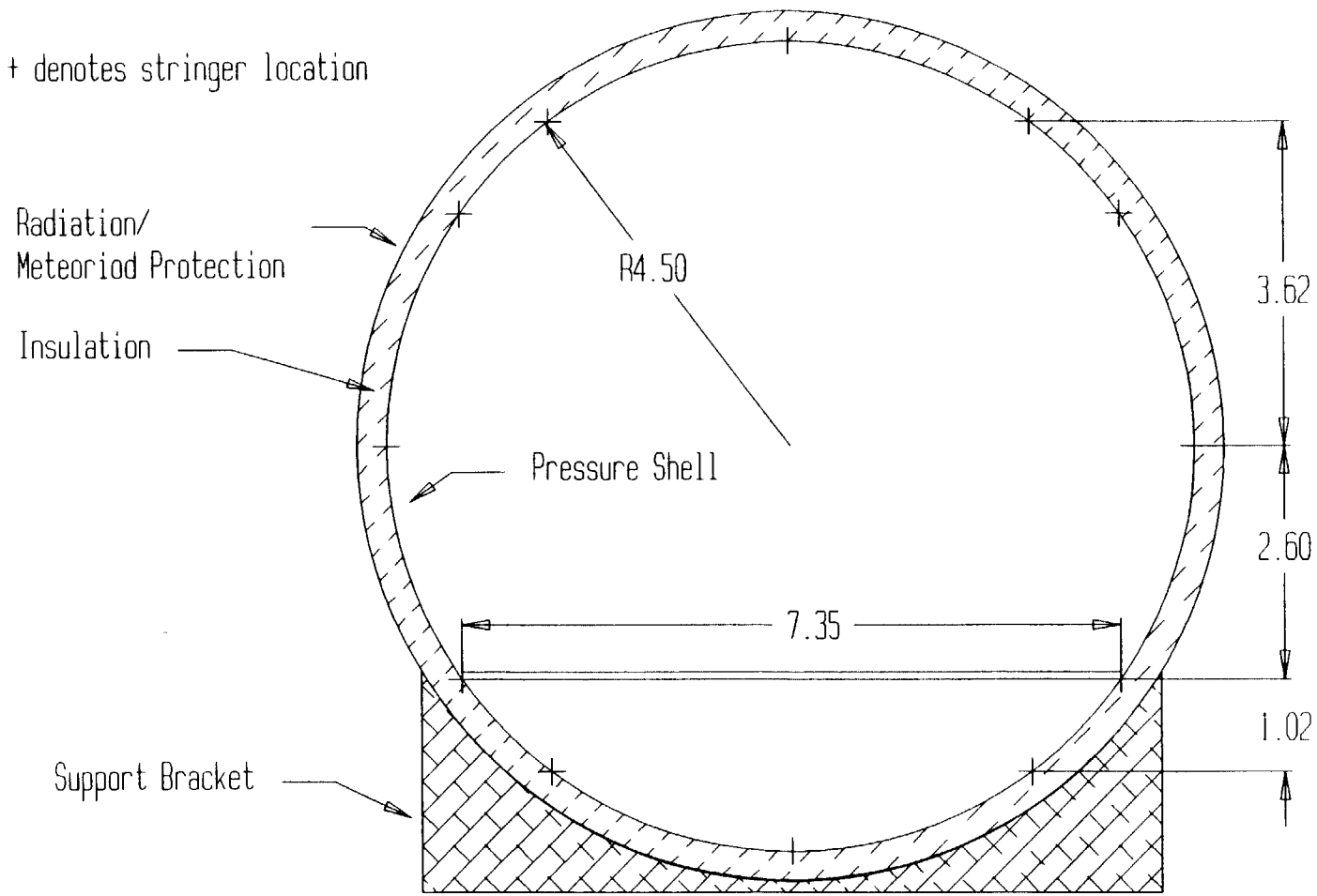

$$\mathscr{E} = \left(\frac{x}{3.47E-3}\right)^{1.73}$$

where

Dp = proton radiation (rad/sec)
De = electron radiation (rad/sec)
Dr = Bremsstrahlung radiation (rad/hr)
$\mathscr{E}$ = shield cutoff energy (Mev)
x = shield thickness (g/cm$^2$).

The first three equations were summed together and set equal to the radiation equivalent that adequately protected the crew. A flux (x) of 1.2 g/cm$^2$ was found that yielded exposure of 54 rad/hr. Using this flux, the thickness was found to be 0.1703", which is greater than the thickness determined for galactic radiation.

Exposure in the most intense regions around 11,880 nmi is not more than 2 hours. Thus, a maximum exposure of 108 (54x2) rads is encountered. The 108 rads exposure is within the limits imposed by both the National Council on Radiation Protection (NCRP) and the U.S. Nuclear Regulatory Commission. Both agencies typically use a number of 150 rems as the limit for maximum exposure. A 150 rem exposure is approximately equivalent to 150 rads, so the protection provided for is sufficient (108 < 150). Also, the insulation and pressure shell provide protection as well as the space suits.

The above analysis assumes that, if the crew is exposed to these levels of radiation at GEO for several days, the exposure will not exceed acceptable limits. This is a reasonable assumption since at GEO most of the Van Allen radiation consists of dispersed protons and very few of the more harmful ions. At altitudes approaching that of GEO, the Van Allen radiation becomes less important, and the more prominent radiation is that of solar flares.

Solar flares consist mainly of alpha particles and protons. Since solar flare radiation is the most intense (with the exception of some areas within the Van Allen belts), a safe haven was designed instead of bulk shielding the entire crew module. The safe haven requires approximately 80% less mass in comparison to bulk shielding. The equation based on aluminum was used to find the flux is:

$$Drad = \frac{15000}{x^{2.78}} + \frac{800}{x^{1.82}}$$

where

x = flux (g/cm$^2$).

A flux of 4 g/cm$^2$ was solved for, while keeping Drad within reasonable limits as discussed earlier. Using this flux, a thickness of 1.44" is needed for the safe haven. However, this aluminum flux was converted to an equivalent flux of 2.4 g/cm$^2$ using polyethylene (thickness

remains at 1.44"). This flux provides the same amount of protection as aluminum but provides a better mass savings since polyethylene has a much lower density than aluminum.

Polyethylene, a nonmetal, was not used for the outer shell because it could not protect against meteoroid impact as well as aluminum. Since the safe haven is inside the crew module, direct impact is not a consideration. Thus, using polyethylene for the haven is better than using aluminum because of the substantial reduction in mass (about 40%).

Now, the flux that was calculated above assumed that the safe haven was directly exposed to space. Since it is not, some additional protection is provided by the outer shell, insulation, and inner shell. This added protection essentially increases the effectiveness of the safe haven.

# Chapter 8

# Navigation, Communication, & Power Systems

*8.1 Guidance, Navigation, and Control*

*8.2 Communication & Data Processing*

*8.3 Electrical Power Systems*

## 8.1 Guidance, Navigation, Control (GNC)

The purpose of the guidance, navigation, and control system is to monitor and correct the trajectory of the vehicle. The GNC becomes extremely important when returning to LEO from GEO by aeroassisted maneuver.

The three major components of the GNC system are: the star tracker, the global positioning system (GPS), and the inertial reference unit (IRU) (Table 8.1). The star tracker provides information on the vehicle's position necessary for the calculation of the magnitude and direction of the propulsive burns.

Table 8.1 GNC Summary

| Component | Mass (lbm) | Power (Btu/hr) | Quantity |
|---|---|---|---|
| Inertial Reference Unit | 35 | 238.8 | 2 |
| Star Tracker | 20 | 61.42 | 2 |
| Global Positioning System | 25 | 194.5 | 1 |
| **Total** | 135 | 494.8 | |

During the transfer orbit, position data is provided by the GPS by means of 18 satellites in various Earth orbits. An update on the vehicle position takes approximately five minutes and during this time, the IRU accumulates acceleration and angular rate data. To provide redundant systems, important for manned missions, two star trackers are used, while the IRU and the GPS are internally redundant.

## 8.2 Communications and Data Processing

The data processing system is responsible for computer interaction with all of the vehicles subsystems. The communications system is comprised of a 2.5W transponder, an amplifier, antenna, and the necessary cabling (Table 8.2). The amplifier boosts the transponder signal to 20W for improved fidelity. For simplicity, all communication will take place over standard NASA communication links, STDN and TDRS. Each computer is internally redundant, and triple redundancy is achieved with an additional computer.



PAGE 120 INTENTIONALLY BLANK

PRECEDING PAGE BLANK NOT FILMED

Table 8.2 Communications and Data Processing Summary

| Component | Mass (lbm) | Power (Btu/hr) | Quantity |
|---|---|---|---|
| Communications | 55 | 511.8 | 2 |
| Data Processing | 250 | 2388 | 5 |
| Instrumentation | 140 | 170.6 | 1 |
| **Total** | 445 | 3071 | |

## 8.3 Electrical Power System

Fuel cells are utilized as the power source because of their proven reliability. Additionally, the short duration of the mission, the relatively low power requirements, and the fact that the system produces water which can be used for life support, all enforce the decision of fuel cells as a power source.

The major systems that require electrical power are: the GNC, communications and data processing, propulsion, and life support. Additionally, there is a 20% emergency reserve. Based on the mission duration and man rated requirements, 600W per crew member is required, for a total of 3kW. The propulsion system, including both engines and all the valves, requires 1.8kW, and 200W is allotted for connection mechanisms on the payload bays and elsewhere (Table 8.3).

Table 8.3 Power Requirements

| System | Power (Btu/hr) |
|---|---|
| GNC | 818.9 |
| Propulsion | 6142 |
| Life Support | 10,236 |
| Communication & Data Processing | 3071 |
| Emergency | 409.5 |
| **Total** | 20,678 |

The power system (Table 8.4) consists of three identical $LH^2/LO_2$ fuel cells, each of which is capable of supplying the maximum power requirement to the vehicle.

Table 8.4 Power System

| System | Mass (lbm) | Quantity |
|---|---|---|
| Fuel Cell | 630 | 3 |
| Distribution | 170 | N/A |
| **Total** | 800 | |

# Chapter 9

# Cost Analysis & Assembly

*9.1 Cost Analysis*

*9.2 On-Orbit Assembly*

PAGE 124 INTENTIONALLY BLANK

PRECEDING PAGE BLANK NOT FILMED

## 9.1 Cost Analysis

As with any large scale design, this project will incur significant costs as it progresses from conceptualization to construction, much of which results from research and development of the design prototype. The cost of the actual craft will diminish significantly once the materials and technology for the project are developed.

This cost analysis is based on several models: a Boeing parametric cost model, an RCA parametric hardware and software model, and the COCOMO model developed by Boehm-TRW. All costs given in Table 9.1 include estimates for design, development, testing, and evaluation. Cost estimates of total support and space station accommodations are based on a Boeing orbital transfer vehicle analysis. The total program cost is estimated at $1.8 billion, with the single unit production cost ranging from $70 - 80 million. All cost estimates are based on 1985 dollars.

## 9.2 On Orbit Assembly

For any spaced-based vehicle, consideration must be given to the way in which its delivery to space will occur. Currently, because of the vehicle's size, there is only one possible means to transport the entire vehicle, and this is by making multiple trips in the Space Shuttle. This is not considered here, as it is expected that the Space Shuttle will be obsolete at the time of the first launch of the SPARC.

There are three vehicles, currently in the design stage, that could be used to transport the craft: the Heavy Lift Launch Vehicle (HLLV), the Shuttle Derived Vehicle (SDV-3R), and the STS-II. The HLLV will have a 50'-diameter, 200'-long payload bay, and a 400,000-lbm capacity--more than enough to handle the SPARC. NASA expects the HLLV to be operational in 2025, sometime after the expected first launch of the SPARC.

The SDV-3R payload bay is 25' in diameter and 90' long. It has a payload capacity of 183,000 lbm. Two trips would be necessary with this vehicle. The first trip could include the aerobrake disassembled into three pieces, the truss structure, the payload bays, and the crew module; the second trip could include all tanks fully fueled, the two engines, and the four RCS clusters. The SDV-3R is expected to be operational for the first SPARC launch.

The STS II has a 25'-diameter, 60'-long payload bay with a capacity of 65,000 lbm. Three trips with this vehicle would be necessary. The payload of the first trip would consist of the main oxygen tank fully fueled, all four RCS clusters, and one of the engines; the second trip would contain the aerobrake in three pieces, the truss structure, and the second engine. The third trip would carry the remaining tanks fully fueled, the payload bays, and the crew module.

Definite delivery plans will have to be made closer to the time of first launch when it is known which of these vehicles, or their derivatives, is operational.



PAGE 126 INTENTIONALLY BLANK

PRECEDING PAGE BLANK NOT FILMED

Table 9.1 SPARC Cost Analysis

| All Values in Millions of 1985 Dollars | |
|---|---|
| Hardware | |
| Structure | 57.28 |
| Advanced Space Engines | 400.00 |
| Tank Shells | 13.50 |
| Auxillary Tanks | 0.50 |
| RCS | 6.80 |
| Propellant | 51.17 |
| Aerobrake | 87.38 |
| Avionics | 61.50 |
| Electrical Power | 6.00 |
| Thermal Control | 5.80 |
| Ground Support | 51.00 |
| Air Support | 19.00 |
| Integration & Assimilation | 18.60 |
| **Total Hardware** | $778.53 |
| **Support** | |
| System Integration | 29.00 |
| Software | 110.00 |
| System Testing | 84.00 |
| Tooling & STE | 26.00 |
| Miscellaneous Costs | 37.00 |
| **Total Support** | $286.00 |
| **SPARC Total** | $1064.53 |
| Spac Station Accomodation | 400.00 |
| Space Transport System | 200.00 |
| Technology | 160.00 |
| **Program Total** | $1824.53 |

Table 9.2 SPARC Component Useable Lifetime

| | |
|---|---|
| Structure & Avionics | 40 flights |
| TPS | 20 flights |
| Engines | 300 firings |

# Chapter 10

# Design Summary

PAGE 130 INTENTIONALLY BLANK

PRECEDING PAGE BLANK NOT FILMED

## 10.1 Summary

The purpose of this vehicle is to provide aeroassisted orbital transfer between the Space Station (LEO) and the GeoShack (GEO) for three separate mission scenarios: a 6,000-lbm payload and crew of five, round trip; a 20,000-lbm payload to GEO and a round trip for a crew of five; and an "expendable" 28,000-lbm trip to GEO with no crew. These missions are accomplished via Hohmann transfers to and from GEO with the return trip, in the 6,000-lbm and the 20,000-lbm cases, including an aeropass. The aeropass includes a 4.68° plane change attaining a minimum altitude of 262,900'. Total $\Delta V$ requirement for the round trip missions is 22,570 fps: a savings of 26.5% from the all-propulsive mission.

A rigid, 45'-diameter ellipsoidally blunted lifting aerobrake was used which was raked at 73° to provide lift at zero angle-of-attack. The aerobrake is detachable for the 28,000-lbm expendable mission. A multi-layer, flexible thermal protection system is used.

Main propulsion is provided by two modified Pratt and Whitney Advanced Expander Engines each providing 16,140 lbf thrust with an Isp of 487 sec. They retract during aerobraking to allow for a smaller aerobrake. A liquid hydrogen and a liquid oxygen propellant provides a high performance-to-mass ratio. The propellant is contained in three cylindrical tanks during the 6,000-lbm and 28,000-lbm missions, and three additional spherical tanks accommodate the fuel required for the 20,000-lbm mission.

The vehicle support structure is composed of eight graphite polyimide truss networks running parallel to the thrust direction and four networks running perpendicular. The truss structure is integrated with the other components of the vehicle, minimizing the required mass. Crew accommodations are provided for five by a 9.5'-diameter cylindrical cabin pressurized with a nitrogen and oxygen atmosphere. The crew module is removable for the expendable mission.

A standard sized payload bay is used so that one is required for the 6,000-lbm mission, two for the 20,000-lbm, and three for the 28,000-lbm mission. The payload bays may be attached in several positions to satisfy c.g. requirements for thrusting and aerobraking. The c.g. of the payload inside the bay also has a large envelope for maximum vehicle flexibility.

Maximum dry mass of the vehicle without payload is 20,535 lbm, and maximum total mass is 120,288 lbm, for the 20,000-lbm mission. Key advantages of this design include its capability to meet all three mission requirements with one vehicle, and a removable aerobrake and crew module for maximum savings in the case of the expendable mission.



PAGE 132 INTENTIONALLY BLANK

Table 10.1 Design Parameter Summary

| | 6,000-lbm mission | 20,000-lbm mission | 28,000-lbm mission |
|---|---|---|---|
| Propulsion | | | |
| Isp | 487 sec | 487 sec | 487 sec |
| Propellant Mass Flow Rate | 35.86 lbm/sec | 35.86 lbm/sec | 35.86 lbm/sec |
| Main Engine Thrust | 16,140 lbf | 16,140 lbf | 16,140 lbf |
| RCS Thrust | 30 lbf each | 30 lbf each | 30 lbf each |
| RCS Isp | 225 sec | 225 sec | 225 sec |
| Masses (lbm) | | | |
| Dry Mass at Launch | 24,577 | 40,535 | 41,469 |
| Dry Mass at GEO | 24,577 | 20,535 | 41,469 |
| Propellant Mass at Launch | 53,930 | 79,753 | 71,951 |
| Propellant Mass at GEO | 13,303 | 10,793 | 0 |
| Total Vehicle Mass at Launch | 78,507 | 120,288 | 113,421 |
| Total Vehicle Mass at GEO | 37,880 | 31,328 | 13,470 |
| Propellant Used LEO to GEO | 40,627 | 68,960 | 71,951 |
| Propellant Used GEO to LEO | 13,303 | 10,826 | N/A |
| Performance | | | |
| Trip Time LEO to GEO | 5.3 hr | 5.3 hr | 5.3 hr |
| Trip Time GEO to LEO | 5.34 hr | 5.34 hr | N/A |
| Payload/Mass Ratio LEO to GEO | 0.101 | 0.233 | 0.328 |
| Payload/Mass Ratio Geo to LEO | 0.188 | 0.0 | N/A |
| Structural Coefficient | 0.256 | 0.205 | 0.158 |

# References

**Chapter 2 SPARC Configuration**

Andrews, D.G., Caluori, V.A., and Bloetscher, F., "Optimization of Aerobraked Orbital Transfer Vehicles," AIAA 81-1126.

Davies, C.B. and Park, C., "Aerodynamic Characteristics of Generalized Bent Biconic Bodies for Aero-Assisted Orbital-Transfer Vehicles," AIAA 83-1512.

Gamble, J.D., Cerimele, C.J., and Spratlin, K., "Aerobraking of a Low L/D Manned Vehicle from GEO Return to Rendezvous With the Space Shuttle," AIAA 83-2110.

Menees, Gene P., "Thermal Protection Requirements for Near-Earth Aeroassisted Orbital Transfer Vehicle Missions," AIAA 83-1513.

Menees, G.P., Park, C., "Design and Performance Analysis of a Conical Aerobrake Orbital Transfer Vehicle Concept," AIAA 84-0410.

Menees, G.P., "Aerothermodynamic Heating Analysis of Aerobraking Orbital Transfer Vehicles," AIAA 84-1711.

Park, C., "A Survey of Aerobraking Orbital Transfer Vehicle Design Concepts," AIAA 87-0514.

Walberg, Gerald D., "A Review of Aeroassisted Orbit Transfer,"AIAA Paper 82-1378, AIAA 9th Atmospheric Flight Mechanics Conference, San Diego, CA., Aug. 1982.

**Chapter 3 Trajectory Analysis**

Desautel, Dick, "Analytic Characterization of AOTV Perigee Aerothermodynamic Regime," AIAA Paper 84-1713, Jun. 1984.

Johannesen, Jennie R., et al., "Effect of Maximum Lift to Drag Ratio on Optimal Aeroassisted Plane Change," AIAA Paper 85-1817.

Mayo, E.E., et al., "Newtonian Aerodynamics for Blunted Raked-off Circular Cones and Raked-off Elliptical Cones," NASA-TN-D-2624, May 1965.

"Orbital Transfer Vehicle Concept Definition Study," Boeing Aerospace Company, Report No. D180-29108-3, Contract NASA-36107.

Reid, R.C., Mayo, E.E., "Equations for the Newtonian Static and Dynamic Aerodynamic Coefficients for a Body of Revolution with an Offset Center-of-Gravity Location," NASA, June 1963.



PAGE 136 INTENTIONALLY BLANK PRECEDING PAGE BLANK NOT FILMED

Scott, Carl D., et al., "An AOTV Aeroheating and Thermal Protection Study," AIAA Paper 84-1710, June 1984.

Walberg, Gerald D., "A Review of Aeroassisted Orbit Transfer," AIAA Paper 82-1378, AIAA 9th Atmospheric Flight Mechanics Conference, San Diego, CA., Aug. 1982.

**Chapter 4 The Aerobrake**

Andrews, D.G., Caluori, V.A., and Bloetscher, F., "Optimization of Aerobraked Orbital Transfer Vehicle", AIAA-81-1126.

Bowles, K.J., "A Thermally Modified Polymer Matrix Composite Material with Structural Integrity to 371 C", NASA-TM-100922, 1988.

Calamito, D.P., "Development of Tailorable Advanced Blanket Insulation for Advanced Space Transportation", NASA-CR-177444, 1987.

Cheatwood, F.M., DeJarnette, and Hamilton, H.H., "Geometrical Description for a Proposed Aeroassist Flight Experiment Vehicle", NASA-TM-87714, 1986.

Clark, R.K. et al, "Vapor Deposited Emittance/Catalysis Coatings for Superalloys in Heatshield Applications", AIAA-85-0403, 1985.

Cleland, J. et al, "Thermal Protection System of the Space Shuttle", NASA-CR-4227, 1989.

Coe, C.F., "An Investigation of the Causes of Failure of Flexible Thermal Protection Materials in an Aerodynamic Environment", NASA-CR-166624, 1987.

Covington, M.A. and Sawko, P.M., "Optical Properties of Woven Fabrics for Flexible Heat Shields", AIAA-86-1281, 1986.

Davies, C.B., "Aerodynamic and Thermal Characteristics of a Modified Raked Off Blunted Cone", AIAA-86-1309, 1986.

Delvings, P., "The 371 Deg C Mechanical Properties of Graphite Polyimide Composites", NASA-TM-87122, 1985.

Dexter, H.B. et al, *Graphite/Polyimide Composites*, NASA-CP-2079, 1979.

Gamble, J., Spratlin, K., Skalecki, L., "Lateral Directional Requirements for a Low L/D Aeromaneuvering Orbital Transfer Vehicle", AIAA-84-2123.

Garber, D.P., "Elastic Properties and fracture behavior of graphite/ polyimide composites at extreme temperatures," Thesis, VPI&SU, 1983.

Glass, C.E. and Hunt, L.R., "Aerothermal Test of Quilted Dome Models on a Flat Plate at a Mach Number of 6.5", NASA-TP-2804, 1988.

Islam, Mahmud., *Artificial Composites for High Temperature Applications*, 1988.

Korites, B.J., *Structural Analysis Software for Microcomputers*, Kern International, Inc., 1975.

Kourtides, D.A., Pitts, W.C., Araujo, M., and Zimmerman, R.S., "High Temperature Properties of Ceramic Fibers and Insulations for Thermal Protection of Atmospheric Entry and Hypersonic Cruise Vehicles", NASA-TM-100059, 1988.

Lubowinski, S.J. et al, "Loading Rate Sensitivty of Open Hole Composistes in Compression", NASA-TM-100634, 1988.

Mayo, E.E., Lamb, R.H., and Romero, P.O., "Newtonian Aerodynamics for Blunted Raked-Off Circular Cones and Elliptical Cones," NASA TN D-2624, 1965.

Menees, G.P., C. Park and J.F. Wilson, "Design and Performance Analysis of a Conical Aerobrake Orbital Transfer Vehicle Concept", AIAA-84-0410, Jan. 1984.

Menees, G.P., "Thermal-Protection Requirements for Near-Earth Aeroassisted Orbital Transfer Vehicle Missions", AIAA-83-1513, June 1983.

Menees, G.P., C.B. Davies, J.F. Wilson and K.G. Brown, "Aerothermodynamic Heating Analysis of Aerobraking and Aeromaneuvering Orbital Transfer Vehicles", AIAA-84-1711, 1984.

Nelson, J.B., "Effect of Long Term Thermal Aging on Coated Celion/LARC-160 Composites", NASA-TM-100495, 1987.

Norman, I. and Ritrivi, C.A., "Thermal Performance of FRSI/Graphite Epoxy Materials for the Orbiter TPS Application", AIAA-84-1769, 1984.

"Orbital Transfer Vehicle Concept Definition Study," Boeing Aerospace Company, Report No. D180-29108-3, Contract NAS8-36107.

Park, C. and Wilson, J.F., "Design and Performance Analysis of a Conical Aerobrake Orbital Transfer Vehicle Concept", AIAA-84-0410, 1984.

Pitts, W.C. and Murbach, M.S., "Thermal Design of AOTV Heat Shields for a Conical Drag Brake", AIAA-85-1052, 1985.

Pitts, W.C. and Murbach, M.S., "Thermal Response of an Aeroassisted Orbital Transfer Vehicle with a Conical Drag Brake", AIAA-84-8412, June 1984.

Preliminary Design Document, "Aeroassisted Flight Experiment," National Aeronautics and Space Administration.

Savage, R.T., "High Temperature Performance of Flexible Thermal Protection Materials", AIAA-84-1770, 1984.

Schwartz, M.M., *Composite Materials Handbook*, McGraw-Hill Book Co., 1984.

Scott, C.D., Roberts B.B., Nagy, K., Taylor, P., Gamble, B., Cerimele, C.J., Kroll, K.R. Li, C.P., and Ried, R.C., "Design Study of an Integrated Aerobraking Orbital Transfer Vehicle," NASA TM-58264, 1985.

Scott, C.D., R.C. Ried, R.J. Maraia, C.P. Li, and S.M. Derry, " An AOTV Aeroheating and Thermal Protection Study", AIAA-Paper 84-1710, June 1984.

Serafini, T.T., "High Temperature Polymer Matrix Composites", NASA-CP-2385, 1985.

"Taxi: Aeroassisted Manned Transfer Vehicle," Department of Aerospace and Ocean Engineering, VPI&SU, 1987.

Tally, T.A., White, N.W., and Naftel, J.C., "Impact of Atmospheric Uncertainties and Viscous Interaction Effects on the Performance of AOTV's", *Thermal Design of AOTV's*, Vol. 96, ed. Nelson, H.F., AIAA, New York, 1985.

Tow, D.M., Barna, B.A., Rodriguez, J.G.,"NDE of the Space Shuttle Orbiter Thermal Protection System: Phase 2 Final Report", EGG-MS-8425, 1989.

Walberg, G.D., "A Survey of Aeroassisted Orbit Transfer," *Journal of Spacecraft and Rockets*, Vol. 22, No. 1, January-February 1985, pp. 3-18.

**Chapter 5 Propulsion Systems**

Aydelott, John, Cryogenic Fluids Technology Office, NASA Lewis Research Center, interview, February, 1990.

Bednar, H.H. P.E., *Pressure Vessel Design Handbook*, 2nd edition, New York, NY, Van Nostrand Reinhold Company, 1986.

Blatt, M.H., "Capillary Acquisition Devices For High Performance Vehicles", NASA CR-159658, Feb. 1980.

Bussard, R.W., *Fundamentals of Nuclear Flight*, New York, McGraw-Hill, 1965.

*CRC Handbook of Chemistry and Physics*, Editor-in-Chief R.C. Weast, Ph.D., 66th edition, Boca Raton, FL, CRC Press, 1985.

Glazer,J., "Mechanical Behavior of Al-Li alloys at Cryogenic Temperatures", *Metallurgical Transactions*, Vol. 18A, Oct. 1987, pp. 1695-1701.

Haselden, G.G., *Cryogenic Fundamentals*, Academic Press, N.Y., 1971, pp. 200-230.

Hill, P.G. and Peterson, C.R., *Mechanics and Thermodynamics of Propulsion*, 3rd edition, Reading, MS, Addison-Wesley Publishing, 1970.

Hsu, Chai-Jung, "Shape Factor Equations for Radiant Heat Transfer between Two Arbitrary Sizes of Rectangular Planes.", *The Canadian Journal of Chemical Engineering*, vol 45, February, 1967, p.58-60.

Mitchell, L.D., and Shigley, J.E., *Mechanical Engineering Design*, McGraw-Hill Book Company, New York, 1983.

NASA SP-8088, NASA Space Vehicle Design Criteria, "Liquid Rocket Metal Tanks and Tank Components", May 1974.

"Orbital Transfer Vehicle Concept Definition Study," Boeing Aerospace Company, Report No. D180-29108-3, Contract NAS8-36107.

Pratt and Whitney Aircraft, NASA Orbit Transfer Rocket Engine Technology Program (Final Report), N84-28901, 23 April, 1984.

Pratt and Whitney Aircraft, RL10 Derivative Engines for the OTV, AIAA 85-1338, 1985.

Pratt and Whitney Aircraft, NASA Orbit Transfer Rocket Engine Technology Program, 1984, pp. 6-11.

Preliminary Design Document, "Aeroassisted Flight Experiment," National Aeronautics and Space Administration.

Shames, Irving, *Mechanics of Fluids*, McGraw-Hill, New York, 1982, pp. 275-287.

Stochl, Robert, "Basic Performance of a MLI System Containing 20 to 160 Layers", NASA Lewis Research Center, April 1974.

Sutton, G.P. and Ross, D.M., *Rocket Propulsion Elements* 4th edition, New York, NY, Wiley-Interscience, 1976.

Torre, Chris N., General Dynamics Space Systems Division, "Analysis of a Low-Vapor-Pressure Cryogenic Propellant Tankage System", *Journal of Spacecraft*, Vol. 26, No. 5, pp. 368-378.

Traister, J.E., *Handbook of Electric Motors*, Prentice-Hall Inc., Englewood Cliffs, New Jersey, 1983.

Williamson, K.D., *Liquid Cryogens*, Vols. 1 & 2, CRC Press, Boca Raton, 1983.

**Chapter 6 Structures**

Froes, F.H, *Journal of Materials*, "Developments of Metallic Materials for Aerospace Applications," May, 1989, pp.12-26.

Hilado, C.J., "Boron Reinforced Aluminum Systems," Technomic Publishing Co., Inc., Westport, CT, 1982.

Hoffner, J.W., "Radiation and Shielding in Space," Academic Press Inc., New York, 1967.

Howard, E.B., "Metals Handbook," American Society for Metals, Metals Park, Ohio, 1985.

Jones, R.M., "Mechanics of Composite Materials," Hemisphere Publishing Corporation, New York, 1975.

Lee, J.A., "Metal and Polymer Matrix Composites," Noyes Data Corporation, Park Ridge, New Jersey, 1987.

"Mechanical Response of Unidirectional Boron/Aluminum Under Combined Loading," Virginia Polytechnic Institute and State University, Blacksburg, VA, 1987.

Stassinopoulos, E.G., *Journal of Spacecraft*, "The Geostationary Radiation Environment," March-April, 1980, pp. 145-152.

"Structural Alloys Handbook," Battelle Publishing Co., Columbus, Ohio, Vol. 3, 1989.

Tsao, C.H., *Aerospace America*, "Radiation hazards in space," October, 1987, pp. 38-41.

**Chapter 7 Crew Module**

Hord, M.R., *CRC Handbook of Space Technology: Status and Projections*, CRC Press, Boca Raton, Fla., 1984.

*Journal of Spacecraft and Rockets*, Vol. 26, #5, 1989.

Kammermyer, Karl., *Atmosphere in Space Cabins and Closed Environments*, MacGruder-Vaughn Inc., 1965.

Korites, B.J., *Structural Analysis Software for Microcomputers*, Kern International, Inc., 1975.

Nicolai, L.M., *Aircraft Design*, L.M. Mets, Inc, 1984.

Space Shuttle: A Triumph in Manufacturing, Society of Manufacturing Engineers, Deerborn, Michigan, 1985.

*Space Systems Technology*, Heitchue, R.D., Deinhold Book Corp., 1968.

*Space Transportation System*, NASA, June 1977.

**Chapter 8 Navigation & Power Systems**

"Orbital Transfer Vehicle Concept Definition Study," Boeing Aerospace Company, Report No. D180-29108-3, Contract NAS8-36107.

Preliminary Design Document, "Aeroassisted Flight Experiment," National Aeronautics and Space Administration.

**Chapter 9 Cost Analysis & Assembly**

Hord, M.R., *CRC Handbook of Space Technology: Status and Projections*, CRC Press, Boca Raton, Fla., 1984.

"Orbital Transfer Vehicle Concept Definition Study," Boeing Aerospace Company, Report No. D180-29108-3, Contract NAS8-36107.

Preliminary Design Document, "Aeroassisted Flight Experiment," National Aeronautics and Space Administration.

# Appendices

*A Stability Equations*

*B Mass Moments of Inertia*

*C Drag Program*

*D Propellant Analysis Program*

PAGE 144 INTENTIONALLY BLANK

PRECEDING PAGE BLANK NOT FILMED

## Appendix A Stability Equations

$$C_m = \frac{\sec^2\theta_{xz}}{s\,l}\int_{-1}^{0}\int_{\phi_L}^{\phi_U}\frac{C_p\,x^2\tan\theta_{xz}\cos\phi}{A^{3/2}}\,d\phi\,dx$$

$$C_p = \frac{2}{m^2 s^2\sin^2\phi + \cos^2\phi}\left(\lambda\sin\theta_{xz}\sqrt{A} + m s\,\nu\cos\theta_{xy}\sin\phi - \omega\cos\theta_{xz}\cos\phi\right)^2$$

$$\phi_U = 90^\circ + \psi(x)$$
$$\phi_U = 270^\circ - \psi(x)$$

$$\psi(x) = \tan^{-1}\left\{\frac{-\tan\delta\left(B + \frac{x}{d}\right) - C}{\frac{1}{m}\sqrt{\left(\frac{x}{d}\right)^2\tan^2\theta_{xz} - \left[-\tan\delta\left(B + \frac{x}{d}\right) - C\right]^2}}\right\}$$

$$-90^\circ \le \psi(x) \ge 90^\circ$$

$$m = \frac{\tan\theta_{xz}}{\tan\theta_{xy}} \qquad s = \frac{\sin\theta_{xz}}{\sin\theta_{xy}}$$

$$\lambda = \cos\alpha\cos\beta \qquad \omega = \sin\alpha\cos\beta \qquad \nu = -\sin\beta$$

$$A = m^2\sin^2\phi + \cos^2\phi$$

$$B = \frac{1}{2}\frac{\sin(\delta - \theta_{xz})}{\sin\theta_{xz}}$$

$$C = \frac{1}{2}\frac{\sin(\delta - \theta_{xz})}{\cos\theta_{xz}}$$



PAGE 146 INTENTIONALLY BLANK

PRECEDING PAGE BLANK NOT FILMED

## Appendix B Mass Moments of Inertia (lb-ft$^2$)

| | Full | Aeropass | At LEO (empty) |
|---|---|---|---|
| 6,000-lbm mission | | | |
| Ixx | 3,312,687.4 | 1,195,484.9 | 1,459,713.9 |
| Iyy | 6,091,613.7 | 2,885,904.7 | 1,798,103.2 |
| Izz | 7,041,929.4 | 3,039,915.3 | 1,818,462.5 |
| 20,000-lbm mission | | | |
| Ixx | 5,305,547.5 | 1,452,454.4 | 1,152,619.7 |
| Iyy | 11,225,959.2 | 1,947,563.7 | 1,512,138.3 |
| Izz | 12,737,323.0 | 2,341,373.0 | 1,684,400.5 |
| 28,000-lbm mission | | | |
| Ixx | 4,640,115.7 | - | 692,838.2 |
| Iyy | 11,930,779.1 | - | 947,238.1 |
| Izz | 13,427,716.4 | - | 1,036,291.5 |

# Appendix C DRAG Program

```
*********************************************************************
*                                                                   *
*   Roni G. Winkler     229-06-8237     Aerobraking Vehicle         *
*                                                                   *
*********************************************************************
*                                                                   *
*   Modified by Aimee Thornton                                      *
*                                                                   *
*********************************************************************
c
      program drag
c
      real mu, mass, nu
c
      open(0,file='PRN')
      open(1,file='atmos.dat')
c
***** VALUES USED TO CALCULATE THE ATMOSPHERIC DRAG ******************
c
      pi = 3.14159265359
c
***** INITIAL ORBIT PARAMETERS IN EARTH CANONICAL UNITS ***************
c
      write(*,*)'ENTER THE VALUE FOR PERIGEE ALTITUDE IN FT'
      read(*,*)rp
      rp = (rp / 20925672.5722) + 1.
      write(*,*)
      ratmos = 1.019115276
      ra = 6.585
      mu = 1.0
c
***** PHYSICAL CHARACTERISTICS OF THE AEROBRAKE:  VEHICLE AREA ********
***** IN FT^2, MASS IN LBM, AND NOSE RADIUS OF CURVATURE IN METERS ****
c
      cd = 1.53
      area = 1590.4313
      Rn = 8.15852064
     0write(*,*)'ENTER THE VALUE FOR TOTAL VEHICLE MASS AT ATMOSP',
     1          'HERIC ENTRY IN lbm'
      read(*,*)mass
c
***** CALCULATE THE INITIAL ORBIT ENERGY AND VELOCITY AT ATMOSPHERIC **
***** ENTRY ***********************************************************
c
      call energ (rp,ra,ratmos,mu,nu,energy,a,vel)
      energy1 = energy
      xnu = 360. - nu
      oldnu = xnu * pi / 180.
      degnu = xnu
      rold = ratmos
      tottof = 0.
      dtofsec = 0.
      totheat = 0.
      tq = 0.
      alt = (rold - 1.) * 2.092567257e7
      vel1 = vel * 25936.24764
      row = .075 * exp(-7.4e-6*alt**1.15)
c
      call pertaccel(cd,area,mass,row,vel1,paccel,accel)
```

```
c
      call heating(row,vel1,Rn,dtofsec,qdot,dq)
      call unitq(qdot)
      totheat = totheat + dq
      tq = totheat
      call unitq(tq)
c
      call unitalt(rold,altitude)
c
***** PRINT OUT THE DATA ***********************************************
c
      write(1,10)
      write(1,9)tottof,vel1,altitude,accel,tq,qdot
c
    9 format(5x,f10.4,3x,f10.2,3x,f10.2,3x,f9.7,3x,f10.4,3x,f10.7)
   100format(6x,'tottof{s}',4x,'vel{ft/s}',5x,'alt{ft}',4x,
     1       'accel{g''s}',2x,'q{Btu/ft^2}',1x,'qdot{Btu/(s*ft^2)}')
   11 format(10x,f9.5,3x,f7.4,3x,f9.7,3x,f10.4,3x,f7.3,3x,f9.3)
   12 format(13x,'Energy',6x,'ra',8x,'Accel',9x,'TOF',7x,'nu',10x,'q')
   130format(10x,'{DU^2/TU^2}',3x,'{DU}',7x,'{g''s}',9x,'{s}',5x,
     1       '{deg}',5x,'{Btu/ft^2}')
c
   14 format(f9.5,3x,f7.4,3x,f9.7,3x,f10.4,3x,f7.3,3x,f9.3)
   15 format(3x,'Energy',6x,'ra',8x,'Accel',9x,'TOF',7x,'nu',10x,'q')
   160format(' {DU^2/TU^2}',2x,'{DU}',7x,'{g''s}',9x,'{s}',5x,
     1       '{deg}',5x,'{Btu/ft^2}')
c
      write(0,12)
      write(0,13)
      write(0,*)
      write(0,11)energy,ra,accel,tottof,degnu,tq
      write(*,15)
      write(*,16)
      write(*,*)
      write(*,14)energy,ra,accel,tottof,degnu,tq
c
***** CALCULATE CHANGES IN ORBITAL ENERGY DUE TO THE FORCE GENERATED **
***** BY SOLAR PRESSURE IN SMALL INCREMENTS UPDATING ENERGY IN SMALL **
***** INCREMENTS FOR EVERY ONE DEGREE CHANGE IN TRUE ANAMOLY ***********

c
      do 100 i = 1,90
c
***** CALCULATE THE INCREMENT OF TRUE ANOMALY *************************
c
         if ((xnu+float(i)).ge.360.) then
            nu = (xnu+float(i)-360.) * pi / 180.
            goto 25
         endif
         nu = (xnu + float(i)) * pi / 180.
c
   25    ra = 2.*a - rp
         e = 1. - rp / a
         pee = a * (1. - e**2)
         rcurrent = pee / (1. + e * cos(nu))
c
***** CONVERT ALTITUDE INTO FEET ***************************************
c
      alt = (rcurrent - 1.) * 2.09256725e7
c
         vel = sqrt( 2.*(mu/rcurrent + energy))
c
```

```
***** CONVERT VELOCITY IN CANONICAL UNITS TO FT/S *********************
c
      vel1 = vel * 25936.24764
c
***** CALCULATE THE TIME OF FLIGHT BETWEEN PREVIOUS AND CURRENT *******
***** POSITION ********************************************************
c
      if(nu.le.pi.and.oldnu.gt.pi) then
        eccanom = acos( (e + cos(nu)) / (1. + e*cos(nu)) )
        eccold = acos((e+cos(2.*pi-oldnu))/(1.+e*cos(2.*pi-oldnu)))
        tof = sqrt(a**3/mu) * ((eccanom-e*sin(eccanom)) + (eccold -
     $        e*sin(eccold)) )
        goto 50
      endif
c
      if (nu.le.pi)then
      eccanom = acos ( (e + cos(nu)) / (1. + e*cos(nu)) )
      eccold = acos ( (e + cos(oldnu)) / (1. + e*cos(oldnu)) )
      tof = sqrt(a**3/mu) * ( (eccanom-e*sin(eccanom)) - (eccold -
     $      e*sin(eccold)) )
      goto 50
      else
      eccanom = acos((e+cos(2.*pi-nu))/(1.+e*cos(2.*pi-nu)))
      eccold = acos((e+cos(2.*pi-oldnu))/(1.+e*cos(2.*pi-oldnu)))
      tof = sqrt(a**3/mu) * ( ( eccold - e*sin(eccold)) - (eccanom -
     $      e*sin(eccanom)) )
      endif
c
***** CALCULATE TOTAL TIME OF FLIGHT **********************************
c
   50 tottof = tottof + tof
c
***** CONVERT TOF TO SECONDS ******************************************
c
      call unittim(tottof,tofsec)
      call unittim(tof,dtofsec)
c
***** CALCULATE THE DISTANCE TRAVELED ALONG THE ORBIT BETWEEN ONE *****
***** DEGREE INCREMENTS IN TRUE ANOMOLY.  APPROXIMATE THE DISTANCE ****
***** AS A CIRCULAR ARC WITH AVERAGE RADIUS AND ONE DEGREE ANGLE. *****
c
        ravg = (rold + rcurrent) / 2.
c
***** CONVERT RAVG FROM CANONICAL UNITS TO FT *************************
c
      ravg = ravg * 2.09256725e7
c
        angle = pi / 180.
        dis = ravg * angle
c
      row = .075 * exp(-7.4e-6*alt**1.15)
c
***** CALCULATE THE PERTURBATIVE ACCELERATION DUE TO ATMOSPHERIC ******
***** DRAG ************************************************************
c
      call pertaccel(cd,area,mass,row,vel1,paccel,accel)
c
***** CALCULATE HEAT FLUX & HEATING RATE ******************************
c
      call heating(row,vel1,Rn,dtofsec,qdot,dq)
      totheat = totheat + dq
      tq = totheat
```

```
c
***** CONVERT HEAT FLUX & HEATING RATE TO BRITISH UNITS ***************
c
      call unitq(tq)
      call unitq(qdot)
c
***** CALCULATE CHANGE IN ENERGY DUE TO FORCE FROM ATMOSPHERIC DRAG ***
c
      deltae =  paccel * dis
c
***** CONVERT CHANGE OF ENERGY TERM INTO EARTH CANONICAL UNITS ********
c
      call uniten (deltae)
c
      energy = energy + deltae
c
      aold = a
      rold = rcurrent
      oldnu = nu
      degnu = nu * 180. / pi
c
      call unitalt(rcurrent,altitude)
c
***** PRINT OUT THE DATA ********************************************
c
      write(*,14)energy,ra,accel,tofsec,degnu,tq
      write(0,11)energy,ra,accel,tofsec,degnu,tq
      write(1,9)tofsec,vel1,altitude,accel,tq,qdot
c
      if (rcurrent.ge.ratmos) goto 250
c
***** CALCULATE A NEW SEMI-MAJOR AXIS *********************************
c
      a = -mu / (2. * energy)
c
  100 continue
  250 write(*,*)'the vehicle has left the atmosphere'
      write(0,*)'          the vehicle has left the atmosphere'
c
      end
c
*********************************************************************
*********************************************************************
c
      subroutine energ (rp,ra,ratmos,mu,nu,energy,a,vel)
c
      real mu,nu
      pi = 3.141592654
      energy = -mu / (rp + ra)
      a = (rp + ra) / 2.
      vel = sqrt(2.*(mu/ratmos + energy) )
      va =  sqrt(2.*(mu/ra + energy) )
      ht = ra * va
      phi = acos (ht/ratmos/vel)*180. / pi
      p = (ra*va)**2/mu
      e = (ra - rp) / (ra + rp)
      nu = acos(( p/ratmos - 1.)/e)  * 180. / pi
c
      write(*,*)
     0write(*,*)'THE FLIGHT PATH ANGLE ENTERING THE ATMOSPHERE IS',
     1          phi,' DEGREES'
      write(*,*)
```

```
      write(*,*)
  170format('          THE FLIGHT PATH ANGLE ENTERING THE ATMOSPHERE',
     1     ' IS',f9.6,' DEGREES')
      write(0,17)phi
      write(0,*)
      write(0,*)
c
      return
      end
c
*********************************************************************
c
      subroutine pertaccel (cd,area,mass,row,vel1,paccel,accel)
c
      real mass
c
      paccel = -.5 * cd * area/mass * row * vel1**2
      accel = paccel / 32.174
c
      return
      end
c
*********************************************************************
c
      subroutine heating (row,vel1,Rn,dtofsec,qdot,dq)
c
      rowSI=row * 16.018463374
      vel1SI = vel1 * 0.3048
      qdot = 18300. * sqrt(rowSI/Rn) * (vel1SI/10.**4)**3.05
      dq = qdot * dtofsec
c
      return
      end
c
*********************************************************************
c
      subroutine uniten (deltae)
c
c     CONVERT FT^2/S^2 TO EARTH CANONICAL UNITS
c
      deltae = deltae / (25936.24764**2)
c
      return
      end
c
*********************************************************************
c
      subroutine unitdis (r)
c
c     CONVERT DU TO KILOMETERS
c
      r = r * 6378.145
c
      return
      end
c
*********************************************************************
c
      subroutine unittim (tottof,tofsec)
c
c     CONVERT TU TO SECONDS
c
```

```
      tofsec = tottof * 806.8118744
c
      return
      end
c
*********************************************************************
c
      subroutine unitq (q)
c
c     CONVERT HEAT FLUX TO BRITISH UNITS {Btu/ft^2} FROM SI UNITS
c     {J/cm^2} OR HEATING RATE TO {Btu/(s*ft^2)} FROM {W/cm^2}
c
      q = q * 0.880550918411
c
      return
      end
c
*********************************************************************
c
      subroutine unitalt (radius,altitude)
c
c     CALCULATE ALTITUDE {ft} FROM RADIUS {DU}
c
      altitude = (radius - 1.) * 20925672.5722
c
      return
      end
c
*********************************************************************
```

# Appendix D Propellant Analysis Program

```
' CODE WRITTEN BY THEODORE F. BUGTONG FOR SPARC DESIGN GROUP
' VERSION DATE: 03-09-90
' THIS PROGRAM TAKES THE NECESSARY ENGINE CHARACTERISTICS AND THE REQUIRED
' DELTA-VEES FOR THE MISSION AND CALCULATES THE AMOUNT OF FUEL NECESSARY
' TO ACCOMPLISH THE MISSION ASSUMING DIFFERENT TYPES OF TANKS
'
' PROGRAM ASSUMPTIONS:
'         FUEL : LIQUID HYDROGEN (DENSITY = 4.42 lbm/ft^3)
'         OXIDIZER : LIQUID OXYGEN (DENSITY = 71.19 lbm/ft^3)
'         OXIDIZER TANK MAT'L : Al-Li 2090 T81 (DENSITY = 161.7 lbm/ft^3)
'         FUEL TANK MAT'L : Ti-5Al-2.5Sn ELI (DENSITY = 278.21 lbm/ft^3)
' PROGRAM FURTHER ASSUMES:
'         6% MORE PROPELLANT IS LEFT IN THE TANKS FOR EMERGENCIES
'         2% MORE PROPELLANT REMAINS IN THE LINES (RESIDUALS)
'         3% MORE VOLUME IS REQUIRED SINCE TANKS CAN ONLY BE FILLED TO 97%
'
' PROGRAM NOMENCLATURE:
'         "SKELATON" REFERS TO ANY MASS WHICH IS NOT TANK SHELL OR PAYLOAD MASS
'          (i.e. AEROBRAKE, MAIN STRUCTURE, SUPPORT FOR MAIN ENGINES, TTL RCS
'           HARDWARE AND RCS PROPELLANT, ETC.)
'
' THE FOLLOWING FIGURES SHOULD BE USED IN SUMMING FOR "SKELATON":
'         TTL RCS HARDWARE AND PROPELLANT : 2188 lbm
'         MASS OF TWO ENGINES: 900 lbm
'         MASS OF ENGINE SUPPORT STRUCTURE : 500 lbm
'         MASS OF PIPING BETWEEN TANKS AND ENGINES : 1000 lbm
'
TITIDENSITY = 278.21
ALLIDENSITY = 161.7
PI = 3.14159265
DEF FNEQUATION(NUMBR,USABLE,TNKVOL)=(-2/3*PI)*NUMBR^3+PI*USABLE*NUMBR^2-TNKVOL
'
CLS
PRINT
INPUT "WILL YOU BE WRITING DATA TO THE DISK (Y/N)";RITE$
IF RITE$ = "Y" THEN
         OPEN "GNU.DAT" FOR OUTPUT AS #1
         PRINT #1 ,"PROGRAM ASSUMPTIONS:"
         PRINT #1 ,"FUEL : LIQUID HYDROGEN (DENSITY = 4.42 lbm/ft^3)"
         PRINT #1 ,"OXIDIZER : LIQUID OXYGEN (DENSITY = 71.19 lbm/ft^3)"
         PRINT #1 ,"OXIDIZER TANK MAT'L : Al-Li 2090 T81 (DENSITY = 161.7 lbm/ft^3)"
         PRINT #1 ,"FUEL TANK MAT'L : Ti-5Al-2.5Sn ELI
         PRINT #1 ,"          (DENSITY = 278.21 lbm/ft^3)"
         PRINT #1 ,"PROGRAM FURTHER ASSUMES:"
         PRINT #1 ,"6% MORE PROPELLANT IS LEFT IN THE TANKS FOR EMERGENCIES"
         PRINT #1 ,"2% MORE PROPELLANT REMAINS IN THE LINES (RESIDUALS)"
         PRINT #1 ,"3% MORE VOLUME IS REQUIRED SINCE TANKS ONLY FILLED TO 97%"
         PRINT #1 ,"AN ASSUMED WALL THICKNESS IS USED FOR EACH TANK"
         PRINT #1 ,"THE FOLLOWING FIGURES USED IN SUMMING FOR 'SKELATAL MASS':"
         PRINT #1 ,"TTL RCS HARDWARE AND PROPELLANT : 2188 lbm"
         PRINT #1 ,"MASS OF TWO ENGINES: 900 lbm"
         PRINT #1 ,"MASS OF ENGINE SUPPORT STRUCTURE : 500 lbm"
         RITE$ = "N"
END IF
'
         CLS
  PRINT "MISSION DATA:"
         INPUT"SKELATAL MASS        = ";SKELATON
         INPUT"1ST PAYLOAD MASS     = ";PAYLOAD1
```

```
        INPUT"1ST DELTAV            = ";DELTAV1
        INPUT"2ND PAYLOAD MASS      = ";PAYLOAD2
        INPUT"2ND DELTAV            = ";DELTAV2
        INPUT "DELTAV POST AEROPASS = ";LASTDELTAV
        INPUT"EXIT VELOCITY         = ";VEXIT
        INPUT"Wo/Wf                 = ";WOWF
        INPUT"NUMBER OF H2 TANKS    = ";NH2
        INPUT"NUMBER OF O2 TANKS    = ";NO2
'
' CALCULATE FOR THE CYLINDRICAL CASE, HEMISPHERICAL ENDS
' --ALL INPUT FROM THE SPHERICAL CASE IS RETAINED AND USED
'
DO
'
' THIS IS THE CASE LOOPER
'
        BAILOUT% = 0
        STOPPER% = 0
        ITERCT% = 0
        TANKS = 0
        CLS
        PRINT
        PRINT "PROCEEDING TO THE CYLINDRICAL"
        PRINT" (WITH HEMISPHERICAL ENDS) TANKS"
        PRINT
'
DO
'
' THIS IS THE TANK GUESSING LOOPER
'
' CALCULATE MASSES + 8% FOR 1ST DELTAV
'
        MASSFINAL1 = SKELATON+PAYLOAD1+TANKS
        MASSINITIAL1 = MASSFINAL1*EXP(DELTAV1/VEXIT)
        MASSFUEL1 = (MASSINITIAL1-MASSFINAL1) + (MASSINITIAL1-MASSFINAL1)*.08
        MH21 = MASSFUEL1/(WOWF+1)
        MO21 = MASSFUEL1 - MH21
'
' CALCUATE MASSES + 8% FOR 2ND DELTAV
'
        MASSFINAL2 = SKELATON+PAYLOAD2+TANKS
        MASSINITIAL2 = MASSFINAL2*EXP(DELTAV2/VEXIT)
        MASSFUEL2 = (MASSINITIAL2-MASSFINAL2) + (MASSINITIAL2-MASSFINAL2)*.08
        MH22 = MASSFUEL2/(WOWF+1)
        MO22 = MASSFUEL2 - MH22
'
' DIVIDE THE MASSES INTO THE NUMBER OF TANKS
'
        MH2 = (MH21 + MH22)/NH2
    MO2 = (MO21 + MO22)/NO2
'
' CALCULATE THE VOLUME THAT EACH OF THE TANKS WOULD ENCLOSE + 3%
' ASSUMES:
'       USABLE LENGTH OF 15 FT FOR OXYGEN TANK
'           USABLE LENGTH OF 15.1 FT FOR HYDROGEN TANK--REC.FR. STRUCTURE GROUP
'           (WALL THICKNESSES FROM STRESS ANALYSIS)
'
        THICKO2 = .0013
        THICKH2 = .00153
        USEH2 = 15.1
        USEO2 = 15
        VOLH2 = (MH2/4.42) + (MH2/4.42)*.03
```

```
        VOLO2 = (MO2/71.19) + (MO2/71.19)*.03
    CALL FINDHEMI(H2RIN,VOLH2,USEH2)
        H2ROUT = THICKH2 + H2RIN
        TANKH2VOL = 1.333333*PI*(H2ROUT^3-H2RIN^3)+(USEH2-2*H2ROUT)*_
                        PI*(H2ROUT^2-H2RIN^2)
        CALL FINDHEMI(O2RIN,VOLO2,USEO2)
        O2ROUT = THICKO2 + O2RIN
        TANKO2VOL = 1.333333*PI*(O2ROUT^3-O2RIN^3)+(USEO2-2*O2ROUT)*_
                        PI*(O2ROUT^2-O2RIN^2)
        SHELLVOLH2 = TANKH2VOL*NH2
    MASSSHELLH2 = SHELLVOLH2 * TITIDENSITY
    SHELLVOLO2 = TANKO2VOL*NO2
        MASSSHELLO2 = SHELLVOLO2 * ALLIDENSITY
        SHELLVOL = SHELLVOLH2 + SHELLVOLO2
        MASSSHELL = MASSSHELLH2 + MASSSHELLO2
'
        ITERCT% = ITERCT% + 1
        LOCATE 1,40
        PRINT "ON ITERATION ";ITERCT%
        LOCATE 2,40
        PRINT "TANK MASS = ";TANKS
        LOCATE 3,40
        PRINT "SHELL MASS= ";MASSSHELL
        LOCATE 4,40
        PRINT "THE DELTAm = ";(TANKS-MASSSHELL)
'
        IF ABS(TANKS-MASSSHELL) <= 10 THEN
                BAILOUT% = 1
                TITLE$ = "CYLINDRICAL TANKS,HEMISPHERICAL ENDS:"
                CALL ECHO1(SKELATON,VEXIT,WOWF,PAYLOAD1,PAYLOAD2,DELTAV1,_
                DELTAV2,MASSFINAL1,MASSFINAL2,MASSINITIAL1,MASSINITIAL2,_
                MASSFUEL1,MASSFUEL2,MH21,MH22,TITLE$)
                BH2 = H2ROUT
                BO2 = O2ROUT
                CALL ECHO2(MO21,MO22,VOLH2,NH2,VOLO2,NO2,H2ROUT,O2ROUT,_
                THICKH2,THICKO2,SHELLVOL,BH2,USEH2,BO2,USEO2)
                CALL ECHO3(TANKS,MASSSHELLO2,MASSSHELLH2)
                PENULTIMATEMASS = SKELATON+PAYLOAD2+TANKS
                EMERGENCY = .08*(MASSFUEL1+MASSFUEL2)
                CALL PENULTIMATE(LASTDELTAV,VEXIT,PENULTIMATEMASS,_
                        EMERGENCY,PENULTIMATEH2,PENULTIMATEO2,WOWF)
                CALL ECHO4(PENULTIMATEH2,PENULTIMATEO2,LASTDELTAV,EMERGENCY)
          INPUT "WRITE RESULTS TO DISK (Y/N)"; RITE$
          IF RITE$ = "Y" THEN
                        CALL HARDCOPY1(SKELATON,VEXIT,WOWF,PAYLOAD1,PAYLOAD2,_
                        DELTAV1,DELTAV2,MASSFINAL1,MASSFINAL2,MASSINITIAL1,_
                                MASSINITIAL2,MASSFUEL1,MASSFUEL2,MH21,MH22,_
                                TITLE$)
                        CALL HARDCOPY2(MO21,MO22,VOLH2,NH2,VOLO2,NO2,H2ROUT,_
                        O2ROUT,THICKH2,THICKO2,SHELLVOL,BH2,USEH2,BO2,USEO2)
                        CALL HARDCOPY3(TANKS,MASSSHELLO2,MASSSHELLH2)
                        CALL HARDCOPY4(PENULTIMATEH2,PENULTIMATEO2,LASTDELTAV,_
                        EMERGENCY)

                END IF
            ELSE
                TANKS = TANKS + 10
        END IF
LOOP UNTIL (BAILOUT%)
'
INPUT "RUN ANOTHER CASE (Y/N)"; ASN$
IF ASN$ <> "Y" THEN
```

```
            STOPPER% = 1
    END IF
    '
    LOOP UNTIL (STOPPER%)
    '
    CLOSE #1
    PRINT "STOPPING..."
    '
    SUB FINDHEMI(RADIUS,TANKVOLUME,USABLE)
    '
    BIGNUM& = 100000
    EPSILON = .0001
    PI = 3.14159265
    '
    ' SOLVE USING METHOD OF FALSE POSITION
    '
    ITER% = 0
    BAILOUT% = 0
    TOOBIG% = 0
    LTSIDE = 0
    RTSIDE = 20
    '
    ' UTILIZING THE METHOD OF FALSE POSITION TO FIND ZERO OF FUNCTION..."
    '
    DO
            BETWEEN =(LTSIDE*FNEQUATION(RTSIDE,USABLE,TANKVOLUME)-_
                    RTSIDE*FNEQUATION(LTSIDE,USABLE,TANKVOLUME))/_
                    (FNEQUATION(RTSIDE,USABLE,TANKVOLUME)-_
                    FNEQUATION(LTSIDE,USABLE,TANKVOLUME))
            INTERMED = FNEQUATION(BETWEEN,USABLE,TANKVOLUME)
            IF ABS(INTERMED) > EPSILON THEN
                    CALL SHUFFLE(LTSIDE,RTSIDE,BETWEEN,USABLE,TANKVOLUME)
                    ITER% = ITER% + 1
               ELSE
                    BAILOUT% = 1
            END IF
            IF ITER% >= BIGNUM& THEN
                    BAILOUT% = 1
                    TOOBIG% = 1
            END IF
    LOOP UNTIL (BAILOUT%)
    '
    ITER% = ITER% + 1
    IF (TOOBIG%) THEN
            PRINT
            PRINT "SEARCH ABORTED AFTER ";BIGNUM&;" CYCLES"
            PRINT "SOLUTION NOT FOUND"
    END IF
    RADIUS = BETWEEN
    '       PRINT "RADIUS =";RADIUS
    '       INPUT "ANY KEY TO LEAVE SUB FINDHEMI ";ANY$
    END SUB
    '
    SUB SHUFFLE(LT,RT,MID,USABLE,TNKVOL)
            PI = 3.14159265
            PRODUCT = FNEQUATION(LT,USABLE,TNKVOL)*FNEQUATION(MID,USABLE,TNKVOL)
            SELECT CASE PRODUCT
                    CASE < 0
                            RT = MID
                    CASE = 0
    ' THIS IS IMPOSSIBLE, BUT IT WAS INCLUDED FOR COMPLETENESS
                    CASE > 0
```

```
                    LT = MID
        END SELECT
END SUB
'
SUB PENULTIMATE(LASTDELTAV,VEXIT,PENULTIMATEMASS,EMERGENCY,PENULTIMATEH2,_
                PENULTIMATEO2,WOWF)
INITMASS = PENULTIMATEMASS*EXP(LASTDELTAV/VEXIT)
MASSFUEL = (INITMASS-PENULTIMATEMASS)+EMERGENCY
PENULTIMATEH2 = MASSFUEL/(WOWF+1)
PENULTIMATEO2 = MASSFUEL-PENULTIMATEH2
END SUB
'
END
```